

國立交通大學

電子工程學系電子研究所

博士論文

以類神經網路為基礎的通訊等化器之研究

The Study of Neural-based Channel Equalizers



研究生：許騰仁

指導教授：李鎮宜

中華民國九十五年七月

以類神經網路為基礎的通訊等化器之研究

The Study of Neural-based Channel Equalizers

研究生：許騰仁

Student：Terng-Ren Hsu

指導教授：李鎮宜 博士

Advisor：Dr. Chen-Yi Lee

國立交通大學

電子工程學系電子研究所



A Dissertation

Submitted to Department of Electronics Engineering & Institute Electronics

College of Electrical and Computer Engineering

National Chiao Tung University

in Partial Fulfillment of the Requirements

for the Degree of Doctor of Philosophy

in

Electronics Engineering

July 2006

Hsinchu, Taiwan, Republic of China.

中華民國 九十五年 七月

以類神經網路為基礎的通訊等化器之研究

研究生：許騰仁

指導教授：李鎮宜教授

國立交通大學電子工程系電子研究所

摘要

在實際的通訊系統中需要以資料等化器來回復一個失真信號的原始波形，近來許多以類神經網路為基礎的等化器設計被應用在嚴重失真的信號回復。在本文，我們提出了一個新的類神經網路模式，使用一個多變數冪級數函數做為人工神經元的集成函數，應用於多層認知器結構倒傳遞類神經網路，由於對應的訓練演算法是以最陡坡降法推導，故收斂解存在。與使用一階多變數多項式當集成函數的傳統方法相比較，這個新方法的樣本空間分割邊界，將由傳統的片段線性分割變成片段非線性分割，傳統的多層認知器結構倒傳遞類神經網路可視為這個新方法的一個線性特別解。因此，可說這個新的模式是一般化的多層認知器結構倒傳遞類神經網路，與其他的片段線性分割的方法相比較，這個新方法因為具有片段非線性分割樣本空間的能力，所以在應用上有更大的彈性。

在有線通訊系統中，我們將以多層認知器結構倒傳遞類神經網路為基礎的通道等化方法應用於不同的地方，在資料速率大於通道頻寬十倍左右的有線頻寬受限通道上，與傳統上使用最小均方誤差演算法為基礎的決策回授等化器相比較，以多層認知器結構倒傳遞類神經網路為基礎的決策回授等化器可提供比較好的效能、容忍比較多的取樣時脈歪斜和允許比較大的通道響應變異。然而對於具有非線性失真的嚴重碼際干擾通道來說，以多層認知器結構倒傳遞類神經網路為基礎的決策回授等化器還有改善的空間，使用一般化的多層認知器結構倒傳遞類神經網路為基礎的決策回授等化器可以提供更好的效能。在多條平行的有線頻寬受限通道上，我們採用多輸入多輸出的以多層認知器結構倒傳遞類神經網路為基礎的決策回授等化器和多輸入多輸出的以一般化多層認知器結構倒傳遞類神經網路為基礎的決策回授等化器，同時抑制碼際干擾、串音干擾和背景雜訊。同樣的，多輸入多輸出的以一般化多層認知器結構倒傳遞類神經網路為基礎的決策回授等化器優於多輸入多輸出的以多層認知器結構倒傳遞類神經網路為基礎的決策回授等化器，而且多輸入多輸出的

以多層認知器結構倒傳遞類神經網路為基礎的決策回授等化器又優於使用最小均方誤差演算法為基礎的決策回授等化器。

對於無線通訊系統，我們提出一個以多層認知器結構倒傳遞類神經網路為基礎的改進方法。在多路徑平坦衰減通道中，我們應用軟性輸出和軟性決策回授的結構於一個以多層認知器結構倒傳遞類神經網路為基礎的通道等化器，並於其後串接一個軟性決策通道解碼器以改進整體的效能。此外，利用輸出層神經元的轉移函數尺度因子的最佳化，以及在訓練型樣加入少量的隨機擾動，可以進一步的改善以多層認知器結構倒傳遞類神經網路為基礎的軟性決策回授等化器的效能。由模擬結果，在多路徑平坦衰減通道中，使用包含位元交錯的軟性決策通道解碼器時，以多層認知器結構倒傳遞類神經網路為基礎的軟性決策回授等化器的效能優於以多層認知器結構倒傳遞類神經網路為基礎的決策回授等化器和軟性輸出的以多層認知器結構倒傳遞類神經網路為基礎的決策回授等化器。



The Study of Neural-based Channel Equalizers

Student: Terng-Ren Hsu

Advisor: Chen-Yi Lee

Department of Electronics Engineering, National Chiao-Tung University

Abstract

In practical communication systems, it is necessary to apply data equalizers to recover the original waveform from the distorted one. Recently, various equalizer designs based on artificial neural networks have been studied to the severely distorting signal recoveries. In this study, we propose a new neural network model that applies a multivariate power series as the summation function of the MLP/BP neural networks. The corresponding training algorithm is deduced by the gradient steepest descent method; consequently, the convergence solutions exist. Compared to the conventional approach using a first order multivariate polynomial, the boundaries separating the pattern space change from piecewise linear into piecewise nonlinear. The traditional method is a special case of the proposed model. Therefore, this new model is a generalized MLP/BP neural network that is more flexible than other piecewise linear approaches because of the nonlinear separating pattern space.

For wireline communications, we apply the MLP/BP-based channel equalization schemes to different applications. In wireline band-limited channels that the data rate is about ten times as much as the channel bandwidth, the MLP/BP-based DFEs provide better performance, tolerate more sampling clock skew, and permit larger channel response variance than LMS DFEs. However, the BER performance of the traditional MLP/BP-based DFEs is not good enough for the severe ISI channels with nonlinear distortions. In such channels, the generalized MLP/BP-based DFEs can outperform the

traditional MLP/BP-based DFEs that do better than the LMS DFEs. In wireline band-limited parallel channels, the MIMO MLP/BP-based DFEs and the MIMO GMLP/BP-based DFEs can suppress ISI, CCI and AWGN, simultaneously. By the simulation results, the MIMO GMLP/BP-based DFE can yield a substantial improvement over the MIMO MLP/BP-based DFE that perform better than the LMS DFEs in such channels.

For wireless communications, a modified approach, which is also based on the MLP/BP neural network, is presented. We apply the soft output and the soft decision feedback structure to the MLP/BP-based channel equalization scheme that concatenates with the soft decision channel decoder to improve whole performance on multi-path fading channels. Moreover, the performance of the MLP/BP-based soft DFE is also increased with the optimal scaling factor searching of the transfer function in the output layer of the MLP/BP neural networks and extra small random disturbances added to the training data. By the simulations, the MLP/BP-based soft DFEs with bit-interleaved TCM outperform the MLP/BP-based DFEs with bit-interleaved TCM and the soft output MLP/BP-based DFEs with bit-interleaved TCM in multi-path fading channels.

Acknowledgements

在這九年的博士班求學過程中，非常感謝指導教授李鎮宜老師的教導，他給學生寬廣的研究自由度，讓創意可以不受限制的盡情發展，並提供良好的研究環境，讓靈感得以驗證實現。在我研究類神經網路的過程中，基礎觀念的建立必須感謝我就讀逢甲大學自動控制工程研究所碩士班時的指導教授蕭肇殷博士和賴啟智副教授，也要謝謝逢甲大學資電學院院長邱創乾教授的教導和關心。此外，感謝口試委員的指導與寶貴的意見。

在我的博士論文研究過程中，特別的感謝給許騰尹和林建青，因為你們的大力幫忙，我的研究才能順利完成。也感謝 University of Minnesota 的 Dr. Yi-ru Chen 和 Prof. Simo Sarkanen 在百忙中抽空幫我修改投稿期刊論文的英文稿件。另外感謝 SI2 實驗室的大師兄蔡哲民學長、有革命情感的張錫嘉、李有山、謝百舉、蘇浩坤、羅偉仁、陳麒旭、楊鎮澤、彭文孝、鍾菁哲、王中正、劉益全、蔡尚峰、劉軒宇、曾順得、陳黎峰、蔡侑庭、游瑞元、陳志龍、賴名威、郭子菁、周伶霞、SI2 實驗室的其他同仁、資工 ISIP 實驗室的林祐賢和其他的學弟、明新科大電子系陳啟文主任、鄧俊修學長、呂明峰學長、李紀萍學長、鴻友科技同事樊勁志先生，謝謝你們的關心和協助。

最後，謹以此論文獻給我敬愛的母親，也以此紀念我的父親，感謝父母的照顧和栽培。此外姊姊的關心和學習路上一路相伴的弟弟，謝謝你們給我最大的支持與鼓勵，也謝謝內人怡霈的陪伴和照顧小孩的辛苦。

人生無常，不是每件事都會有好的結果。在我最鬱悶的時候帶來最大的欣喜，卻在一切將要順利之際，給我嘎然而止的震驚。淺淺的緣分，一生的思念。



Contents

Abstract in Chinese	<i>i</i>
Abstract	<i>iii</i>
Acknowledgements	<i>v</i>
Contents	<i>vii</i>
List of Tables	<i>xi</i>
List of Figures	<i>xiii</i>
1. Introduction	1
1-1 Thesis Motivation	1
1-2 Paper Survey	4
1-3 Thesis Organization	9
2. Generalized MLP/BP Neural Networks	11
2-1 Traditional MLP/BP Neural Networks	12
2-1-1 Architecture	12
2-1-2 Backpropagation Algorithm	14
2-2 Generalized MLP/BP Neural Networks	18
2-1-1 Architecture	19
2-1-2 Corresponding Backpropagation Algorithm	20
2-3 Complexity Analysis	24

3. SISO GMLP/BP-based DFEs for Wireline Applications	27
3-1 MLP/BP-based DFEs with High Skew Tolerance for Band-limited Channels	28
3-1-1 System Overview	28
3-1-2 MLP/BP-based DFEs	32
3-1-3 Simulation Results	33
3-1-4 Summary	43
3-2 GMLP/BP-based DFEs for Severe ISI Channels with Nonlinearity	44
3-2-1 Severe ISI Channels and Nonlinear Distortions	45
3-2-2 GMLP/BP-based DFEs	49
3-2-3 Simulation Results	51
3-2-4 Summary	62
4. MIMO GMLP/BP-based DFEs for Wireline Applications	63
4-1 MIMO MLP/BP-based DFEs for Overcoming ISI and CCI	64
4-1-1 Multi-channel Environment	64
4-1-2 MIMO MLP/BP-based DFE	68
4-1-3 Simulation Results	69
4-1-4 Summary	79
4-2 MIMO GMLP/BP-based DFEs for Overcoming ISI and CCI	80
4-2-1 Multi-channel Environment within a Plane	81
4-2-2 MIMO GMLP/BP-based DFE	82
4-2-3 Simulation Results	83
4-2-4 Summary	87

5. MLP/BP-based Soft DFEs with TCM for Wireless Communications	89
5-1 Wireless Channel Environment	90
5-2 Error Control Coding	93
5-3 Architecture	93
5-3-1 The MLP/BP-based Soft DFEs	94
5-3-2 Soft Decision Channel Coding and Interleaving	96
5-4 Simulation Results	96
5-5 Summary	103
6. Conclusion and Future Works	105
6-1 Conclusion	105
6-2 Future Works	107
References	109





List of Tables

Table 2-1: The comparison of computational complexity.	25
Table 3-1: Transfer functions of several wireline band-limited channels.	31
Table 3-2: The comparison of sampling clock skew tolerance.	44
Table 3-3: Transfer functions of different wireline severe ISI channels.	47
Table 3-4: The BER vs. SNR performance comparison with different equalizers for Channel 1, 2, and 3 without truncations at BER = 10^{-4} .	61
Table 3-5: The BER vs. SNR performance comparison with different equalizers for Channel 1, 2, and 3 with 30% truncations at BER = 10^{-3} .	62
Table 4-1: Weighting of co-channel interference between different channels in space.	67
Table 4-2: Simulation conditions for MIMO MLP/BP-based DFE.	71
Table 4-3: Weighting of co-channel interference between different channels on a plane.	81
Table 4-4: Simulation conditions for MIMO GMLP/BP-based DFE.	86
Table 5-1: System configurations and simulation conditions.	99
Table 5-2: The PER and BER performance improvement.	103



List of Figures

Fig. 2-1: MLP Neural Network Architecture.	13
Fig. 2-2: Neuron of MLP Neural Networks.	14
Fig. 2-3: Neuron of Generalized MLP/BP Neural Networks.	19
Fig. 3-1: System diagram.	30
Fig. 3-2: Equivalent model for the band-limited channels.	30
Fig. 3-3: Frequency responses of several similar wireline band-limited channels.	31
Fig. 3-4: MLP/BP-based DFEs.	32
Fig. 3-5: BER performance for different types of equalizers in different channels.	35
Fig. 3-6: BER performance for different types of equalizers with different clock skews in Channel 1.	36
Fig. 3-7: BER performance for different types of equalizers with different clock skews in Channel 3.	36
Fig. 3-8: BER performance for different types of equalizers with different clock skews in Channel 5.	37
Fig. 3-9: BER performance for different channel conditions with regular input pattern configuration at SNR=20dB.	37

Fig. 3-10: BER performance for different channel conditions with modified input pattern configuration at SNR=20dB.	38
Fig. 3-11: BER performance for different ADC resolution at SNR=15, SNR=18, and SNR=20.	40
Fig. 3-12: BER performance with different ADC resolution.	40
Fig. 3-13: BER performance for different ADC resolution with internal resolution enhancement.	41
Fig. 3-14: BER performance for different types of equalizers in different channels.	41
Fig. 3-15: BER performance for different types of equalizers with different clock skews in Channel 3.	42
Fig. 3-16: BER performance for different channel conditions with modified input pattern configuration at SNR=20dB.	42
Fig. 3-17: Equivalent model for the severe ISI channels.	47
Fig. 3-18: Frequency responses of different severe ISI channels.	48
Fig. 3-19: The comparison of the transmitted data and the received waveform.	48
Fig. 3-20: Generalized MLP/BP-based DFEs.	50
Fig. 3-21: Minimum MSE and standard deviation of MSEs of the training set in Channel 1 at SNR=15dB.	56

Fig. 3-22: Minimum MSE and standard deviation of MSEs of the evaluation set in Channel 1 at SNR=15dB.	56
Fig. 3-23: BER of the evaluation set and the test set in Channel 1 at SNR=15dB	57
Fig. 3-24: BER performance for different levels of the nonlinearity with different hidden neuron multipliers in Channel 1 at SNR=15dB.	57
Fig. 3-25: Channel 1 test results.	58
Fig. 3-26: Channel 2 test results.	58
Fig. 3-27: Channel 3 test results.	59
Fig. 3-28: Channel 4 test results.	59
Fig. 3-29: Channel 5 test results.	60
Fig. 3-30: Channel 6 test results.	60
Fig. 3-31: Channel 7 test results.	61
Fig. 4-1: Equivalent model for the band-limited channels with co-channel interference.	66
Fig. 4-2: Frequency responses of the ISI and the CCI responses.	67
Fig. 4-3: MIMO MLP/BP-based DFEs.	68
Fig. 4-4: BER vs. SNR for different types of equalizers in the band-limited channels with co-channel interference at SIR=10, 15 and 20dB.	72



Fig. 4-5: BER vs. SIR for different types of equalizers in the band-limited channels with co-channel interference at SNR= 15 and 20dB.	72
Fig. 4-6: BER performance under SIR=15dB, 17.5dB, and 20dB for different ADC resolution at SNR=15dB, 17.5dB, and 20dB.	74
Fig. 4-7: BER performance vs. SNR for different ADC resolution at SIR=15dB, 17.5dB, and 20dB.	75
Fig. 4-8: BER performance under SIR=15dB, 17.5dB, and 20dB for different ADC resolution with internal resolution enhancement technique at SNR=20dB.	77
Fig. 4-9: BER performance vs. SNR with different ADC resolution and different internal resolution at SIR=15dB, 17.5dB, and 20dB.	78
Fig. 4-10: BER performance vs. SNR for the LMS DFEs and MIMO MLP/BP-based DFEs at SIR=15.0dB, 17.5dB, and 20.0dB.	79
Fig. 4-11: The MIMO generalized MLP/BP-based DFEs.	83
Fig. 4-12: BER vs. SNR for different types of equalizers in the wireline band-limited channels with co-channel interference at SIR=10, 15 and 20dB.	85
Fig. 4-13: BER vs. SIR for different types of equalizers in the wireline band-limited channels with co-channel interference at SNR= 15 and 20dB.	87
Fig. 5-1: System Diagram.	90
Fig. 5-2: The Equivalent Model for the Multi-path Fading Channels.	91

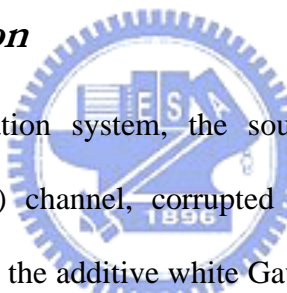
Fig. 5-3: Channel Responses of Multi-path Fading Channels.	92
Fig. 5-4: Frequency Responses of Multi-path Fading Channels.	92
Fig. 5-5: MLP/BP-based Soft DFEs for Wireless Applications.	95
Fig. 5-6: PER Performance for different types of equalizers when packet data length is equal to 10^3 .	100
Fig. 5-7: PER Performance for different types of equalizers when packet data length is equal to 8×10^3 .	100
Fig. 5-8: PER Performance for different types of equalizers with different packet data length at $E_b/N_0 = 7.5\text{dB}$ and 10.0dB .	101
Fig. 5-9: BER Performance for different types of equalizers when packet data length is equal to 10^3 .	101
Fig. 5-10: BER Performance for different types of equalizers when packet data length is equal to 8×10^3 .	102
Fig. 5-11: BER Performance for different types of equalizers with different packet data lengths at $E_b/N_0 = 7.5\text{dB}$ and 10dB .	102



CHAPTER 1

Introduction

1-1 Thesis Motivation



In a digital communication system, the source signal is transmitted over an intersymbol interference (ISI) channel, corrupted by noise, and then received as a distorted signal. In most cases, the additive white Gaussian noise (AWGN) can be used to model the background noise; however, the noise includes not only ISI and AWGN but the nonlinear distortion as well. If the channel response introduces both intersymbol interference and nonlinear distortions, transmitted signal will be corrupted nonlinearly, leading to worse performance. For example, the saturation of non-ideal amplifier and automatic gain control (AGC) loss in transceivers will produce nonlinear distortions that further degrade the performance of equalizers. Therefore, it is necessary to apply data equalizers to recover the original waveform from the distorted one in practical communication systems [1], [2]. A good equalization design can enhance the whole system performance with an acceptable cost.

Conventionally, the NRZ signal recovery is based on either linear equalizers (LEs)

[1], [3], or decision feedback equalizers (DFEs) [1], [2], [3]. A linear equalizer can restore the original transmitted signal in a wireline band-limited channel, where the channel distortion is linear without spectral nulls in the channel frequency response. Nevertheless, as the channel frequency response has spectral nulls, the received noise will be enhanced in the process of compensating these nulls, resulting in degraded performance. For linear equalization scheme, such channels that lead to malfunctions of equalizers have been termed “severe” ISI channels [4].

The decision feedback equalizer employing previous decisions to remove the ISI on the current symbol has been extensively exploited to serve intersymbol interference rejection. The least mean squares (LMS) algorithm is used to estimate the coefficients of the equalizer [1], [2], [3] whose accuracy determines the system performance.

For wireline high data rate applications, timing uncertainty degrades the system performance [5]. The channel response variance that is caused by manufacturing deviation makes the worse situation. It is necessary that using an equalizer to overcome clock skew and channel response variance. In addition, interconnect paths of parallel data I/O would cause the co-channel interference (CCI) [6]. The transmitted signals are tainted by the intersymbol interference that caused by the band-limited channel, the co-channel interference that caused by crosstalk between different channels, and background white noise. For recover the distorted data as well as suppress ISI, CCI and AWGN, a multi-input multi-output (MIMO) channel equalizer is essential.

Error control codes (ECC) are applied to enhance the accuracy of the transmitted data in wireless applications. The channel decoder with soft information inputs is widely employed to improve the error correction capability [7], and the bit interleaving is included [8] in wireless fading channels. With the soft output [9] and soft feedback [10] channel equalizers, the soft decision channel decoder will receive more information from

the channel and therefore precisely decode the data sequence, leading to better BER performance.

Besides, the equalization schemes can be thought of a mapping from the received waveform to the transmitted data. The pattern recognition techniques have been used to identify the severely distorting data. Having the capability of classifying the sampling pattern and fault tolerance, artificial neural networks are very suitable for the channel equalizations. Recently, various equalizer designs based on artificial neural networks have been studied to the severely distorting signal recoveries [11]. Neural-based approaches have more flexibility and better performance than conventional equalization techniques. The proposed approaches are based on the most popular multi-layer perceptron neural network with backpropagation algorithm (MLP/BP) [12], [13], [14], [15], [16]. As well, the MLP architecture can be regarded as a separateness-summation modus operandi in separating pattern space.

For wireline applications, we apply the MLP/BP-based channel equalization schemes to different applications. In the wireline band-limited channel that the data rate is ten times as much as the channel bandwidth, the MLP/BP-based feedforward equalizer (FFE) can recover the distorted data [17]. The MLP/BP-based DFE provide better performance, tolerate sampling clock skew, and permit channel response variance [18]. In wireline parallel I/O channels, the MIMO MLP/BP-based DFE can suppress ISI, CCI and AWGN, simultaneously [19]. However, the traditional MLP/BP-based DFEs are not good enough for the severe ISI channels with nonlinear distortions. We present a new neural network model, which is based on the MLP/BP neural network. This model utilizes a multivariate power series for the summation function of the MLP/BP neural networks [20], [21]. The corresponding training algorithm is deduced by the gradient steepest descent method; consequently, the convergence solutions exist. Compared to the conventional approach

using a first order multivariate polynomial, the boundaries separating the pattern space change from piecewise linear into piecewise nonlinear. Therefore, this novel model is a generalized MLP/BP neural network (GMLP/BP) that is more flexible than other piecewise linear approaches because of the nonlinear separating pattern space. In such channels, the GMLP/BP-based DFE can outperform the traditional MLP/BP-based equalization schemes [22]. Also, the performance of the MIMO GMLP/BP-based DFE is better than that of the MIMO MLP/BP-based DFE in wireline parallel channels that contain ISI, CCI, and background white noise [23].

For wireless applications, a modified approach, which is also based on the most popular MLP/BP neural network, is presented. We apply the soft output and the soft decision feedback structure to the MLP/BP-based channel equalizer that concatenates with the soft decision channel decoder to improve whole performance on multi-path fading channels. Moreover, the performance of the MLP/BP-based soft DFE is also increased with the optimal scaling factor searching of the transfer function in the output layer of the MLP/BP neural networks and extra small random disturbances added to the training data [24].

1-2 Paper Survey

There are various channel equalization schemes that are applied to different channel conditions. We survey the representative equalization approaches for wireline and wireless communications in these few years. These papers treat of different channel equalization schemes for wireline band-limited channels, wireline severe ISI channels, and wireless fading channels, respectively.

The linear equalizers can recover the distorted data in wireline band-limited channels

[1], [2], [3]. For wireline severe ISI channels or wireless fading channels, the linear equalization schemes are unsuitable [4], [5].

In severe ISI channels, the DFEs [1], [2], [3], [5] can avoid the influence of the spectral nulls and outperform the LEs. For wireline high data rate communications, DFEs are applied to improve the data rate or reduce the error rate [25], [26], [27]. In practice circuits, the channel responses of different interconnect paths of parallel data I/O are different. The receiver must tolerate channel responses variance and sampling clock skew. Besides, CCI makes the problem more severely.

The most popular training algorithm of DFEs is the least mean squares (LMS) algorithm, which is a minimum mean square error (MMSE) solution. One of the great methods for improving DFEs, support vector machines (SVM) based DFEs [28], [29], [30] uses the minimum bit error rate (MBER) solution instead of the MMSE solution to enhance system performance, but requires the estimation of channel impulse response (CIR) to compute the weighting vectors. Although the performance of SVM DFE is better than LMS DFE, the complexity of SVM DFE is much higher due to the additional channel estimator.

The Viterbi Equalizer (VE) [31] that requires CIR estimation can also be used in severe ISI channels and achieve much better performance. However, the accuracy of CIR dominates the performance particularly, and a nonlinear distortion of received signal will cause significant performance degradation to VE.

Because feed-forward neural network based channel equalization schemes are the most suitable architectures for very large-scale integration (VLSI) implementation, we survey the several well-liked neural network models that contain single layer perceptron (SLP) neural networks [13], [14], [16], polynomial perceptron (PP) neural network [14], [16], functional-link (FL) neural networks [14], [16], [32], radial basis function (RBF)

neural networks [14], [15], [16], counterpropagation (CP) neural networks [14], [16], [33], and MLP/BP neural networks [12], [13], [14], [15], [16].

The single layer perceptron neural network is the simplest neural network model, but it can't solve the linear non-separable problem. In wireline applications, SLP-based channel equalizers [34] are better than LMS-based linear equalizers.

The polynomial perceptron neural network uses a polynomial function to represent the input data and then a SLP neural network to combine these represented data and generate the output. By the input data represented, PP neural networks can solve linear non-separable problems. In severe ISI channels, PPNN-based channel equalizers outperform linear equalizers [35]. In multi-path fading channels, PPNN-based channel equalizers can suppress ISI and CCI [36], [37], simultaneously. The complexity of the PPNN-based channel equalization schemes is depended on tap number and polynomial degree.

Based on the same concept, the functional-link neural networks are proposed. The higher-order input terms of the FL neural networks can be generated by the expanded functions, which comprise polynomial functions, trigonometric functions, signum functions and other nonlinear functions. The PP neural network is a special case of FL neural network. In severe ISI channels, FLNN-based channel equalizers can recover severe distorted data [38], [39], [40]. In multi-path fading channels, FLNN-based channel equalizers can suppress ISI and CCI with better performance than LEs and DFEs [41], [42], [43].

Excluding above definitely defined functions, a set of radial basis functions, which paves the input space with overlapping receptive fields, can be taken as the functional expander of the RBF neural networks. The most frequently used radial basis function is the Gaussian function. The output of the radial basis function is maximized by minimized

the Euclidean distance between the input vector and the centroid. To find the correct centers of the radial basis functions is very important. Thus, the clustering technique is the key issue [44]. The RBF-based channel equalization schemes [45], [46], [47], [48], [49] can be applied to wireline band-limited channels, severe ISI channels with or without nonlinearity, severe ISI channels with CCI, and wireless fading channels.

Overall, the architecture of PP neural networks, FL neural networks, and RBF neural networks consists of two main parts, the functional expander and the linear combiner. The functional expander, which performs nonlinear mapping for the input data, and make the linear non-separable problem become linear separable. Afterward, a SLP neural network, which is trained by the simple delta-learning rule, is taken as the linear combiner to associate the represented input data with the desired outputs. The pattern space separating boundaries of such neural networks are nonlinear.

The counterpropagation neural network is two-layer structure. The first layer is a winner-take-all network, and the second layer is perceptron-based architecture. The learning speed of CP neural networks is faster than MLP/BP neural networks, but the accuracy is worse. The CP-based channel equalizers outperform LEs under nonlinear channel characteristics [50].

Since late 1980s, the MLP/BP neural network is the most important and most popular neural network model [12], [13], [14], [15], [16]. The MLP neural network can be regarded as a separateness-summation modulus operandi. Because the summation function of the MLP/BP neural network is a first order multivariable polynomial function, the boundaries of neighbors are linear or piecewise linear. Also, it is treated as continuous linear mapping processes.

In severe ISI channels, the MLP/BP-based feedforward equalizers [51], [52], and the MLP/BP-based decision feedback equalizers [53], [54], [55] have been widely used to

distorted signal recovery. The MLP/BP neural network combined decoder and equalizer [4] merges forward equalization and data decoder in an MLP/BP neural network. It can offer higher system integration and better performance than the traditional separate solutions. The MLP/BP DFE with lattice filter [56] uses a lattice filter to whiten its input signal. The lattice filter can reject a quantity of the noise and make the signal clear. The convergence rate of the neural network, the steady state mean square error, and the bit error rate of whole system can be improved in chorus.

For constant envelope signal processing, we can separate in-phase and quadrature-phase components and then the real-value activation functions can handle this problem. Besides, there are two main approaches for the development of a complex neural network. One looks for fully complex activation function [57], [58], and has been applied to distorted QPSK signal recovery [59]. Another has used split complex activation function [60], [61], and has been also employed to channel equalization [62].

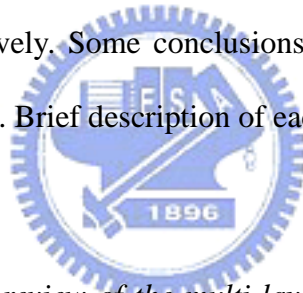
For wireless communications, the MLP/BP-based DFEs are applied to indoor radio channels [63] and digital satellite channels [64]. In wireless applications, the length of the training symbols and the number of the training epochs are sternly limited. As well, the MLP/BP-based DFEs can be used to suppress not only ISI but also CCI that is due to other co-channel users [65], [66].

The MLP neural network with hierarchical backpropagation algorithm (HBP) combines the hierarchical approach and BP algorithm [67]. It can solve some problems of the local minimum in the BP algorithm and improve the system performance. Except MMSE based learning rule, the least relative entropy (LRE) [68], [69] based learning algorithm has been applied to SLP neural network based equalizers and MLP neural network based equalizers. The dynamics of the LRE based algorithm is better than that of the MMSE based learning rule. It means that the learning speed of the LRE based

algorithm is faster than the MMSE based one. Moreover, neural networks can be trained by fuzzy if-then rules [16]. For nonlinear channel equalization applications, an adaptive neural fuzzy filter provides good performance [70].

1-3 Thesis Organization

The rest of this thesis is organized as follows. The traditional MLP/BP neural networks and the generalized MLP/BP neural networks are first addressed in chapter 2. The detail of proposed neural-based channel equalization schemes for wireline SISO applications, wireline MIMO applications, and wireless applications are described in chapters 3, 4, and 5, respectively. Some conclusions and future works of the proposed methods are made in chapter 6. Brief description of each chapter is given below:



- *In chapter 2, the brief review of the multi-layer perceptron neural networks with backpropagation algorithm is introduced at first. Subsequently, the generalized multi-layer perceptron neural networks and corresponding backpropagation algorithm is proposed. At last, the comparison of computational complexity is made.*
- *In chapter 3, the MLP/BP-based DFEs with high skew tolerance for wireline band-limited channels are presented at the beginning. Afterward, the generalized MLP/BP-based DFEs for wireline severe ISI channels are proposed.*
- *In chapter 4, the MIMO MLP/BP-based DFEs and the MIMO generalized MLP/BP-based DFEs for overcoming ISI and CCI in wireline band-limited channels are given.*

- *In chapter 5, the MLP/BP-based soft decision feedback equalizers for wireless communications are delivered.*
- *In chapter 6, some concluding remarks will be derived from this research. Then briefly discussions illustrate our research activities in the future.*



CHAPTER 2

Generalized MLP/BP Neural Networks

Artificial neural networks are systems that are deliberately constructed to make use of some organizational principles resembling those of the human brain. In 1943, McCulloch and Pitts proposed a simple mathematical model of the biological neuron, usually called an M-P neuron. The generalizations or variations of the M-P neuron are the basic component of artificial neural networks. An artificial neural network consists of a set of highly interconnected neurons such that each neuron output is connected to other ones or/and to itself through weights, which with or without lag. In 1957, Rosenblatt created the perceptron neural networks that include single-layer feedforward networks, which without hidden layers; and multi-layer feedforward networks, which with a hidden layer or more. But there is no suitable training algorithm for multi-layer perceptron neural networks until the backpropagation algorithm [12] had been proposed. Today, there are many different artificial neural networks had been proposed, but the multi-layer perceptron neural network with backpropagation algorithm is the most important and most popular one [13], [14], [15], [16].

In this work, we treat the MLP/BP neural network model and make a key

modification to offer a new approach, the generalized MLP/BP neural network. At the beginning of this chapter, we make a review for the traditional MLP/BP neural network. Afterward, a detail arrangement of the generalized MLP/BP neural network is given.

2-1 Traditional MLP/BP Neural Networks

Although the MLP neural network had been treated in late 1950s, the suitable training algorithm wasn't appeared until the backpropagation algorithm [12] presented. Bryson and Ho in 1969, Werbos in 1974, LeCun in 1985, Parker in 1985, and Rumelhart in 1986 proposed the backpropagation algorithm. The most influential publication of the backpropagation algorithm is Rumelhart's contribution. Since late 1980s, the MLP/BP neural network has been widely used to pattern recognition, and signal processing [13], [14], [15], [16].

In this section, we treat the MLP/BP neural network because it is the basis of our proposed model. At first, we show the detail of the MLP neural network architecture. Subsequently, the deduced process of the backpropagation algorithm is presented.

2-1-1 Architecture

The architecture of a multi-layer perceptron neural network [12], [13], [14], [15], [16] is shown in Fig. 2-1. The neurons are arranged into several layers. The first layer is the input layer, the final layer is the output layer, and other in-between layers are hidden layers. The neuron number of each layer could be singular form or plural form. In the input layer, each neuron includes a single input and a single output. In other layers, there

are several inputs and one output in each neuron. The different neurons, which situate in neighbor layers, connect together through respective weights without lag.

A neuron, the processing unit, of the MLP neural networks [12], [14], [16] is shown in Fig. 2-2. The output of a neuron is the value obtained from applying a transfer function to a weighted sum of its inputs, where each input is the output of a neuron situated in the previous layer. The weighted sum of the inputs can be described as a first order polynomial function. As well, commonly used transfer functions include hard limit functions (step functions), ramp functions (linear functions), unipolar sigmoid functions (log-sigmoid functions), bipolar sigmoid functions (tan-sigmoid functions), and so on. For different purposes, we can select dissimilar transfer functions to meet the requirement or constraint. In this work, we choose the unipolar sigmoid function as the transfer function of a neuron.

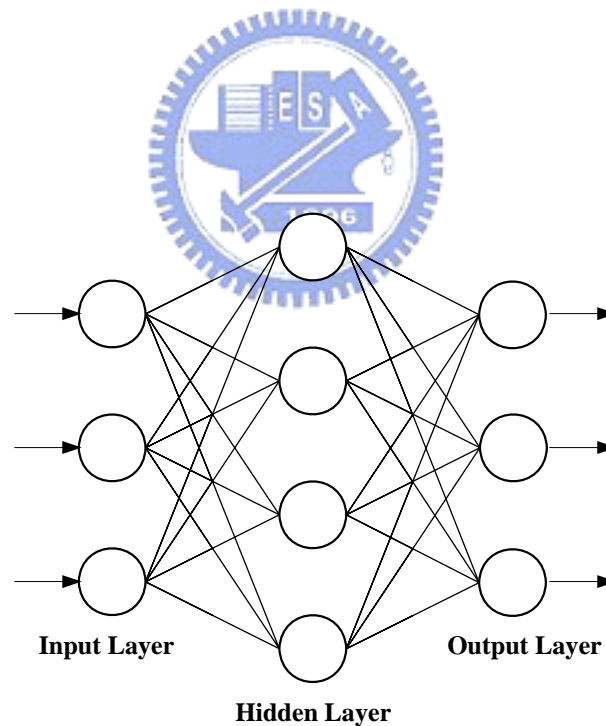


Fig. 2-1: MLP Neural Network Architecture.

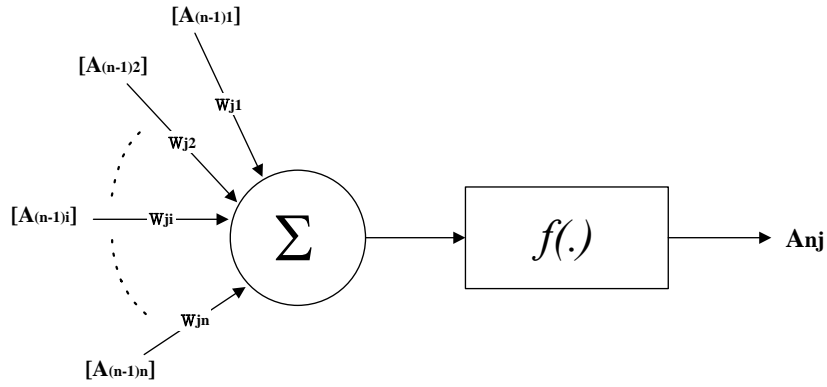


Fig. 2-2: Neuron of MLP Neural Networks.

2-1-2 Backpropagation Algorithm

The MLP/BP neural networks are supervised learning. It means that a training set includes an input vector and a desired output vector. Using the MLP/BP neural networks to solve problems includes two phases, one is training procedure and another is testing procedure. In the training phase, we base on the gradient steepest descent method to minimize the error function for updating the weights. After that we apply the training result to obtain the network response in testing phase. Now, a mathematical description of backpropagation algorithm [12], [15] is shown as follows:

$$Output = A_{nj} = f(net_{nj}), \quad (2-1)$$

where A_{nj} is the output of neuron j in the n -th layer, $f(\cdot)$ is the transfer function obtaining the output of a neuron, and net_{nj} is the output of the summation function of neuron j in the n -th layer. Furthermore,

$$net_{nj} = Summation_Function = \sum_j W_{ji} A_{(n-1)i} - \theta_j, \quad (2-2)$$

where W_{ji} represents the weight of the connection between neuron j in the n -th layer and neuron i in the $(n-1)$ -th layer, and θ_j is the threshold (bias) of neuron j . The W_{jim} should be

trained to minimize the error function

$$E = \text{Error_Function} = \frac{1}{2} \cdot \sum_j (T_j - A_{nj})^2, \quad (2-3)$$

where T_j is the desired output of neuron j in the output layer.

By the gradient steepest descent method, the error function (2-3) can be minimized by

$$\Delta W_{ji} = -\eta \cdot \frac{\partial E}{\partial W_{ji}}, \quad (2-4)$$

the update quantity for W_{ji} , and η is the learning rate.

By chain rule,

$$\frac{\partial E}{\partial W_{ji}} = \frac{\partial E}{\partial \text{net}_{nj}} \cdot \frac{\partial \text{net}_{nj}}{\partial W_{ji}}, \quad (2-5)$$

$$\frac{\partial E}{\partial W_{ji}} = \frac{\partial E}{\partial A_{nj}} \cdot \frac{\partial A_{nj}}{\partial \text{net}_{nj}} \cdot \frac{\partial \text{net}_{nj}}{\partial W_{ji}}, \quad (2-6)$$

$$\frac{\partial \text{net}_{nj}}{\partial W_{ji}} = \frac{\partial}{\partial W_{ji}} \left(\sum_k W_{jk} \cdot A_{(n-1)k} - \theta_j \right) = A_{(n-1)i}, \quad (2-7)$$

$$\frac{\partial A_{nj}}{\partial \text{net}_{nj}} = \frac{\partial}{\partial \text{net}_{nj}} \cdot f(\text{net}_{nj}) = f'(\text{net}_{nj}). \quad (2-8)$$

For $\frac{\partial E}{\partial A_{nj}}$, there are two cases that should be discussed:

(1) When the n -th layer is the output layer,

$$\frac{\partial E}{\partial A_{nj}} = \frac{\partial}{\partial A_{nj}} \left[\frac{1}{2} \cdot \sum_k (T_k - A_{nk})^2 \right] = -(T_j - A_{nj}). \quad (2-9)$$

(2) When the n -th layer is a hidden layer,

$$\begin{aligned} \frac{\partial E}{\partial A_{nj}} &= \sum_k \left(\frac{\partial E}{\partial \text{net}_{(n+1)k}} \right) \cdot \left(\frac{\partial \text{net}_{(n+1)k}}{\partial A_{nj}} \right) \\ &= \sum_k \left(\frac{\partial E}{\partial \text{net}_{(n+1)k}} \right) \cdot \left[\frac{\partial}{\partial A_{nj}} \left(\sum_i W_{ki} \cdot A_{ni} - \theta_k \right) \right] \\ &= \sum_k \left(\frac{\partial E}{\partial \text{net}_{(n+1)k}} \right) \cdot W_{kj} \end{aligned} \quad (2-10)$$

Let $\frac{\partial E}{\partial net_{nk}} = -\delta_{nk}$ be the error signal of neuron k in n -th layer, $\frac{\partial E}{\partial net_{(n+1)k}} = -\delta_{(n+1)k}$ can

be deduced and (2-10) can be rewritten as

$$\frac{\partial E}{\partial A_{nj}} = -\sum_k \delta_{(n+1)k} \cdot W_{kj} \quad (2-11)$$

Furthermore, according to (2-7), the deviation in (2-5) can be rewritten as

$$\frac{\partial E}{\partial W_{ji}} = -\delta_{nj} \cdot A_{(n-1)i} \quad (2-12)$$

By (4) and (12),

$$\Delta W_{ji} = -\eta \cdot \frac{\partial E}{\partial W_{ji}} = \eta \cdot \delta_{nj} \cdot A_{(n-1)i} \quad (2-13)$$

Similarly, the following equation can be obtained

$$\Delta \theta_j = -\eta \cdot \delta_{nj}, \quad (2-14)$$

where $\Delta \theta_j$ is the update quantity of θ_j .

From the above deductions, there are two possible cases:

(1) If W_{ji} is between the output layer and its anterior layer (a hidden layer), (2-7), (2-8),

and (2-9) can be applied to (2-6),

$$\frac{\partial E}{\partial W_{ji}} = -(T_j - A_{nj}) \cdot f'(net_{nj}) \cdot A_{(n-1)i} \quad (2-15)$$

After comparing (2-12) and (2-15), we can obtain

$$\delta_{nj} = (T_j - A_{nj}) \cdot f'(net_{nj}) \quad (\text{for output layer}). \quad (2-16)$$

(2) If W_{ji} is between a hidden layer and its anterior layer (a hidden layer or the input

layer), (2-7), (2-8), and (2-11) can be applied to (2-6),

$$\frac{\partial E}{\partial W_{ji}} = [-\sum_k \delta_{(n+1)k} \cdot W_{kj}] \cdot f'(net_{nj}) \cdot A_{(n-1)i} \quad (2-17)$$

The following equation can be obtained from comparing equations (2-12) and (2-17)

$$\delta_{nj} = [\sum_k \delta_{(n+1)k} \cdot W_{kj}] \cdot f'(net_{nj}) \quad (\text{for hidden layer}). \quad (2-18)$$

In this work, a unipolar sigmoid function is used to the transfer function of a neuron. The first derivative of the unipolar sigmoid function can be represented as the terms of itself, as shown in (2-19) and (2-20).

$$f(net_{nj}) = \frac{1}{1 + e^{-net_{nj}}}, \quad (2-19)$$

$$\begin{aligned} f'(net_{nj}) &= \frac{e^{-net_{nj}}}{(1 + e^{-net_{nj}})^2} = \frac{1}{1 + e^{-net_{nj}}} \cdot \left(1 - \frac{1}{1 + e^{-net_{nj}}}\right) \\ &= f(net_{nj}) \cdot [1 - f(net_{nj})] = A_{nj} \cdot (1 - A_{nj}), \end{aligned} \quad (2-20)$$

By such representation, (2-16) and (2-18) can be rewritten as (2-21) and (2-22).

$$\delta_{nj} = (T_j - A_{nj}) \cdot A_{nj} \cdot (1 - A_{nj}) \quad (\text{for output layer}), \quad (2-21)$$

$$\delta_{nj} = [\sum_k \delta_{(n+1)k} \cdot W_{kj}] \cdot A_{nj} \cdot (1 - A_{nj}) \quad (\text{for hidden layer}). \quad (2-22)$$

In each iteration, the weights and thresholds are updated. When the whole set of training data has been cycled once, calculate mean square error (MSE) of this training epoch. We repeat such epoch and record the best result, which consists of weights and thresholds and leads to the minimal MSE among past training epochs. Check whether the current MSE is smaller than the maximum tolerable error, which the result meets the training object, and the entire training epochs have been completed, which stands for the maximum patient training time. If the alternative conditions have been reached, the training process is terminated. At this moment, the training result is harvested. In general, reduce training time and enhance system performance are certain exclusive property. [14], [15], [16]

Because the MLP/BP neural network is an MMSE approach, the training results will converge on local optima. Using different network configurations, different initial condition and different learning rate, will conduce to different performance [13], [14], [16]. In general, could perform quite a few independent training runs and choose the most suitable result as the final solution.

Moreover, the MLP/BP neural network can be regarded as a separateness-summation modus operandi in separating pattern space. Because the summation function of the MLP/BP neural network is linear, the boundaries of neighbors are linear or piecewise linear. [14], [16] For a complex system, the number of neurons should increase for better approximation.

2-2 Generalized MLP/BP Neural Networks

To achieve more flexibility and better performance, a multivariate power series is used to replace a first order multivariate polynomial as the summation function of the MLP/BP neural networks, leading to a significant modification for the traditional MLP/BP neural network. Therefore, regarded as a general form of the MLP/BP neural network, the proposed model can be termed as a generalized MLP/BP neural network. This key modification comes from the previous study of speech recognition where a better performance can be attained by using the multivariate power series [20], [21]. In this work, this new method is applied to the waveform equalization and results in a significant improvement in performance.

In this section, we show the architecture of the generalized MLP/BP neural network at first. Subsequently, the deduced process of the corresponding backpropagation algorithm is presented. Referring to the traditional MLP/BP neural network and the

generalized MLP/BP neural network, we find that the traditional method is a special case of the proposed model.

2-2-1 Architecture

The network architecture of our proposition is the same as the traditional MLP/BP neural networks. That has been shown in Fig. 2-1. However, the construction of neurons of the both is different. A neuron of this new approach is shown in Fig. 2-3. The output of a neuron of the proposed scheme is the value obtained from applying a transfer function to a weighted sum of the power terms of its inputs, where each input is the output of a neuron situated in the previous layer. The weighted sum of the power terms of the inputs can be represented as a multivariate power series. On the other word, the summation function of the generalized MLP/BP neural networks is a multivariate power series that substitute for the first order multivariate polynomial. Similarly, we can select dissimilar transfer functions to meet the requirements of different purposes.

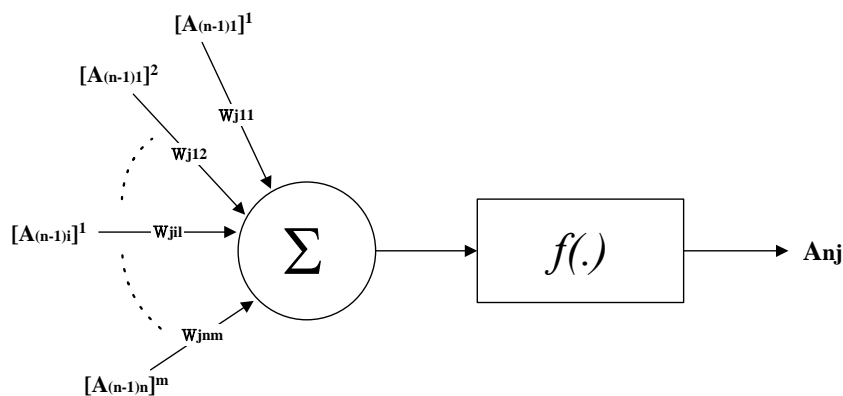


Fig. 2-3: Neuron of Generalized MLP/BP Neural Networks.

2-2-2 Corresponding Backpropagation Algorithm

In this subsection, we present the training algorithm for the generalized MLP/BP neural network. It is similar to the traditional training algorithm. Diversely, the multivariate power series is used to replace the first order multivariate polynomial as the summation function of the MLP/BP neural networks. The corresponding backpropagation algorithm of the proposed approach is deduced by the gradient steepest descent method and is shown as follows:

$$Output = A_{nj} = f(net_{nj}), \quad (2-1)$$

where A_{nj} is the output of neuron j in the n -th layer, $f(.)$ is the transfer function obtaining the output of a neuron, and net_{nj} is the output of the summation function of neuron j in the n -th layer. Furthermore,

$$net_{nj} = Summation_Function = \sum_i \sum_m W_{jim} A_{(n-1)i}^m - \theta_j, \quad (2-23)$$

where m is the order of the summation function, W_{jim} represents the weight of the connection between neuron j in the n -th layer and neuron i in the $(n-1)$ -th layer corresponding to order m , and θ_j is the threshold (bias) of neuron j . The W_{jim} should be trained to minimize the error function

$$E = Error_Function = \frac{1}{2} \cdot \sum_j (T_j - A_{nj})^2, \quad (2-3)$$

where T_j is the desired output of neuron j in the output layer.

By the gradient steepest descent method, the error function (2-3) can be minimized by

$$\Delta W_{jim} = -\eta \cdot \frac{\partial E}{\partial W_{jim}}, \quad (2-24)$$

the update quantity for W_{jim} , and η is the learning rate.

By chain rule,

$$\frac{\partial E}{\partial W_{jim}} = \frac{\partial E}{\partial net_{nj}} \cdot \frac{\partial net_{nj}}{\partial W_{jim}}, \quad (2-25)$$

$$\frac{\partial E}{\partial W_{jim}} = \frac{\partial E}{\partial A_{nj}} \cdot \frac{\partial A_{nj}}{\partial net_{nj}} \cdot \frac{\partial net_{nj}}{\partial W_{jim}}, \quad (2-26)$$

$$\frac{\partial net_{nj}}{\partial W_{jim}} = \frac{\partial}{\partial W_{jim}} \left[\sum_k \sum_{m=1}^p W_{jim} \cdot A_{(n-1)k}^m - \theta_j \right] = A_{(n-1)i}^m, \quad (2-27)$$

$$\frac{\partial A_{nj}}{\partial net_{nj}} = \frac{\partial}{\partial net_{nj}} \cdot f(net_{nj}) = f'(net_{nj}). \quad (2-28)$$

For $\frac{\partial E}{\partial A_{nj}}$, there are two cases that should be discussed:

(1) When the n -th layer is the output layer,

$$\frac{\partial E}{\partial A_{nj}} = \frac{\partial}{\partial A_{nj}} \left[\frac{1}{2} \cdot \sum_k (T_k - A_{nk})^2 \right] = -(T_j - A_{nj}). \quad (2-29)$$

(2) When the n -th layer is a hidden layer,

$$\begin{aligned} \frac{\partial E}{\partial A_{nj}} &= \sum_k \left(\frac{\partial E}{\partial net_{(n+1)k}} \right) \cdot \left(\frac{\partial net_{(n+1)k}}{\partial A_{nj}} \right) \\ &= \sum_k \left(\frac{\partial E}{\partial net_{(n+1)k}} \right) \cdot \left[\frac{\partial}{\partial A_{nj}} \left(\sum_i \sum_{m=1}^p W_{kim} \cdot A_{ni}^m - \theta_k \right) \right]. \\ &= \sum_k \left(\frac{\partial E}{\partial net_{(n+1)k}} \right) \cdot \left[\sum_{m=1}^p m \cdot W_{kjm} \cdot A_{nj}^{(m-1)} \right] \end{aligned} \quad (2-30)$$

Let $\frac{\partial E}{\partial net_{nk}} = -\delta_{nk}$ be the error signal of neuron k in n -th layer, $\frac{\partial E}{\partial net_{(n+1)k}} = -\delta_{(n+1)k}$ can

be deduced and (2-30) can be rewritten as

$$\frac{\partial E}{\partial A_{nj}} = -\sum_k \delta_{(n+1)k} \cdot \left[\sum_{m=1}^p m \cdot W_{kjm} \cdot A_{nj}^{(m-1)} \right]. \quad (2-31)$$

Furthermore, according to (2-27), the deviation in (2-25) can be rewritten as

$$\frac{\partial E}{\partial W_{jim}} = -\delta_{nj} \cdot A_{(n-1)i}^m. \quad (2-32)$$

By (2-24) and (2-32),

$$\Delta W_{jim} = -\eta \cdot \frac{\partial E}{\partial W_{jim}} = \eta \cdot \delta_{nj} \cdot A_{(n-1)i}^m \quad (2-33)$$

Similarly, the following equation can be obtained

$$\Delta \theta_j = -\eta \cdot \delta_{nj}, \quad (2-34)$$

where $\Delta \theta_j$ is the update quantity of θ_j .

From the above deductions, there are two possible cases:

- (1) If W_{jim} is between the output layer and its anterior layer (a hidden layer), (2-27), (2-28), and (2-29) can be applied to (2-26),

$$\frac{\partial E}{\partial W_{jim}} = -(T_j - A_{nj}) \cdot f'(net_{nj}) \cdot A_{(n-1)i}^m \quad (2-35)$$

After comparing (2-32) and (2-35), we can obtain

$$\delta_{nj} = (T_j - A_{nj}) \cdot f'(net_{nj}) \quad (\text{for output layer}). \quad (2-36)$$

- (2) If W_{jim} is between a hidden layer and its anterior layer (a hidden layer or the input layer), (2-27), (2-28), and (2-31) can be applied to (2-26),

$$\frac{\partial E}{\partial W_{jim}} = \left[-\sum_k \delta_{(n+1)k} \cdot \left(\sum_{m=1}^p m \cdot W_{kjm} \cdot A_{nj}^{(m-1)} \right) \right] \cdot f'(net_{nj}) \cdot A_{(n-1)i}^m \quad (2-37)$$

The following equation can be obtained from comparing equations (2-32) and (2-37)

$$\delta_{nj} = \left[\sum_k \delta_{(n+1)k} \cdot \sum_{m=1}^p m \cdot W_{kjm} \cdot A_{nj}^{(m-1)} \right] \cdot f'(net_{nj}) \quad (\text{for hidden layer}). \quad (2-38)$$

In this work, a unipolar sigmoid function is used to the transfer function of a neuron.

The first derivative of the unipolar sigmoid function can be represented as the terms of itself, as shown in (2-19) and (2-20).

$$f(net_{nj}) = \frac{1}{1 + e^{-net_{nj}}}, \quad (2-19)$$

$$f'(net_{nj}) = \frac{e^{-net_{nj}}}{(1+e^{-net_{nj}})^2} = \frac{1}{1+e^{-net_{nj}}} \cdot \left(1 - \frac{1}{1+e^{-net_{nj}}}\right)$$

$$= f(net_{nj}) \cdot [1 - f(net_{nj})] = A_{nj} \cdot (1 - A_{nj}), \quad (2-20)$$

By such representation, (2-36) and (2-38) can be rewritten as (2-39) and (2-40).

$$\delta_{nj} = (T_j - A_{nj}) \cdot A_{nj} \cdot (1 - A_{nj}) \quad (\text{for output layer}), \quad (2-39)$$

$$\delta_{nj} = \left[\sum_k \delta_{(n+1)k} \cdot \left(\sum_{m=1}^p m \cdot W_{kjm} \cdot A_{nj}^{(m-1)} \right) \right] \cdot A_{nj} \cdot (1 - A_{nj}) \quad (\text{for hidden layer}). \quad (2-40)$$

Referring to the traditional MLP/BP neural network and the generalized MLP/BP neural network, we make comparisons between (2-16) and (2-36); (2-18) and (2-38); (2-21) and (2-39); (2-22) and (2-40). The generalized MLP/BP neural network is actually equivalent to the traditional MLP/BP neural network when $m=1$, indicating that the traditional method is a special case of the proposed model. Thus the new approach being presented is a generalized model. Moreover, the network configuration of this scheme has more degrees of freedom than the traditional one.

Because the summation function of the GMLP/BP neural networks is a multivariate power series (nonlinear function), the boundaries of neighbors become either nonlinear or piecewise nonlinear. As the nonlinear summation function within each neuron is materialization in each layer of the GMLP/BP neural networks, the proposed approaches present continuous nonlinear pattern space mapping potential. Theoretically, increases of the summation function order and the number of neurons can achieve better approximation to fit a nonlinear system. Therefore, the proposed scheme will have more flexibility and better performance than traditional MLP/BP neural networks do.

Similar to the traditional approach, the training procedure of this GMLP/BP neural network attains different performance by varying initial conditions, learning rates,

network parameters or summation function orders. Moreover, designers could perform numerous independent training runs and select the most suitable result as the final solution.

Generally, the order of the fitting function is equal to or less than that of the target function. In most cases, the target function is complex or even unknown, and the best fitting function order is determined by experimentation or experience. To simplify the problem, the fitting function order is selected as low as possible while the error is set to be less than the maximum tolerable bound. In general, the order of the most approximation system is equal to or less than three; however, in high performance systems or special applications, the order may be higher. In algebraic, this new approach extends the traditional scheme from the first order approximation to infinity. The most suitable summation function order of this scheme can be determined by computer simulations for different applications.

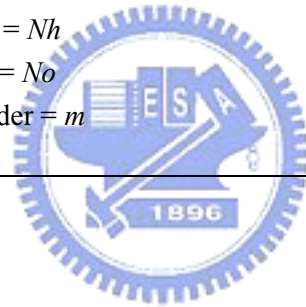


2-3 Complexity Analysis

Because the order of the neuron of the generalized MLP/BP neural networks is more than one, it is necessary to generate the power terms for the inputs in each layer. In addition, the training algorithm of the generalized MLP/BP neural networks is modified from “generalized delta-learning rule”. The complexity and cost of the generalized MLP/BP neural networks will be higher than the traditional MLP/BP neural networks but the former results in better pattern space separability and better performance. The comparison of computational complexity in terms of additions, multiplications and sigmoid function substitution between the traditional MLP/BP neural networks and the generalized MLP/BP neural networks is shown in Table 2-1.

Table 2-1: The comparison of computational complexity.

Operation	MLP/BP neural networks (Single Hidden Layer)	GMLP/BP neural networks (Single Hidden Layer)
Addition	$(N_i + 1) \cdot N_h + (N_h + 1) \cdot N_o$	$(m \cdot N_i + 1) \cdot N_h + (m \cdot N_h + 1) \cdot N_o$
Multiplication	$N_i \cdot N_h + N_h \cdot N_o$	$(2m - 1) \cdot N_i \cdot N_h + m \cdot N_h \cdot N_o$
Function Substitution	$N_h + N_o$	$N_h + N_o$
<p>Notations: Input Neuron Number = N_i Hidden Neuron Number = N_h Output Neuron Number = N_o Summation Function Order = m</p>		

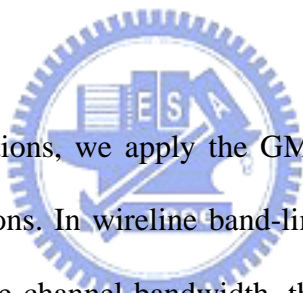




CHAPTER 3

SISO GMLP/BP-based DFEs

for Wireline Applications



For wireline communications, we apply the GMLP/BP-based channel equalization schemes to different applications. In wireline band-limited channels that the data rate is about ten times as much as the channel bandwidth, the traditional MLP/BP-based DFEs provide better performance, tolerate more sampling clock skew, and permit larger channel response variance than LMS DFEs. Because the frequency response of a wireline band-limited channel is without spectral nulls, the high order approximation has no benefit. The first order ones can satisfy the system requirements. However, the traditional MLP/BP-based DFEs are not good enough for the severe ISI channels with nonlinear distortions. The frequency responses of severe ISI channels contain spectral nulls and nonlinear distortions lead to worse situations. In such channels, the generalized MLP/BP-based DFEs can outperform the traditional MLP/BP-based DFEs that do better than the LMS DFEs.

This chapter is organized as follows. The traditional MLP/BP-based DFEs with high

skew tolerance for wireline band-limited channels are presented at the beginning. Afterward, the GMLP/BP-based DFEs for wireline severe ISI channels are proposed.

3-1 MLP/BP-based DFEs with High Skew Tolerance for Band-limited Channels

A traditional MLP/BP neural network is realized as a waveform equalizer for distorted nonreturn-to-zero (NRZ) data recovery in band-limited channels. Moreover, the proposed approach can tolerate sampling clock skew and channel response variance. According to simulation results, the proposed design can recover severe distorted NRZ data with better performance than LMS DFEs in the band-limited channel that the data rate is about ten times as much as the channel bandwidth. Under the 20% channel response variance and the 30% sampling clock skew, the MLP/BP-based DFE can provide an acceptable performance. By fixed-point simulations, the proposed scheme is realizable and outperforms the LMS DFE. Further, the internal resolution enhancement technique provides a better compromise between cost and performance.

This section is organized as follows. The system overview is presented in subsection 1 while subsection 2 shows the MLP/BP-based DFEs. Afterward, the simulation results show in subsection 3. Finally, we make a brief summary in subsection 4.

3-1-1 System Overview

In practice circuits of wireline communications, the channel characteristic of different interconnect paths of parallel data I/O channels are different but analogous.

Besides, sampling clock skew makes the problem more severely. In such conditions, the received signal is deteriorated substantially by intersymbol interference, clock skew and background noise. The system diagram of a single clock source is shown in Fig. 3-1.

If the data rate of transmitted signals is higher than the channel capacity, the received signal pulse is unable to complete its transition within a symbol interval. The equivalent model for the wireline band-limited channels is shown in Fig. 3-2 where a finite impulse response (FIR) filter is used to model the ISI channel response with the AWGN as the background noise.

The ISI channel response with AWGN can be written as follows:

$$H(z) = f_0 + f_1 \cdot z^{-1} + f_2 \cdot z^{-2} + \dots + f_L \cdot z^{-L}, \quad (3-1)$$

$$y_k = \sum_{i=0}^L f_i \cdot x_{k-i}, \quad (3-2)$$

$$\hat{y}_k = y_k + n, \quad (3-3)$$

where $H(z)$ is the transfer function of the ISI channel; L is the length of the channel response; x_k is the input sequence; y_k is the channel output which is warped by ISI only; n_k is the AWGN; \hat{y}_k is the received signal which is distorted by both ISI and AWGN.

In this work, several wireline band-limited parallel I/O channels that consist of analogous channel responses and different sampling clock skews are used to verify the proposed approaches. Their transfer functions with different F_{3dB}/F ratio are shown in Table 3-1. The frequency responses of these channels are illustrated in Fig. 3-3. These frequency responses are without spectral nulls. Base on foregoing channels, clock skews between +/- 30% are considered to represent a worse situation of the practical wireline high-speed communications.

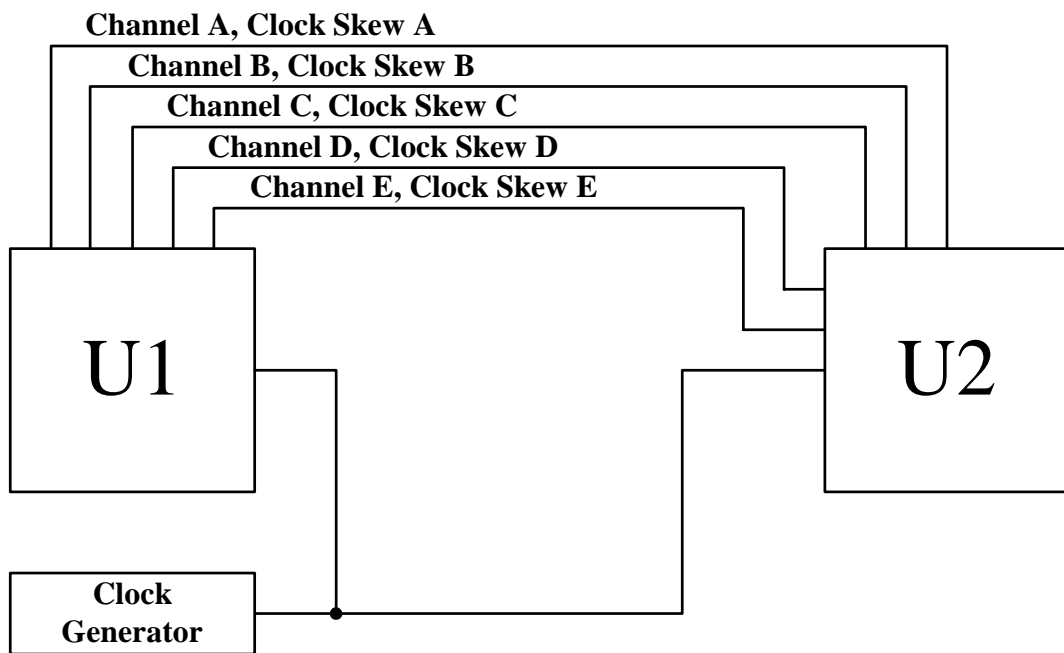


Fig. 3-1: System diagram.

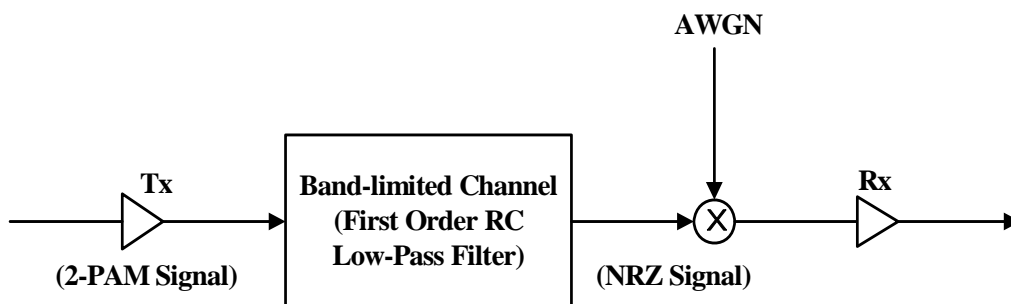


Fig. 3-2: Equivalent model for the band-limited channels.

Table 3-1: Transfer functions of several wireline band-limited channels.

ID	F_{3dB}/F	Channel Impulse Response
1	0.08	[0.3951 0.2390 0.1446 0.0875 0.0529]
2	0.09	[0.4319 0.2454 0.1394 0.0792 0.0450]
3	0.10	[0.4665 0.2489 0.1328 0.0708 0.0378]
4	0.11	[0.4990 0.2500 0.1252 0.0627 0.0314]
5	0.12	[0.5295 0.2491 0.1172 0.0551 0.0259]

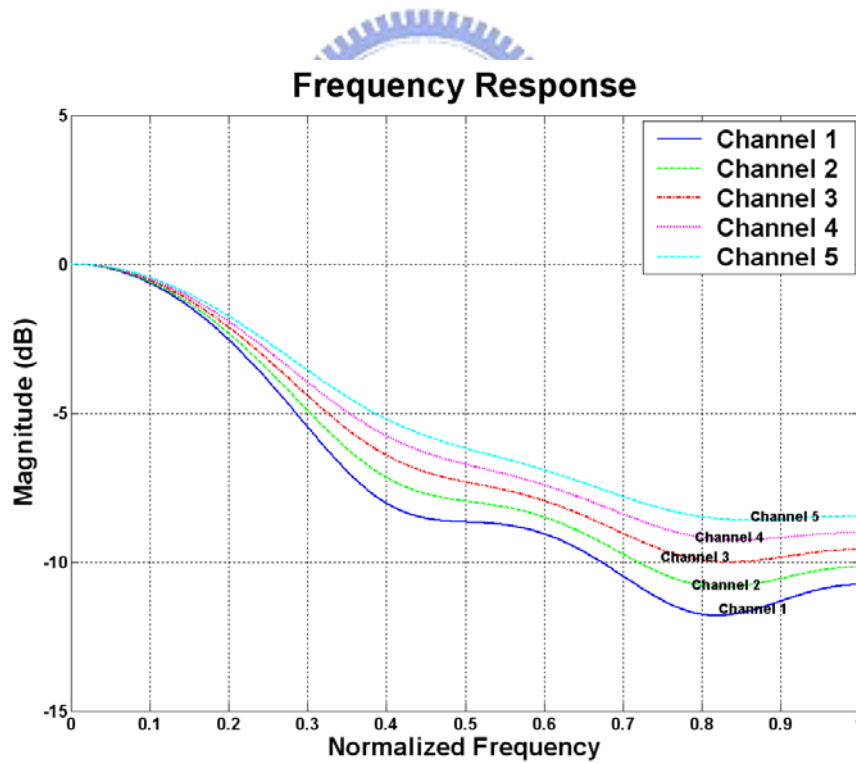


Fig. 3-3: Frequency responses of several similar wireline band-limited channels.

3-1-2 MLP/BP-based DFEs

The block diagram of the MLP/BP-based DFEs is shown in Fig. 3-4. This MLP/BP-based DFE is the single hidden layer MLP architecture. The inputs of the MLP/BP-based DFE consist of feed-forward signals, which come from the input symbols by a tapped-delay-line register, and feedback signals, which come from previous decisions by another tapped-delay-line register.

We evaluate different tap numbers in the forward part and the feedback part of the equalization schemes and select the most suitable arrangement. In this work, all equalization schemes have 11 symbols in the forward part and 5 symbols in the feedback part. The number of neurons in the input layer is equal to 16. The MLP/BP-based DFEs uses the single hidden layer MLP architecture. The number of neurons in the hidden layer is 2 times of that in the input layer. Since all the proposed equalization schemes have a single output, the number of neurons in the output layer is equal to 1.

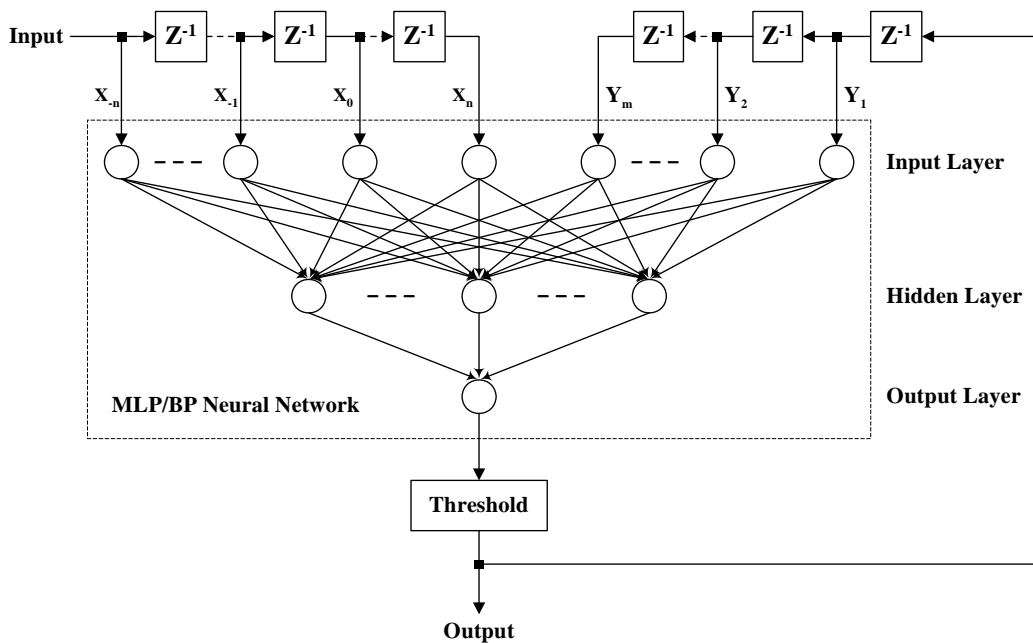


Fig. 3-4: MLP/BP-based DFEs.

3-1-3 Simulation Results

The performance of the MLP/BP-based DFE is evaluated through the simulations for the distorted NRZ signal recovery in the band-limited channel that the data rate is ten times of the channel bandwidth. In this section, a regular input pattern configuration of the equalization schemes is presented first followed by the modified configuration. At last, the fixed-point simulations and its enhancement are discussed in detail.

3-1-3-1 Regular Configuration

Because the MLP/BP neural networks are supervised learning, a training set includes an input vector and a desired output vector. The training patterns must represent the system characteristic as exact as possible. Suitable training patterns can improve the training quality. In wireline applications, we can select a longer training set to achieve better performance.

In the training procedure, the length of the training set is equal to 10^4 symbols and the total training epochs are 10^2 . The two-phase learning is used with the learning rate of 0.5 when the mean square error of the training set is larger than 10^{-3} , and the learning rate of 0.125, otherwise. When the training epochs exceed eighty percent of the total epochs, the best parameters will be recorded to achieve the lowest mean square error of the training set in the last twenty percent of the training epochs. Hence the steady-state training results can be recognized. In fact, the simulations indicate no unstable problems as all training processes are converged.

Because different initial conditions lead to different effects, the non-training evaluation set that has 10^5 symbols is used to examine the training quality of numerous independent simulation outcomes. After numerous independent training and evaluation

runs, those yielding better outcomes will be chosen to perform a long trial with the test set, and then the best one will be the final test result. We execute fifty independent runs and select the best one as the final result. The length of the test set is 10^6 symbols, and the evaluation set is a subset of it.

At first, we follow the regular input pattern configuration of the equalizers. A band-limited channel (Channel 3) described by the transfer function, $H_3=0.4665 + 0.2489z^{-1} + 0.1328z^{-2} + 0.0708z^{-3} + 0.0378z^{-4}$, is used to estimate the system performance of the LMS DFE and the MLP/BP-based DFE, where the training noise and the evaluation noise are assumed to be SNR=20dB, and SNR of the test signal is between 10dB and 25dB. This channel response indicates that the data rate is ten times of the channel bandwidth.

Subsequently, several different band-limited ISI channels (Channels 1, 2, 4, and 5) are used to describe different channel bandwidth vs. data rate ratios that the data rates are eight, nine, eleven, and twelve times the channel bandwidth, respectively. The training result of Channel 3 is applied to these channels, directly. These experiments are used to evaluate the tolerance under different channel response variances. The BER performance for the LMS DFE and the MLP/BP-based DFE in different channels is shown in Fig. 3-5. The proposed approach can outperform the LMS DFE.

At last, -30%, -20%, -10%, +10%, +20%, and +30% sampling clock skews are considered, respectively. Similarly, the training result of Channel 3 is applied to these situations, directly. The comparisons of the BER performance for the LMS DFE and the MLP/BP-based DFE in different channels with different clock skews are shown in Fig. 3-6, Fig. 3-7 and Fig. 3-8, respectively.

The advantage of the proposed approach can be represented in Fig. 3-9. In view of different channel response variances without sampling clock skew at SNR=20dB, the

BER performance of the LMS DFE and the BPN DFE is shown in Fig. 3-9 (a). Considering different clock skews in different channels at SNR=20dB, the comparisons of the BER performance for the LMS DFE and the BPN DFE are shown in Fig. 3-9 (b) to Fig. 3-9(f).

From these simulation results, the proposed approach reports better BER performance under +/- 20% channel response variances and +/- 30% sampling clock skews. With $F_{3dB}/F=0.08$ at $BER=10^{-3}$, the LMS DFE endure about +5% / -8% sampling clock skews and the proposed approach can tolerate over +/- 15%. With $F_{3dB}/F=0.10$, the LMS DFE endure about +13% / -20% and the proposed approach tolerate over +/- 20%. With $F_{3dB}/F=0.12$, the LMS DFE endure about +15% / -25% and the proposed approach tolerate over +20 % / -25%. As the variances increase, the proposed approach achieves more improvement over the LMS DFEs.

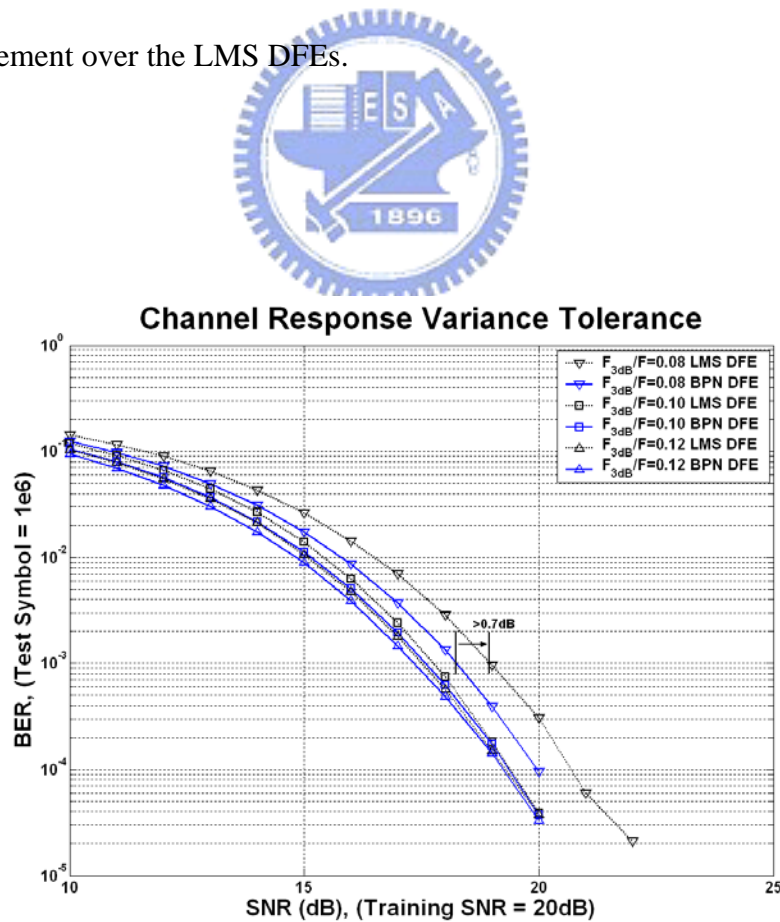


Fig. 3-5: BER performance for different types of equalizers in different channels.

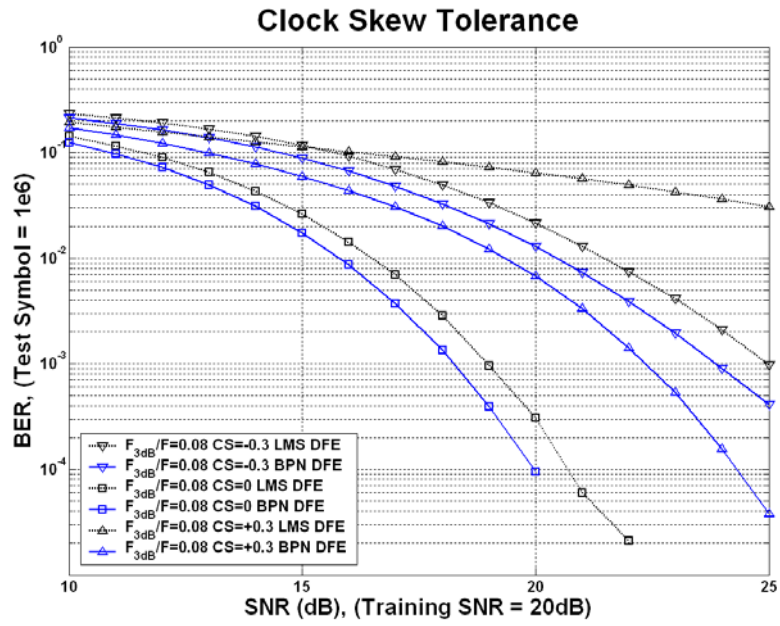


Fig. 3-6: BER performance for different types of equalizers with different clock skews in Channel 1.

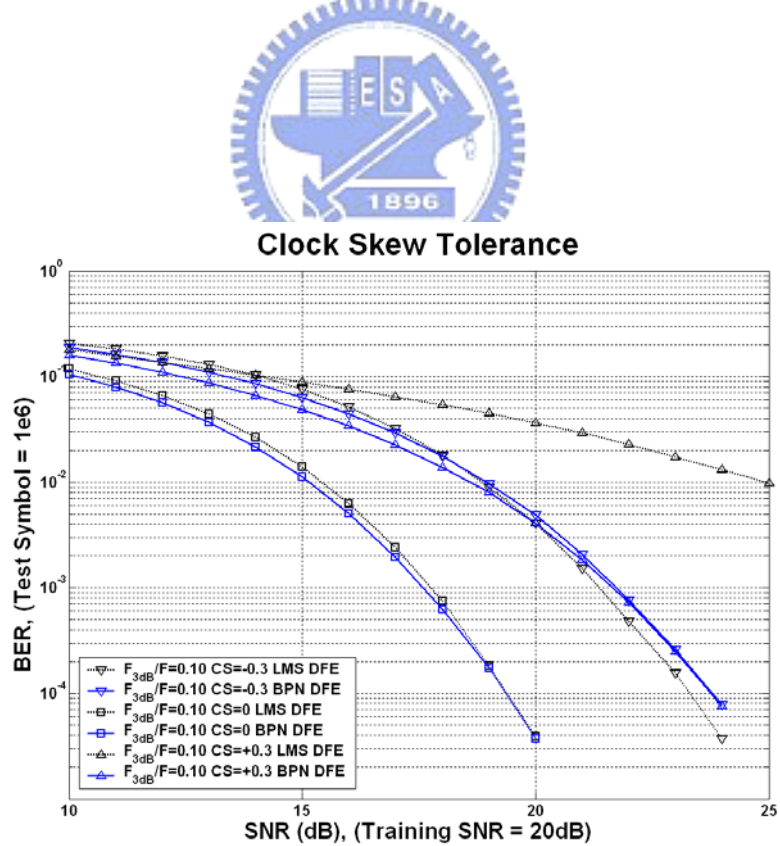


Fig. 3-7: BER performance for different types of equalizers with different clock skews in Channel 3.

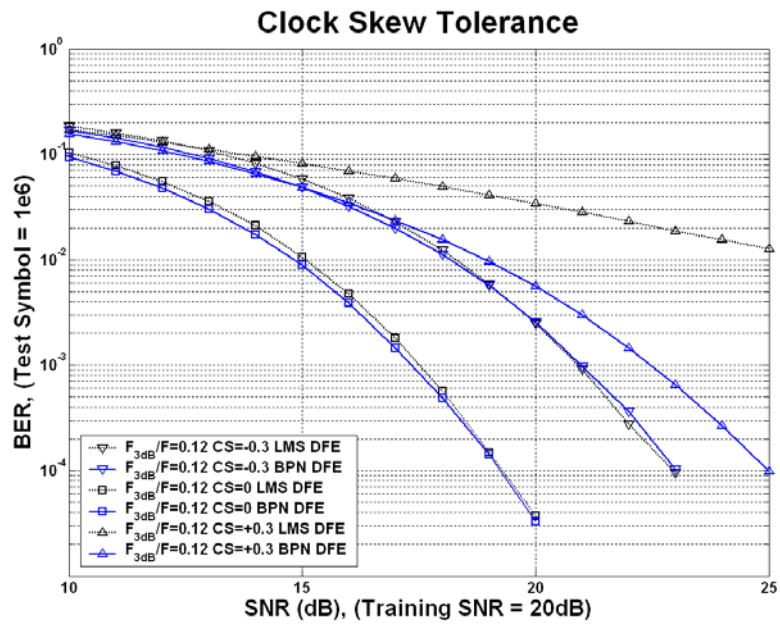


Fig. 3-8: BER performance for different types of equalizers with different clock skews in Channel 5.

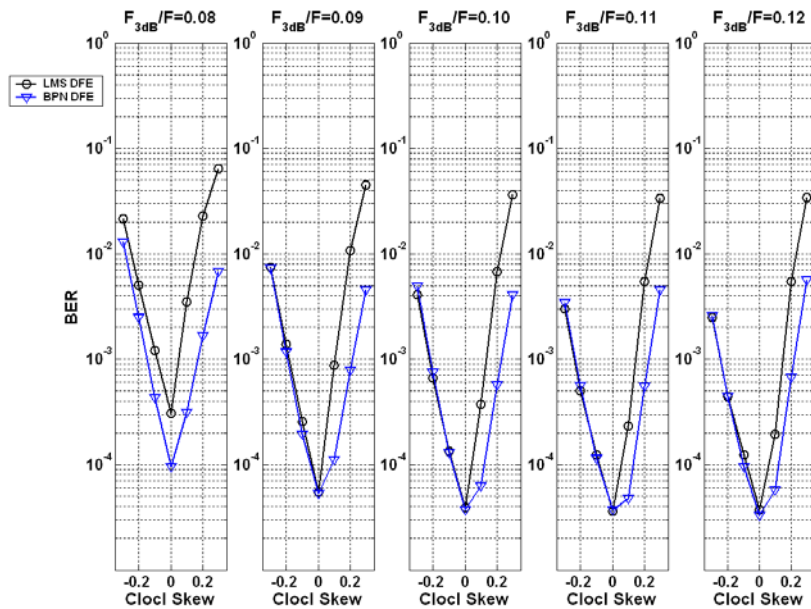


Fig. 3-9: BER performance for different channel conditions with regular input pattern configuration at SNR=20dB.

3-1-3-2 Modified Configuration

Because the input patterns relate with the training quality and the overall performance, we modify the input pattern configuration that contains more variance by using Channel 1, Channel 3, and Channel 5 with and without +/- 10 percent sampling clock skews to generate the training patterns. By this way, the MLP/BP neural network can provide better fault tolerant capability. The simulation results are shown in Fig. 3-10. From Fig. 3-9 and Fig. 3-10, the modified input pattern configuration can improve the overall performance.

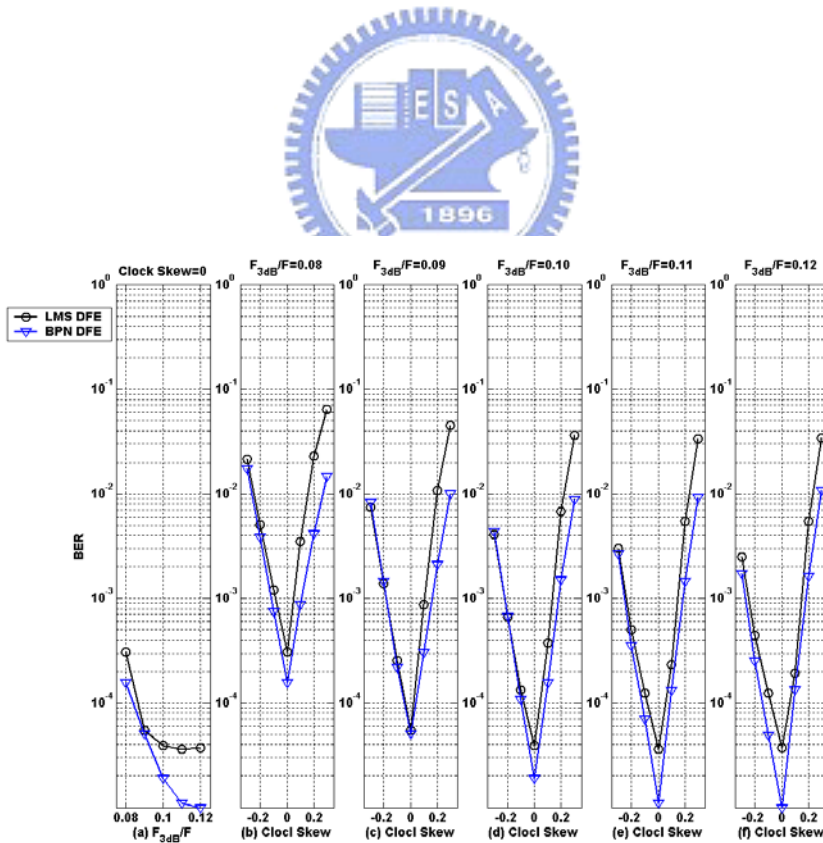


Fig. 3-10: BER performance for different channel conditions with modified input pattern configuration at SNR=20dB.

3-1-3-3 Fixed-Point Simulations

In this subsection, the fixed-point simulations and its enhancement of the MLP/BP-based DFE are presented. In general, higher ADC resolution leads to better performance and higher cost. It is a trade-off problem. We consider that added internal resolution to increase the performance under the same ADC resolution. By this way, we can use a lower resolution ADC to replace a higher resolution one and obtain a similar performance.

In the fixed-point simulations, we use a hard limiter to replace the log-sigmoid function for low cost consideration. The performance of the MLP/BP neural network should be decreased. The training results of the modified configuration are applied to the fixed-point simulations.

The BER performance for different ADC resolution at SNR=15, SNR=18, and SNR=20 are shown in Fig. 3-11. A BER performance comparison with different ADC resolution is shown in Fig. 3-12. The BER performance for different ADC resolution and different internal resolution at SNR=20 are shown in Fig. 3-13.

The BER performance for the LMS DFE and the MLP/BP-based DFE in different channels is shown in Fig. 3-14. The fixed-point simulation comparison for the MLP/BP-based DFE in Channel 3 with different clock skews is shown in Fig. 3-15. The BER performance for different channel conditions with modified input pattern configuration under different resolution at SNR=20dB is shown in Fig. 3-16.

From Fig. 3-11, the acceptable ADC resolution is five or six bits. From Fig. 3-13, the most suitable combination is five bits ADC with ten bits internal resolution. This internal resolution enhancement technique can provide better performance under the same ADC resolution. In the fixed-point simulations, the performance of the proposed equalizer is better than the LMS DFE.

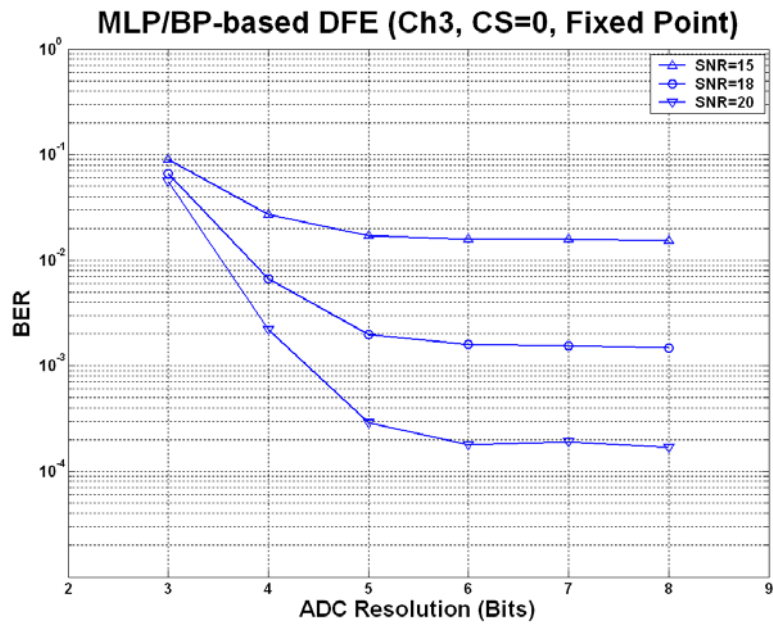


Fig. 3-11: BER performance for different ADC resolution at SNR=15, SNR=18, and SNR=20.

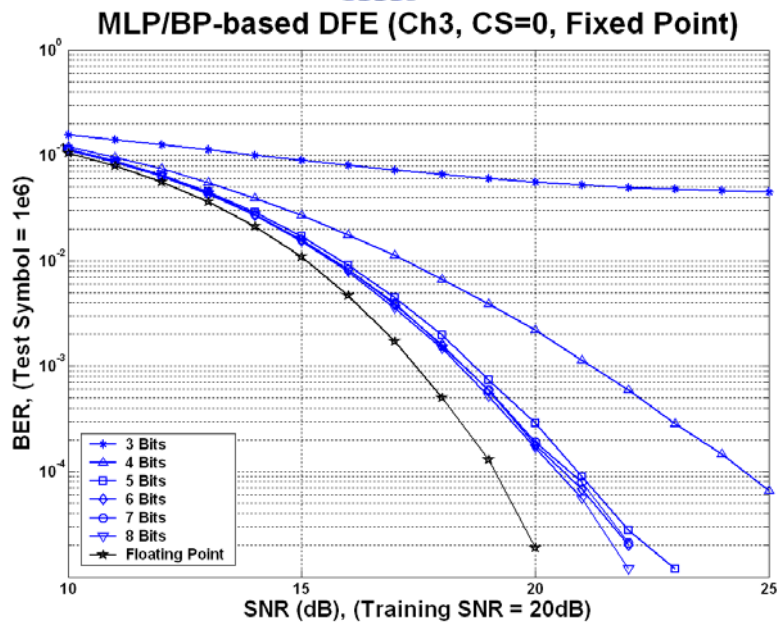


Fig. 3-12: BER performance with different ADC resolution.

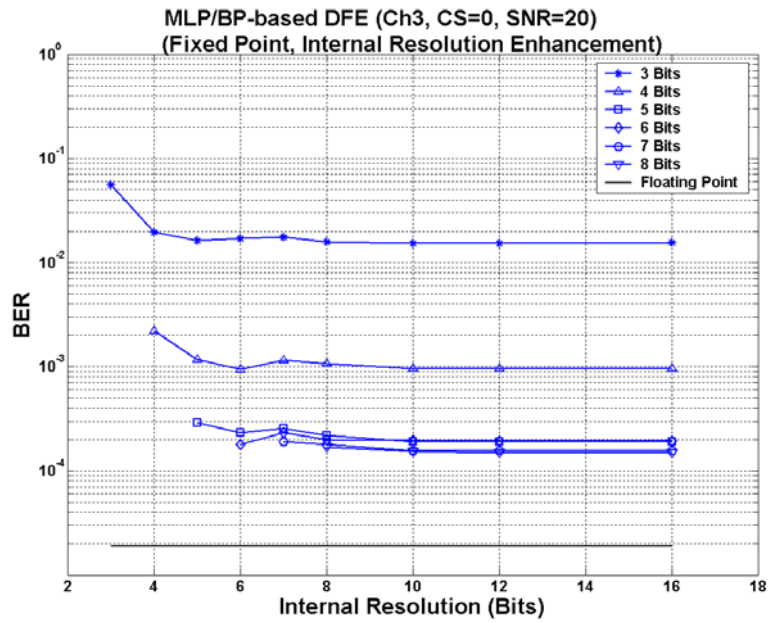


Fig. 3-13: BER performance for different ADC resolution with internal resolution enhancement.

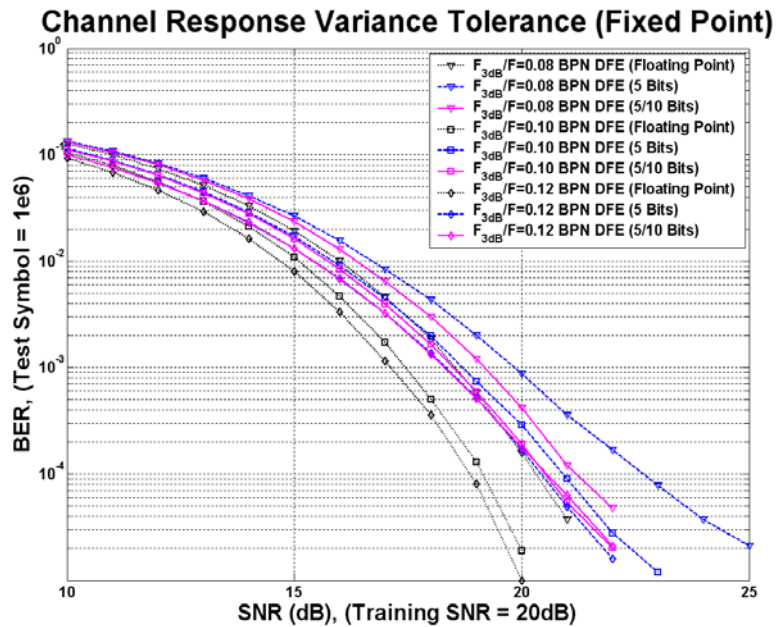


Fig. 3-14: BER performance for different types of equalizers in different channels.

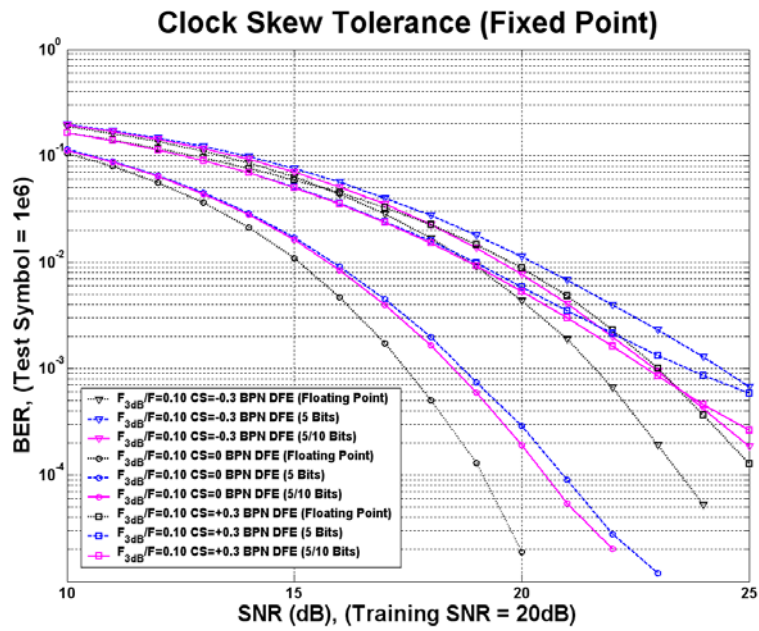


Fig. 3-15: BER performance for different types of equalizers with different clock skews in Channel 3.

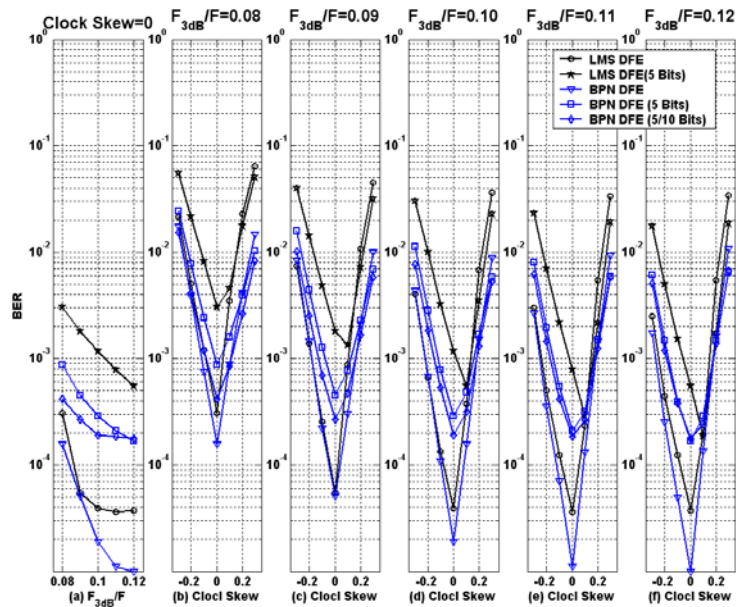


Fig. 3-16: BER performance for different channel conditions with modified input pattern configuration at SNR=20dB.

3-1-3 Summary

The simulation results show that the proposed approach reports better BER performance under +/- 20% channel response variances with +/- 30% sampling clock skews in the band-limited channels that the data rate is about ten times of the channel bandwidth. With different channel responses at $BER=10^{-3}$, the comparison of sampling clock skew tolerance between the LMS DFEs and the MLP/BP-based DFEs is shown in Tab. 3-2. Because the proposed approach can tolerate more clock skews and large channel response variances, the clock tree design and data interconnection planning can be simplified. For low cost considerations, we can use a preset equalizer to replace an adaptive one.

In the fixed-point simulations, the proposed equalizer is realizable and outperforms the LMS DFE. Further, the internal resolution enhancement technique makes the proposed scheme with a better compromise between cost and performance. By the fixed-point simulations, the most suitable combination is five bits ADC with ten bits internal wordlength.

However, the performance of the traditional MLP/BP-based DFEs is not good enough for the severe ISI channels with nonlinear distortions. The frequency responses of severe ISI channels contain spectral nulls and nonlinear distortions lead to worse situations. For such channels, we propose the generalized MLP/BP-based DFEs for better performance and show the details in next section.

Table 3-2: The comparison of sampling clock skew tolerance.

ID	F_{3dB}/F	LMS DFEs	MLP/BP-based DFEs
1	0.08	+5% / -8%	+11% / -12%
2	0.09	+11% / -18%	+17% / -18%
3	0.10	+13% / -20%	+20% / -20%
4	0.11	+14% / -22%	+20% / -23%
5	0.12	+15% / -25%	+20% / -25%

Simulation Conditions for MLP/BP-based DFEs:
 Input Neural Number = 16 (Forward part: 11, and Feedback part: 5),
 Hidden Neural Number = 32 (Hx=2),
 Output Neural Number = 1,
 Training Set = 10^4 symbols,
 Evaluation Set = 10^5 symbols,
 Test Set = 10^6 symbols,
 Training Epoch = 10^2 ,
 Learning Rate = 0.5 / 0.125 (Two Phase Learning, MSE Bound = 10^{-3}),
 Re-training Times = 10 Independent Runs.

3-2 GMLP/BP-based DFEs for Severe ISI Channels

Based on the MLP/BP neural network, we suggest a general model that uses a multivariate power series as the summation function of the MLP/BP neural networks. For more effective data transmissions, this new neural-based channel equalizer is proposed to compensate for severe ISI and nonlinear distortions in wireline applications. As compared with LMS DFE and the traditional MLP/BP-based DFE under the severe ISI channel, simulation results show that the GMLP/BP-based DFE can improve about 2dB and 1dB without nonlinearity at $BER=10^{-4}$, and improve about 4dB and 1dB with 30% signal

truncation at $\text{BER}=10^{-3}$.

This section is organized as follows. The severe ISI channels with nonlinearity are presented in subsection 1. Subsection 2 shows the proposed GMLP/BP-based DFEs. Afterward, the simulation results show in subsection 3. Finally, we make a summary in subsection 4.

3-2-1 Severe ISI Channels and Nonlinear Distortions

In wireline band-limited channels, the traditional MLP/BP-based DFEs provide better performance, tolerate sampling clock skew, and permit channel response variance. However, the traditional MLP/BP-based DFEs are not good enough for the severe ISI channels with nonlinear distortions. In this work, we consider the possible situation in wireline applications, for example ATA-like interface, USB-like interface, Ethernet, etc. Such applications use pulse amplitude modulation schemes that may suffer severe ISI channels with nonlinearity. Therefore, we simulate the practical wireline environments.

The description of the equivalent channel model for wireline digital transmission systems is shown in Fig. 3-17. In this model, a finite impulse response (FIR) filter is used to model the ISI channel response with the AWGN as the background noise. When a nonlinear distortion is introduced, a piecewise linear approximation or a Volterra series will be utilized to represent the nonlinearity.

The severe ISI channel response with AWGN can be written as follows:

$$H(z) = f_0 + f_1 \cdot z^{-1} + f_2 \cdot z^{-2} + \dots + f_L \cdot z^{-L}, \quad (3-1)$$

$$y_k = \sum_{i=0}^L f_i \cdot x_{k-i}, \quad (3-2)$$

$$\hat{y}_k = y_k + n, \quad (3-3)$$

where $H(z)$ is the transfer function of the ISI channel; L is the length of the channel

response; x_k is the input sequence; y_k is the channel output which is warped by ISI only; n_k is the AWGN; \hat{y}_k is the received signal which is distorted by both ISI and AWGN.

The mathematical describe of the severe ISI channels are same to that of the band-limited channels. Moreover, a piecewise linear approximation is used to represent the nonlinear distortion. In a receiver, the output saturation characteristics of non-ideal amplifiers due to the AGC loss, can be expressed by:

$$\tilde{y}(n) = \begin{cases} +V_H & , \text{if } \hat{y}(n) > +V_H \\ -V_L & , \text{if } \hat{y}(n) < -V_L \\ \hat{y}(n) & , \text{otherwise} \end{cases} \quad (3-4)$$

where V_H and V_L represent the saturation values and are considered to be equal because of the symmetrical characteristics of most real amplifiers.

In practical communication circuits, the accuracy of AGC relates to the problem of nonlinearity. If the AGC is perfect, the nonlinear distortion due to non-ideal amplifiers will not occur. Under this ideal condition, the circuits work at the linear region of the characteristic curve of practical amplifiers and the amplifiers can be regarded as ideal ones. However, in practical situations, the AGC is not perfect. When the AGC loss presents, the gain of amplifiers becomes too large, and the output signal is truncated. In this work, we use the hard-limiter to model the output characteristic of real amplifiers. This corresponds to the worst situation of practical communication circuits.

In this section, several different ISI channels, with or without deep nulls of frequency response, are used to verify the proposed approaches. These channels are practical in many wireline communication systems, whose transfer functions of ISI channels with normalized power are shown in Table 3-3. Their frequency responses are illustrated in Fig. 3-18. The transmitted signal is expected to be deteriorated substantially by the ISI channel, the AWGN, and the nonlinearity. The comparison of the transmitted data and the received waveform is shown in Fig. 19.

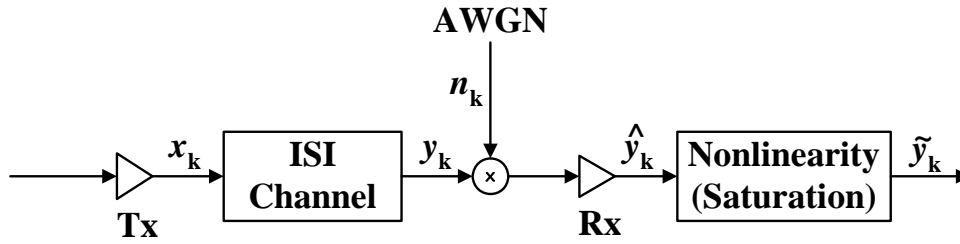


Fig. 3-17: Equivalent model for the severe ISI channels.

Table 3-3: Transfer functions of different wireline severe ISI channels.

Channel ID	Transfer Function
I	$H_1(z) = 0.4575 + 0.7625z^{-1} + 0.4575z^{-2}$ (0.6, 1.0, 0.6)
II	$H_2(z) = 0.408 + 0.816z^{-1} + 0.408z^{-2}$ (0.5, 1.0, 0.5)
III	$H_3(z) = 0.3482 + 0.8704z^{-1} + 0.3482z^{-2}$ (0.4, 1.0, 0.4)
IV	$H_4(z) = 0.227 + 0.460z^{-1} + 0.688z^{-2} + 0.460z^{-3} + 0.227z^{-4}$ (0.33, 0.67, 1.0, 0.67, 0.33)
V	$H_5(z) = 0.108 + 0.215 z^{-1} + 0.430 z^{-2} + 0.717 z^{-3} + 0.430 z^{-4} + 0.215 z^{-5} + 0.108z^{-6}$ (0.15, 0.3, 0.6, 1.0, 0.6, 0.3, 0.15)
VI	$H_6(z) = 0.147 + 0.295 z^{-1} + 0.590 z^{-2} + 0.295 z^{-3} + 0.590 z^{-4} + 0.295 z^{-5} + 0.147z^{-6}$ (0.25, 0.5, 1.0, 0.5, 1.0, 0.5, 0.25)
VII	$H_7(z) = 0.226 + 0.516 z^{-1} + 0.645 z^{-2} + 0.516 z^{-3}$ (0.35, 0.8, 1.0, 0.8)

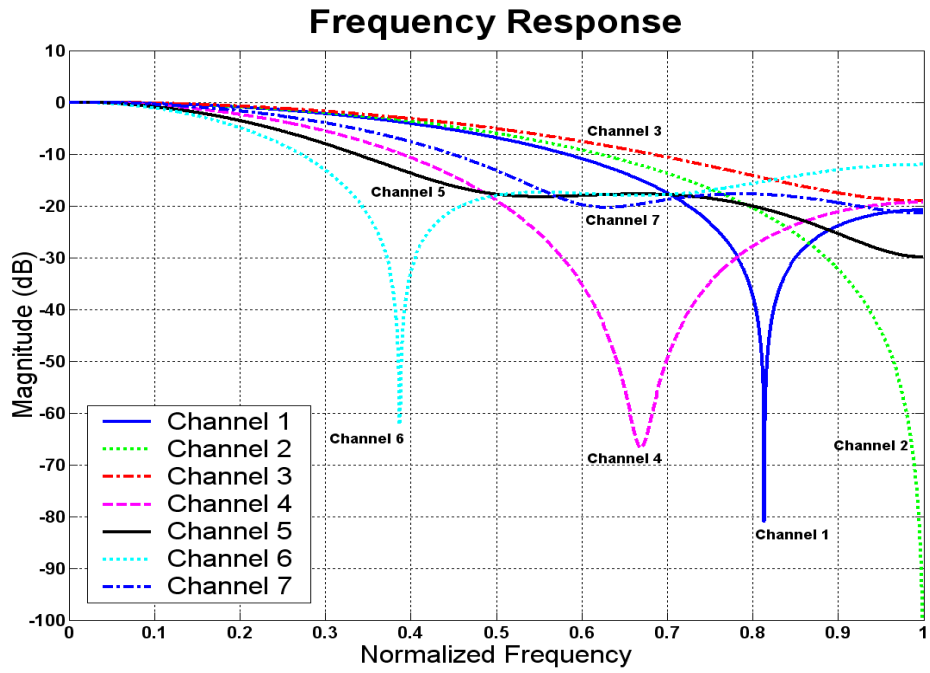


Fig. 3-18: Frequency responses of different severe ISI channels.

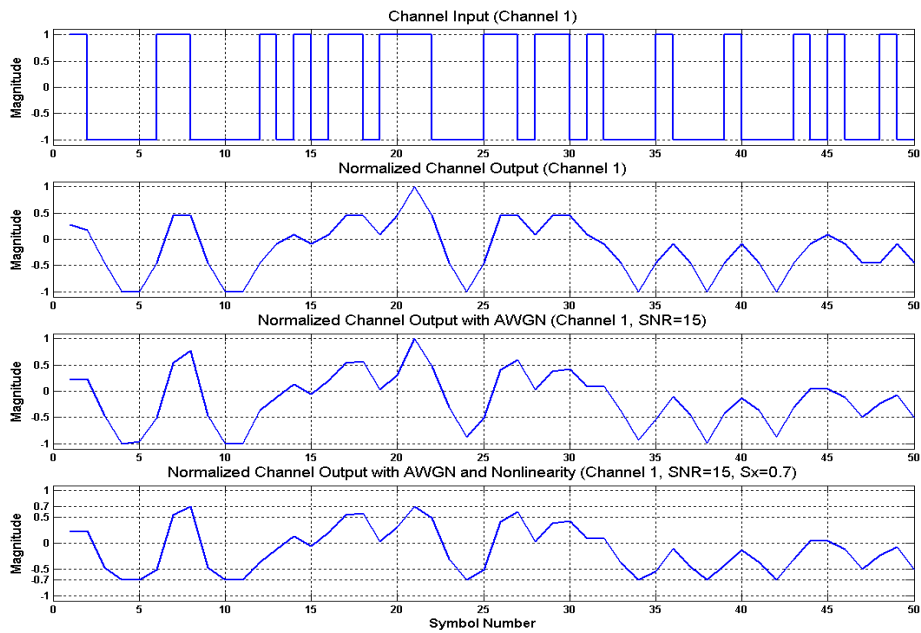


Fig. 3-19: The comparison of the transmitted data and the received waveform.

3-2-2 *GMLP/BP-based DFEs*

The block diagram of the generalized MLP/BP-based DFEs is shown in Fig. 3-20. The inputs of the generalized MLP/BP-based DFE consist of feed-forward signals, which come from the input symbols by a tapped-delay-line register, and feedback signals, which come from previous decisions by another tapped-delay-line register. Because the order of the neuron of the generalized MLP/BP neural networks is more than one, it is necessary to generate the power terms for the inputs in each layer.

We evaluate different symbol numbers in the forward part and the feedback part of the equalization schemes and select the most suitable arrangement. In this work, all equalization schemes have 5 symbols in the forward part and the feedback part, respectively. Both the MLP/BP-based DFEs and the GMLP/BP-based DFEs use the single hidden layer MLP architecture. The number of neurons in the input layer is equal to 10. For different MLP neural network configurations, the number of neurons in the hidden layer is 0.5, 1, 2, or 4 times of that in the input layer, and denoted by “ $H_x=0.5$ ”, “ $H_x=1$ ”, “ $H_x=2$ ”, and “ $H_x=4$ ”, respectively. Since all the proposed equalization schemes have a single output, the number of neurons in the output layer is equal to 1. The summation function order of the generalized MLP/BP-based DFEs is restricted to 1-6 that is denoted by “Order 1” to “Order 6”. Furthermore, total 24 different configurations need to be evaluated.

For practical issues, the summation function order should be minimized. First, the order of the approximation function needs not to be larger than that of the real separating boundary of pattern space. The critical order is regarded as the point where the system performance has only slight improvement when the summation function order increases further as shown in simulation results. Second, a high order approximation leads to a complex and impractical architecture for current very large scale integration (VLSI)

technology. However, in light of the rapid progress of VLSI technology, more complex approaches could potentially be introduced for better performance with acceptable cost.

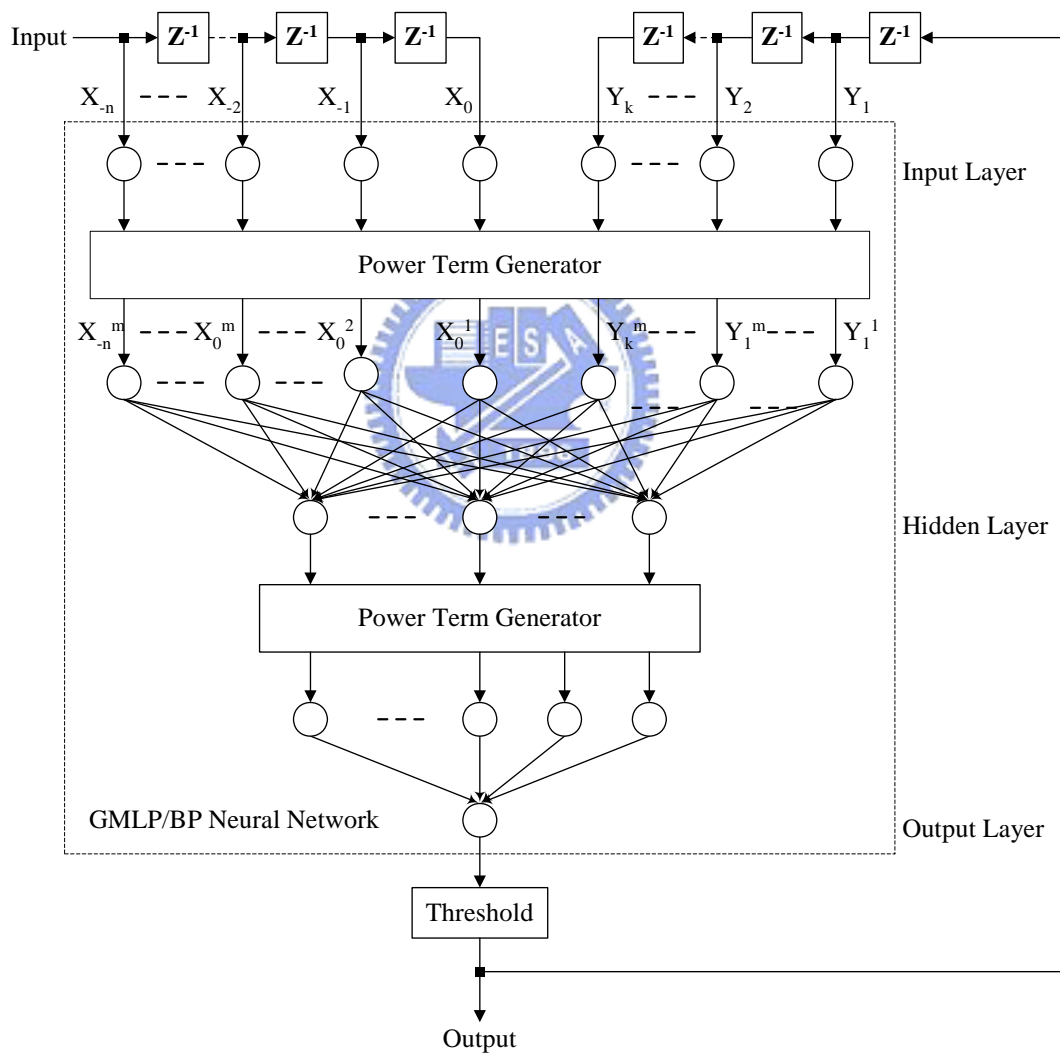


Fig. 3-20: Generalized MLP/BP-based DFEs.

3-2-3 Simulation Results

The performance of the generalized MLP/BP-based DFEs is evaluated through the simulations for the (2-PAM sequences) NRZ signal recovery in a severe ISI channel (Channel 1). The training stability for different configurations of the traditional and the generalized MLP/BP neural networks is analyzed by the standard deviation (Std) of the mean square errors (MSE) of the training and the evaluation sets in numerous independent simulations with different random initiations. In addition, different levels of the nonlinear distortions in the channel that model the circuit saturation characteristics have been considered. These include the 0%, 10%, 20%, and 30% truncations of the output swing, denoted by “ $S_x=1.0$ ”, “ $S_x=0.9$ ”, “ $S_x=0.8$ ”, and “ $S_x=0.7$ ”, respectively. Furthermore, the proposed approach is applied to compensate the distorted NRZ signals in the several different ISI channels (Channels 2, 3, 4, 5, 6 and 7) and results in a significant performance improvement.

In a training procedure, the length of the training set is equal to 10^4 symbols and the total training epochs are 10^3 . The two-phase learning is used with the learning rate of 0.5 when the mean square error of the training set is larger than 10^{-4} , and the learning rate of 0.1, otherwise. When the training epochs exceed ninety percent of total epochs, the best parameters will be recorded to achieve the lowest mean square error of the training set in the last ten percent of training epochs. Hence the steady-state training results can be recognized. In fact, the simulations indicate no unstable problems as all training processes are converged.

Because different initial conditions lead to different effects, the non-training evaluation set that has 10^5 symbols is used to examine the training quality of numerous independent simulation outcomes. After numerous independent training and evaluation runs, those yielding better outcomes will be chosen to perform a long trial with the test set,

and then the best one will be the final test result. The length of the test set is 10^7 symbols, and the evaluation set is a subset of it.

At first, a severe ISI channel (Channel 1) described by the transfer function, $H_1=0.4575 + 0.7625z^{-1} + 0.4575z^{-2}$, is used to estimate the system performance of different equalization schemes, where the training noise and the evaluation noise are assumed to be SNR=15dB, and SNR of the test signal is between 10dB and 20dB.

Considering the distortions due to ISI and AWGN only, the training stability of different configurations is estimated by the standard deviation of MSEs of both the training and the evaluation sets. For each configuration, the results are analyzed according to 50 independent simulation outcomes.

Fig. 3-21 and Fig. 3-22 show the minimum MSE and the standard deviation of MSEs of the training and the evaluation sets for different hidden neuron multipliers and different summation function orders at SNR=15dB. Note that the increase of the neuron numbers in the hidden layer can decrease both the training error and the standard deviation of MSEs of the training set which can also be improved by increasing the summation function order. Further improvements can be achieved by increasing both the neuron numbers in the hidden layer and the summation function order. However, the reciprocal advance for the evaluation set is difficult to obtain. An increase in the neuron numbers in the hidden layer can also lead to a decrease in both the training error and the standard deviation of MSEs of the evaluation set. When the summation function order is equal to 2 or 3, the evaluation error can be reduced efficiently. Beyond the order of 3 very little improvement can be observed. Therefore, the critical order can be defined as the order where the system has little enhancement with higher orders.

Although larger neuron number in the hidden layer increases the complexity, both the training error and the standard deviation of MSEs can be improved. In this work, we

select a larger scale MLP/BP neural network for better training stability and higher performance. However, in practical applications, a smaller size can be selected while considering the trade-off between performance and complexity.

In addition, there are no obvious improvements for the standard deviation of MSEs of the evaluation set with a larger summation function order. Since the training results may be located on a local minimum that leads to a limited performance, in most neural-based applications many independent runs are regularly carried out in search of the best outcomes. This demonstrates the reason for using non-training data to evaluate the training quality.

Fig. 3-23 illustrates the BERs of both the evaluation set and the test set for different hidden neuron multipliers and different summation function orders at SNR=15dB. The analogous trend in Fig. 3-23 that confirms our simulation assumption implies the estimation of training results with the evaluation set is feasible.

The BER performance for different levels of the nonlinearity with different hidden neuron multipliers at SNR=15dB is shown in Fig. 3-24. The critical order of the system with the nonlinearity is higher than the one without the nonlinearity. For “ $S_x=1.0$ ” and “ $S_x=0.9$ ” with “ $H_x=4$ ”, the critical order is 3, while for “ $S_x=0.8$ and “ $S_x=0.7$ ” with “ $H_x=4$ ”, the critical order increases to 4. This appearance is reasonable and confirms our expectation.

Based on the aforementioned results, the summation function order of the generalized MLP/BP-based DFEs is set to 3, and the hidden neuron multiplier is set to 4. A comparison with the LMS DFEs, the ideal VE, the traditional MLP/BP-based DFEs and the generalized MLP/BP-based DFEs is shown in Fig. 3-25. With channel 1 and $S_x=1.0$, the proposed approach at BER= 10^{-4} improves 0.8dB over the traditional MLP/BP-based DFE and 1.9dB over the LMS DFE. The proposed approach performs better than LMS

DFE and the traditional MLP/BP-based DFE in the severe ISI channel without the nonlinearity, but degrades 1.7dB as compared to the ideal VE. Nevertheless, at $S_x=0.7$ (30% truncations) with the BER is 10^{-3} , the proposed scheme improves the traditional MLP/BP-based DFE by 0.8dB, the ideal VE by 2.2dB, and the LMS DFE by 4.4dB. As the distortions increase in the received signal, the proposed approaches achieve more improvement over the others.

Subsequently, several different ISI channels are described by transfer functions, which are $H_2(z) = 0.408 + 0.816z^{-1} + 0.408z^{-2}$, $H_3(z) = 0.3482 + 0.8704z^{-1} + 0.3482z^{-2}$, $H_4(z) = 0.227 + 0.460z^{-1} + 0.688z^{-2} + 0.460z^{-3} + 0.227z^{-4}$, $H_5(z) = 0.108 + 0.215 z^{-1} + 0.430 z^{-2} + 0.717 z^{-3} + 0.430 z^{-4} + 0.215 z^{-5} + 0.108z^{-6}$, $H_6(z) = 0.147 + 0.295 z^{-1} + 0.590 z^{-2} + 0.295 z^{-3} + 0.590 z^{-4} + 0.295 z^{-5} + 0.147z^{-6}$, and $H_7(z) = 0.226 + 0.516 z^{-1} + 0.645 z^{-2} + 0.516 z^{-3}$, respectively. The time domain responses of these channels are symmetric, except that of channel 7 is asymmetric. The lengths of channel response in channels 1, 2 and 3 are the same, but the influences of ISI are different — channel 1 is the worst case, channel 2 is a better one and channel 3 is with the least interference. Moreover, channel 4, 5, 6, and 7 with longer ISI and lower signal-to-interference ratio results in a worse signal quality compared to others. Specially, the channel response of channel 7 is not symmetric. These channels will be further used to evaluate the system performance of the equalization schemes.

The simulation results based on channels 2 and 3, where the simulation conditions are identical to those of channel 1, are shown in Fig. 3-26 and Fig. 3-27, respectively. Note that the proposed approaches result in a better improvement over the LMS DFE and the traditional MLP/BP-based DFE in the severer ISI channel. In these three channels without nonlinearity, the ideal VE appear to outperform the traditional MLP/BP-based DFEs and the generalized MLP/BP-based DFEs. However, the accuracy of the CIR

estimator dominates the performance particularly, and thus the improvement of VE may be lower in real cases. Furthermore, the nonlinear distortions of the received signal will compromise the VE performance significantly. In the severer ISI channel with more nonlinearity, the traditional MLP/BP-based DFEs and the generalized MLP/BP-based DFEs outperform VE. The BER vs. SNR performance comparison with different equalizers for channels 1, 2, and 3 without truncations at $\text{BER}=10^{-4}$ is illustrated in Tab. 3-4. That with 30% truncations at $\text{BER}=10^{-3}$ is presented in Tab. 3-5.

Fig. 3-28 shows the simulation results with channel 4, where the training noise and the evaluation noise are assumed to be $\text{SNR}=20\text{dB}$ and the SNR of the test signal is between 10dB and 25dB . Fig. 3-29, Fig. 3-30, and Fig. 3-31 show the simulation results with channel 5, 6, and 7, where the training noise and the evaluation noise are assumed to be $\text{SNR}=15\text{dB}$ and the SNR of the test signal is between 10dB and 20dB . For these channels, the ideal VE is still the best method without nonlinear distortion in the received signal. Similarly, the performance of the LMS DFE and the ideal VE is limited due to large truncations. In these severe ISI channels, the MLP/BP-based DFEs and the GMLP/BP-based DFEs provide better robustness when large truncations present.

By above simulation results, the proposed GMLP/BP-based DFEs can yield a substantial improvement over the traditional MLP/BP-based DFE that performs better than the LMS DFE. In such applications, the proposed schemes can provide more improvement when larger truncation occurred. The proposed schemes present better capability of classifying the sampling patterns, and tolerate distortions.

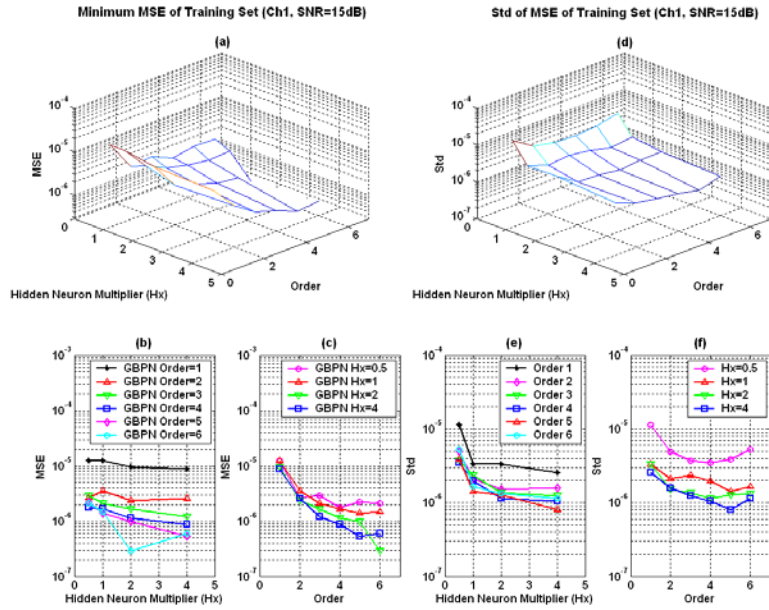


Fig. 3-21: Minimum MSE and standard deviation of MSEs of the training set in Channel 1 at SNR=15dB: (a) Minimum MSE for different hidden neuron multipliers (Hx) and different summation function orders (Order), (b) Minimum MSE for different orders, (c) Minimum MSE for different multipliers, (d) Standard deviation of MSEs for different multipliers and different orders, (e) Standard deviation of MSEs for different orders, (f) Standard deviation of MSEs for different multipliers.

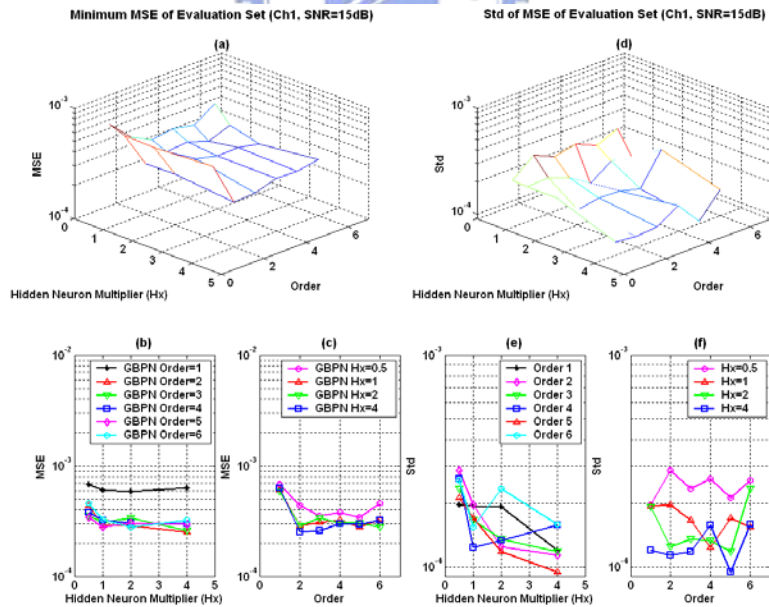


Fig. 3-22: Minimum MSE and standard deviation of MSEs of the evaluation set in Channel 1 at SNR=15dB: (a) Minimum MSE for different hidden neuron multipliers (Hx) and different summation function orders (Order), (b) Minimum MSE for different orders, (c) Minimum MSE for different multipliers, (d) Standard deviation of MSEs for different multipliers and different orders, (e) Standard deviation of MSEs for different orders, (f) Standard deviation of MSEs for different multipliers.

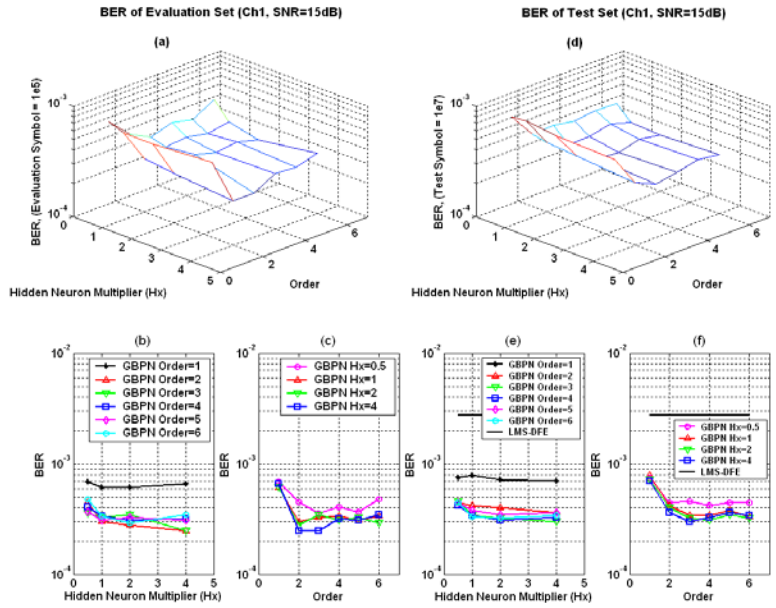


Fig. 3-23: BER of the evaluation set and the test set in Channel 1 at SNR=15dB: (a) BER of the evaluation set for different hidden neuron multipliers (Hx) and different summation function orders (Order), (b) BER of the evaluation set for different orders, (c) BER of the evaluation set for different multipliers, (d) BER of the test set for different multipliers and different orders, (e) BER of the test set for different orders, (f) BER of the test set for different multipliers.

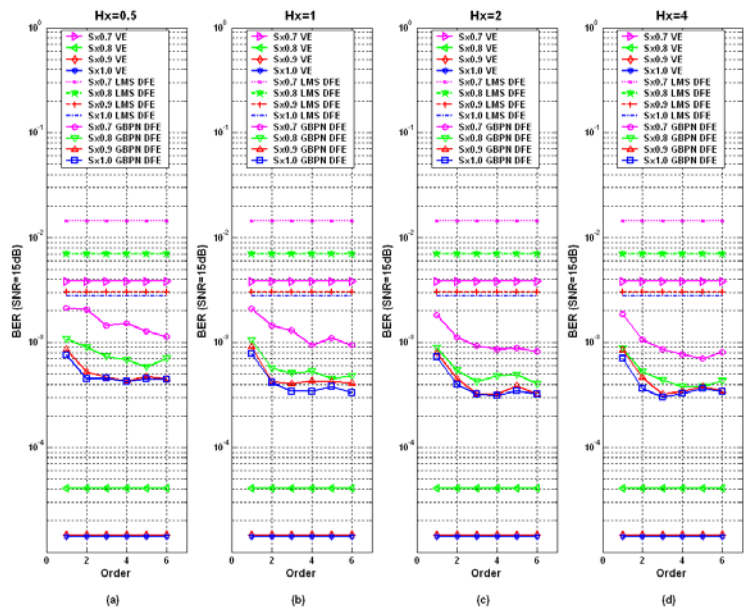


Fig. 3-24: BER performance for different levels of the nonlinearity (Sx) with different hidden neuron multipliers (Hx) in Channel 1 at SNR=15dB.

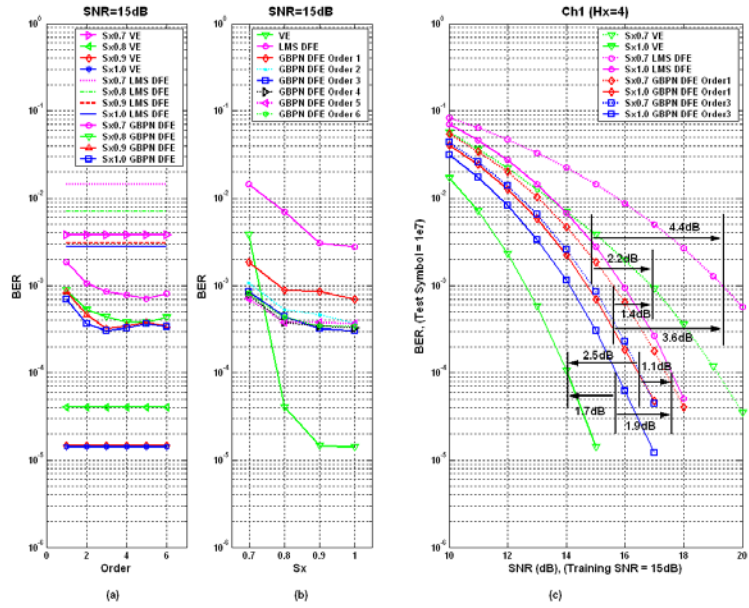


Fig. 3-25: Channel 1 test results: (a) BER performance for different levels of the nonlinearity (S_x) at SNR=15dB, (b) BER performance for different summation function orders at SNR=15dB, (c) BER performance for different types of equalizers under training at SNR=15dB.

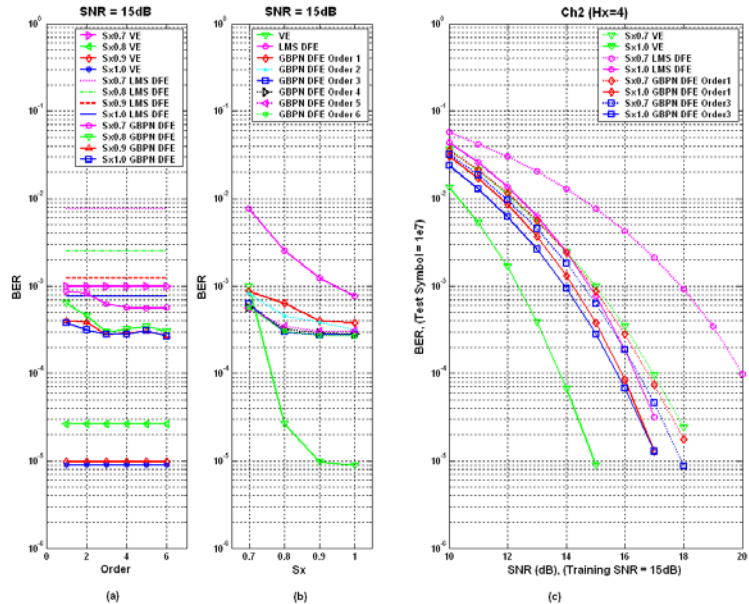


Fig. 3-26: Channel 2 test results: (a) BER performance for different levels of the nonlinearity (S_x) at SNR=15dB, (b) BER performance for different summation function orders at SNR=15dB, (c) BER performance for different types of equalizers under training at SNR=15dB.

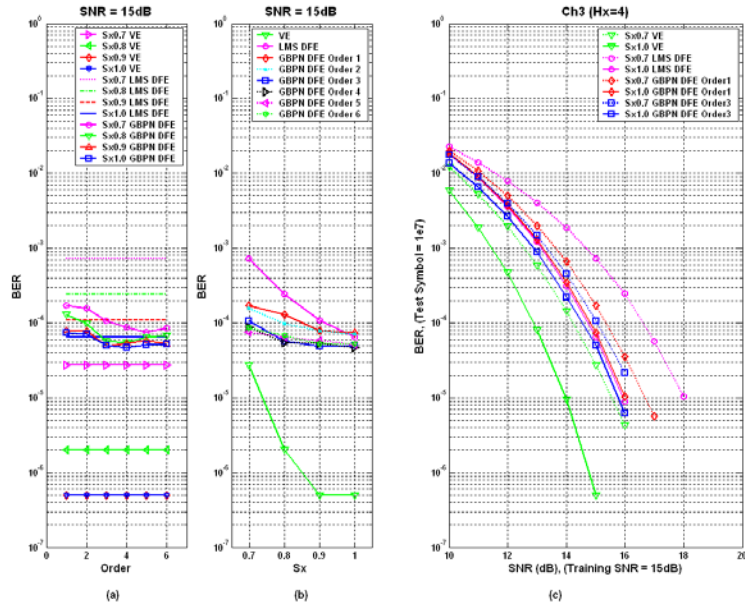


Fig. 3-27: Channel 3 test results: (a) BER performance for different levels of the nonlinearity (S_x) at SNR=15dB, (b) BER performance for different summation function orders at SNR=15dB, (c) BER performance for different types of equalizers under training at SNR=15dB.

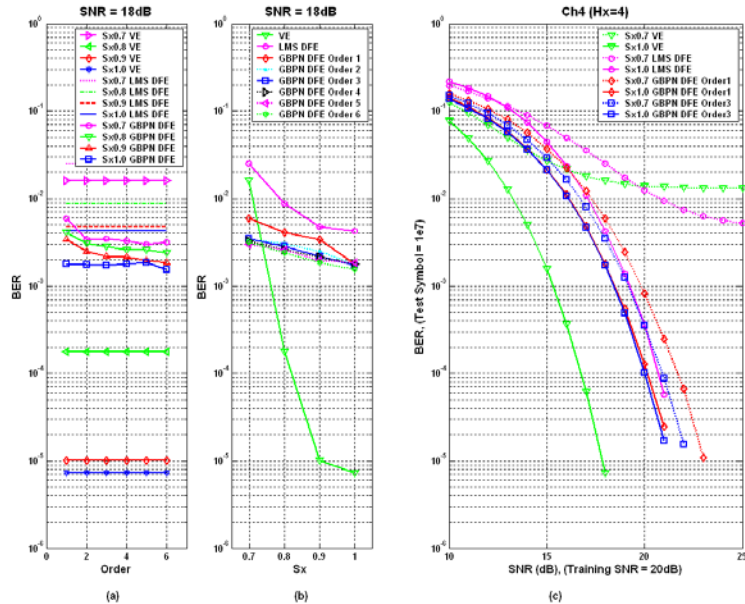


Fig. 3-28: Channel 4 test results: (a) BER performance for different levels of the nonlinearity (S_x) at SNR=18dB, (b) BER performance for different summation function orders at SNR=18dB, (c) BER performance for different types of equalizers under training at SNR=20dB.

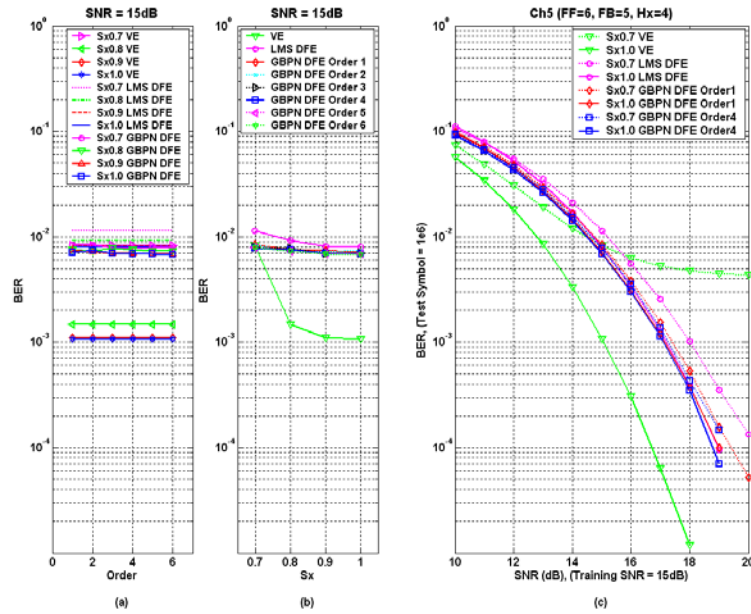


Fig. 3-29: Channel 5 test results: (a) BER performance for different levels of the nonlinearity (S_x) at SNR=15dB, (b) BER performance for different summation function orders at SNR=15dB, (c) BER performance for different types of equalizers under training at SNR=15dB.

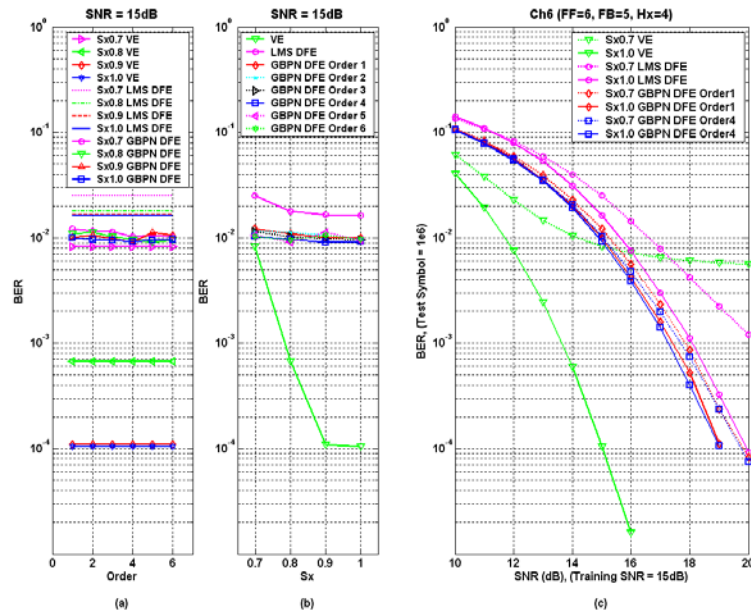


Fig. 3-30: Channel 6 test results: (a) BER performance for different levels of the nonlinearity (S_x) at SNR=15dB, (b) BER performance for different summation function orders at SNR=15dB, (c) BER performance for different types of equalizers under training at SNR=15dB.

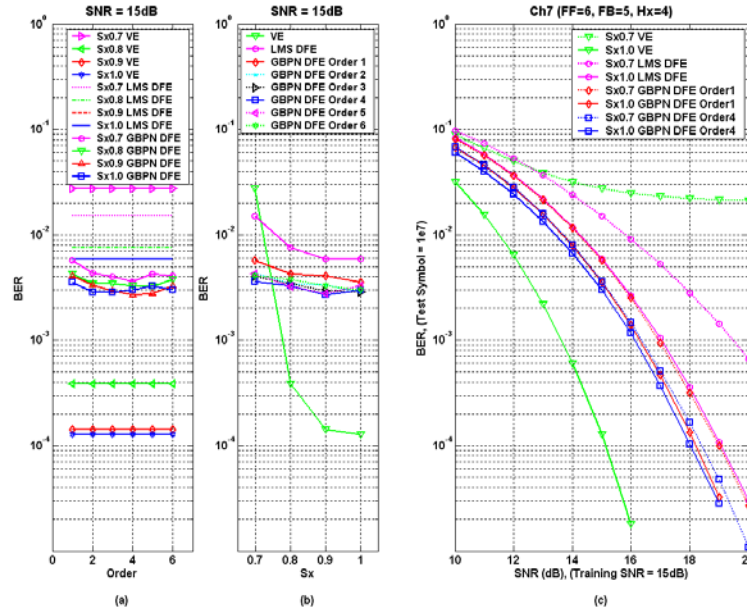


Fig. 3-31: Channel 7 test results: (a) BER performance for different levels of the nonlinearity (S_x) at SNR=15dB, (b) BER performance for different summation function orders at SNR=15dB, (c) BER performance for different types of equalizers under training at SNR=15dB.

Table 3-4: The BER vs. SNR performance comparison with different equalizers for Channel 1, 2, and 3 without truncations at BER= 10^{-4} .

Channel ID	S_x	Ideal VE	LMS DFEs	MLP/BP-based DFEs	GMLP/BP-based DFEs (Order=3)
1	1.0	14.0 dB	17.6 dB	16.5 dB	15.7 dB
2	1.0	13.8 dB	16.3 dB	15.9 dB	15.7 dB
3	1.0	12.9 dB	14.7 dB	14.7 dB	14.5 dB

Simulation Conditions for Neural-based Schemes:

Input Neural Number = 10 (Forward part: 5, and Feedback part: 5),
 Hidden Neural Number = 40 ($H_x=4$),
 Output Neural Number = 1,
 Training Set = 10^4 symbols,
 Evaluation Set = 10^5 symbols,
 Test Set = 10^7 symbols,
 Training Epoch = 10^3 ,
 Learning Rate = 0.5 / 0.1 (Two Phase Learning, MSE Bound = 10^{-3}),
 Re-training Times = 50 Independent Runs.

Table 3-5: The BER vs. SNR performance comparison with different equalizers for Channel 1, 2, and 3 with 30% truncations at $BER=10^{-3}$.

Channel ID	S_x	Ideal VE	LMS DFEs	MLP/BP-based DFEs	GMLP/BP-based DFEs (Order=3)
1	0.7	17.0 dB	19.2 dB	15.6 dB	14.8 dB
2	0.7	15.0 dB	17.9 dB	14.9 dB	14.6 dB
3	0.7	12.5 dB	14.6 dB	13.6 dB	13.3 dB

Simulation Conditions for Neural-based Schemes:
 Input Neural Number = 10 (Forward part: 5, and Feedback part: 5),
 Hidden Neural Number = 40 ($H_x=4$),
 Output Neural Number = 1,
 Training Set = 10^4 symbols,
 Evaluation Set = 10^5 symbols,
 Test Set = 10^7 symbols,
 Training Epoch = 10^3 ,
 Learning Rate = 0.5 / 0.1 (Two Phase Learning, MSE Bound = 10^{-3}),
 Re-training Times = 50 Independent Runs.



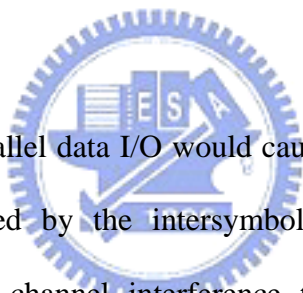
3-2-4 Summary

With multivariate power series as the summation function, the generalized MLP/BP neural network based decision feedback equalizer has been developed to compensate the distorted NRZ signal for severe ISI channels in wireline applications. In addition, the proposed approaches present continuous nonlinear pattern space mapping potential, leading to a better space mapping capability than the traditional MLP/BP neural networks in nonlinear applications. The simulation results show that the proposed equalizer can provide a significant improvement over the other schemes such as the LMS DFEs, the ideal VE, and the traditional MLP/BP-based DFEs when the received signal contains more distortions caused by ISI, AWGN and the nonlinearity.

CHAPTER 4

MIMO GMLP/BP-based DFEs

for Wireline Applications



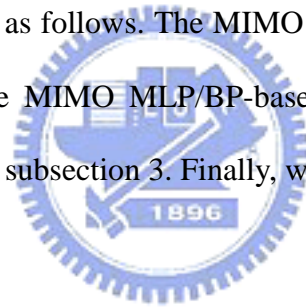
Interconnect paths of parallel data I/O would cause the co-channel interference. The transmitted signals are tainted by the intersymbol interference that caused by the band-limited channel, the co-channel interference that caused by crosstalk between different channels, and background white noise. For recover the distorted data as well as suppress ISI, CCI and AWGN, a multi-input multi-output (MIMO) channel equalizer is essential. In wireline band-limited parallel channels, the MIMO MLP/BP-based DFEs and the MIMO GMLP/BP-based DFEs can suppress ISI, CCI and AWGN, simultaneously. By the simulations, the MIMO GMLP/BP-based DFEs can yield a substantial improvement over the MIMO MLP/BP-based DFEs that perform better than a set of the LMS DFEs.

This chapter is organized as follows. The MIMO MLP/BP-based DFEs are presented at the beginning. Afterward, the MIMO GMLP/BP-based DFEs are proposed.

4-1 MIMO MLP/BP-based DFEs for Overcoming ISI and CCI in Wireline Band-limited Parallel Channels

An MIMO MLP/BP neural network is realized as a waveform equalizer for distorted nonreturn-to-zero data recovery in band-limited channels with co-channel interference. From the simulation results, we note that the proposed design can recover severe distorted NRZ data as well as suppress ISI and CCI. As a result, the better performance as compared to a set of LMS DFEs is achieved in the band-limited channels where the data rate is ten times as much as the channel bandwidth. By fixed-point simulations, the proposed scheme outperforms a set of LMS DFEs. Further, the internal resolution enhancement technique provides a better compromise between cost and performance.

This section is organized as follows. The MIMO system is presented in subsection 1 while subsection 2 shows the MIMO MLP/BP-based DFE. Afterward, the simulation conditions and results show in subsection 3. Finally, we make a summary in subsection 4.



4-1-1 Multi-channel Environment

If the data rate of transmitted signals is higher than the channel capacity, the received signal pulse is unable to complete its transition within a symbol interval. Moreover, interconnect paths of parallel data I/O would cause the co-channel interference and taint the received signals. The equivalent model for the band-limited channels with co-channel interference is shown in Fig. 4-1 where FIR filters are used to model the ISI channel responses and the CCI responses with the AWGN as the background noise.

The ISI channel responses and CCI responses with AWGN can be written as follows:

$$H(z) = f_0 + f_1 \cdot z^{-1} + f_2 \cdot z^{-2} + \dots + f_L \cdot z^{-L}, \quad (4-1)$$

$$C_r(z) = g_{r0} + g_{r1} \cdot z^{-1} + g_{r2} \cdot z^{-2} + \dots + g_{rM} \cdot z^{-M}, \quad (4-2)$$

$$y_k = \sum_{i=0}^L f_i \cdot x_{k-i}^0, \quad (4-3)$$

$$c_k = \sum_{j=0}^r \sum_{j=0}^M g_j \cdot x_{k-j}^r, \quad (4-4)$$

$$\hat{y}_k = y_k + c_k + n_k, \quad (4-5)$$

where $H_\theta(z)$ is the transfer function of the ISI channel responses; L is the length of the ISI channel response; $C_r(z)$ is the transfer function of the CCI responses; M is the length of the CCI response; x_k^0 is the input sequence of ISI response; x_k^r is the input sequence of r -th CCI response; y_k is the channel output which is warped by ISI only; c_k is the sum of co-channel interference; n_k is the AWGN; \hat{y}_k is the received signal which is distorted by ISI, CCI and AWGN.

In this work, we assume that the transfer function of the band-limited channels is $H_\theta(z) = 0.4665 + 0.2489z^{-1} + 0.1328z^{-2} + 0.0708z^{-3} + 0.0378z^{-4}$ and the transfer function of the co-channel interference is $C_r(z) = 0.408 + 0.816z^{-1} + 0.408z^{-2}$. Such channel condition is practical in many wireline communication systems. The frequency responses of the ISI and CCI are illustrated in Fig. 4-2. Moreover, we use uniform distribution random values to build an N-by-N matrix A . We also construct a symmetric matrix $(A+A^T)$ and normalize this matrix to make the sum of squares of all elements be N. The weighting of co-channel interference between different channels is shown in Table 4-1 where N is equal to 8. Table 4-1 represents the co-channel interference of parallel I/O channels in space. For example, a cable includes several parallel I/O wires.

The received signals include the intersymbol interference that caused by the band-limited channel, and the co-channel interference that caused by crosstalk between

different channels. The transmitted signal is expected to be deteriorated substantially by ISI, CCI, and AWGN.

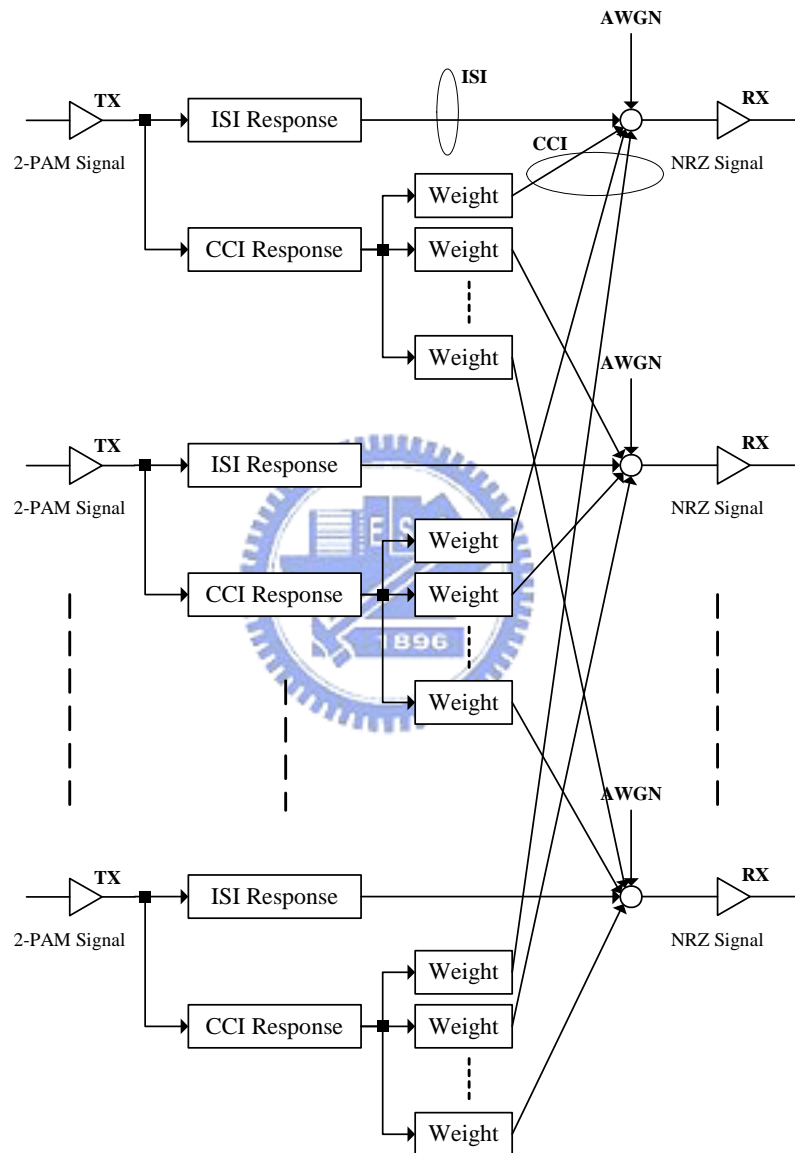


Fig. 4-1: Equivalent model for the band-limited channels with co-channel interference.

Table 4-1: Weighting of co-channel interference between different channels in space.

	1	2	3	4	5	6	7	8
1	0.2253	0.5402	0.3404	0.3298	0.4465	0.2831	0.4023	0.3974
2	0.5402	0.0944	0.4480	0.2017	0.4642	0.5114	0.3507	0.4017
3	0.3404	0.4480	0.0822	0.4380	0.4010	0.2750	0.3313	0.3290
4	0.3298	0.2017	0.4380	0.1737	0.2754	0.1670	0.2886	0.4169
5	0.4465	0.4642	0.4010	0.2754	0.1135	0.2877	0.3738	0.4772
6	0.2831	0.5114	0.2750	0.1670	0.2877	0.1451	0.0898	0.1779
7	0.4023	0.3507	0.3313	0.2886	0.3738	0.0898	0.3009	0.5230
8	0.3974	0.4017	0.3290	0.4169	0.4772	0.1779	0.5230	0.0227

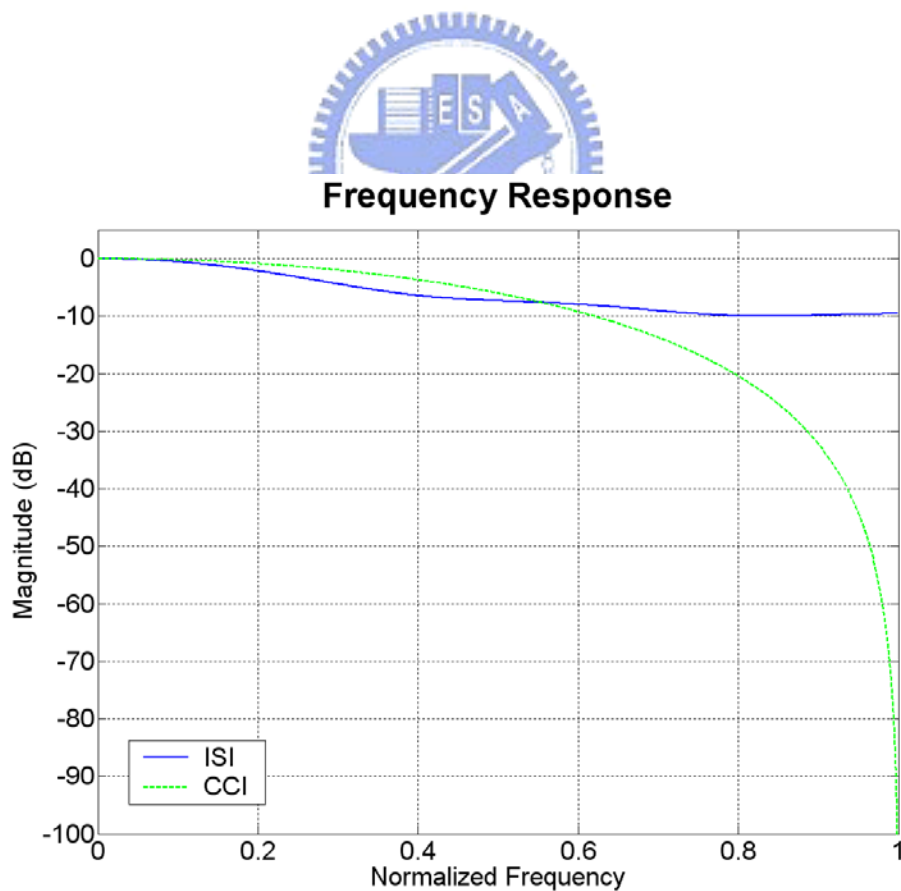


Fig. 4-2: Frequency responses of the ISI and the CCI responses.

4-1-2 MIMO MLP/BP-based DFE

The block diagram of the MIMO MLP/BP-based DFE is shown in Fig. 4-3. This MIMO MLP/BP-based DFE is the single hidden layer MLP architecture. The inputs of the MIMO MLP/BP-based DFE consist of feed-forward signals, which come from the input symbols by tapped-delay-line registers, and feedback signals, which come from previous decisions by another tapped-delay-line registers.

Based on the results of chapter 3, all equalization schemes in this work have 11 symbols per channel in the forward part and 5 symbols per channel in the feedback part. We assume there are 8 parallel channels in this system. The number of neurons in the input layer is equal to 128 (16-by-8). The MLP/BP-based DFEs uses the single hidden layer MLP architecture. The number of neurons in the hidden layer is 16. Since all the proposed equalization schemes have a single output per channel, the number of neurons in the output layer is equal to 8 (1-by-8).

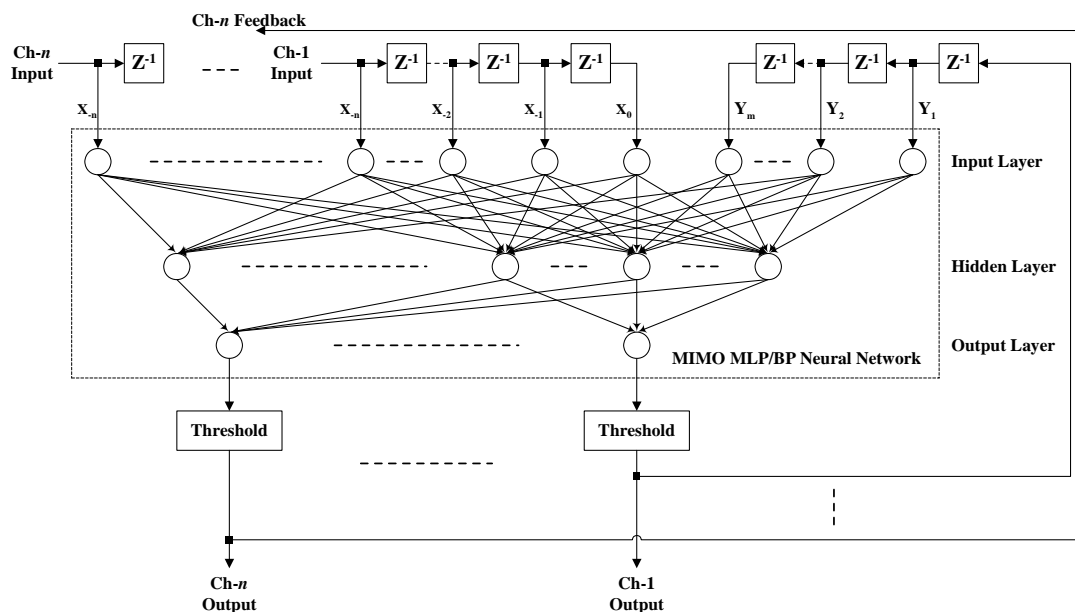


Fig. 4-3: MIMO MLP/BP-based DFEs.

4-1-3 Simulation Results

The performance of the MIMO MLP/BP-based DFE is evaluated through the simulations for the distorted NRZ signal recovery in the band-limited channels with co-channel interference. The data rate is ten times of the channel bandwidth. In this section, floating-point simulations of the equalization schemes are presented first followed by the fixed-point simulations. Finally, the internal resolution enhancement technique is discussed in detail.

4-1-3-1 Floating-Point Simulations

In this work, we apply the MIMO MLP/BP-base DFE to recover the distorted NRZ data in the band-limited channels with CCI. It is also a wireline application so we select a longer training set to achieve better performance.

In the training procedure, the length of the training set is equal to 10^4 symbols and the total training epochs are 10^2 . The two-phase learning is used with the learning rate of 0.5 (2^{-1}) when the mean square error of the training set is larger than 10^{-3} , and the learning rate of 0.125 (2^{-3}), otherwise. When the training epochs exceed eighty percent of the total epochs, the best parameters will be recorded to achieve the lowest mean square error of the training set in the last twenty percent of the training epochs. Hence the steady-state training results can be recognized. In fact, the simulations indicate no unstable problems as all training processes are converged.

Because different initial conditions lead to different effects, the non-training evaluation set that has 10^5 symbols is used to examine the training quality of numerous independent simulation outcomes. After numerous independent training and evaluation runs, those yielding better outcomes will be chosen to perform a long trial with the test set,

and then the best one will be the final test result. The length of the test set is 10^7 symbols, and the evaluation set is its subset. In this work, we execute ten independent runs and select the best one as the final result.

In this work, we compare the performance of our proposed approach with that of a set of LMS DFEs. We use a LMS DFE without cross inputs for a channel among these parallel channels. The simulation conditions are listed in Tab. 4-2.

The band-limited channel described by the transfer function, $H_0(z) = 0.4665 + 0.2489z^{-1} + 0.1328z^{-2} + 0.0708z^{-3} + 0.0378z^{-4}$, with the co-channel interference described by the transfer function, $C_r(z) = 0.408 + 0.816z^{-1} + 0.408z^{-2}$, is used to estimate the system performance of the LMS DFE and the MLP/BP-based DFE. This ISI channel response indicates that the data rate is ten times of the channel bandwidth. The training noise and the evaluation noise are assumed to be SNR=20dB, and SNR of the test signal is between 10dB and 25dB. The signal to co-channel interference ratio (SIR) is equal to 10, 12.5, 15, 17.5, and 20, respectively.

Fig. 4-4 shows the comparisons of the BER performance vs. SNR for the LMS DFE and the MIMO MLP/BP-based DFE in the band-limited channels with different SIR. The MIMO MLP/BP-based DFE outperform a set of LMS DFEs. Considering different SIR in the band-limited channels at SNR = 15dB and 20dB, Fig. 4-5 also shows the comparisons of the BER performance vs. SIR between a set of the LMS DFEs and the MIMO MLP/BP-based DFE. At SNR = 20dB, the BER performance vs. SIR for the MIMO MLP/BP-based DFE can improve about 2.4dB over that for a set of LMS DFEs. From Fig. 4-4 and Fig. 4-5, the MIMO MLP/BP-based DFE reports better performance under larger intersymbol interference and larger co-channel interference.

Table 4-2: Simulation conditions for MIMO MLP/BP-based DFE.

Simulation Conditions	LMS DFEs	MIMO MLP/BP-based DFE
Input Channel Number	1	8
Forward Length	11 symbols	
Feedback Length	5 symbols	
Input Number per Channel	16 symbols	
Input Numbers	16	128 (16x8)
Hidden Neuron Number	---	16
Output Number	1	8
Training Set	10 ⁴ symbols	
Evaluation Set	10 ⁵ symbols	
Test Set	10 ⁶ symbols	
Training Epochs	100 cycles	
Re-training Times	1	10
Learning Rate Searching Range	2 ⁰ ~ 2 ⁻¹⁰	2 ⁰ ~ 2 ⁻⁴ / 2 ⁰ ~ 2 ⁻⁴
Most Suitable Learning Rate	2 ⁻⁸	2 ⁻¹ / 2 ⁻³ (Two phase learning, MSE Bound=10 ⁻³)
Training SNR	20 dB	
Test SNR	10 to 25 dB (Step = 1 dB)	
SIR	10, 12.5, 15, 17.5, and 20 dB	
Equalizer Number for 8 channels	8	1

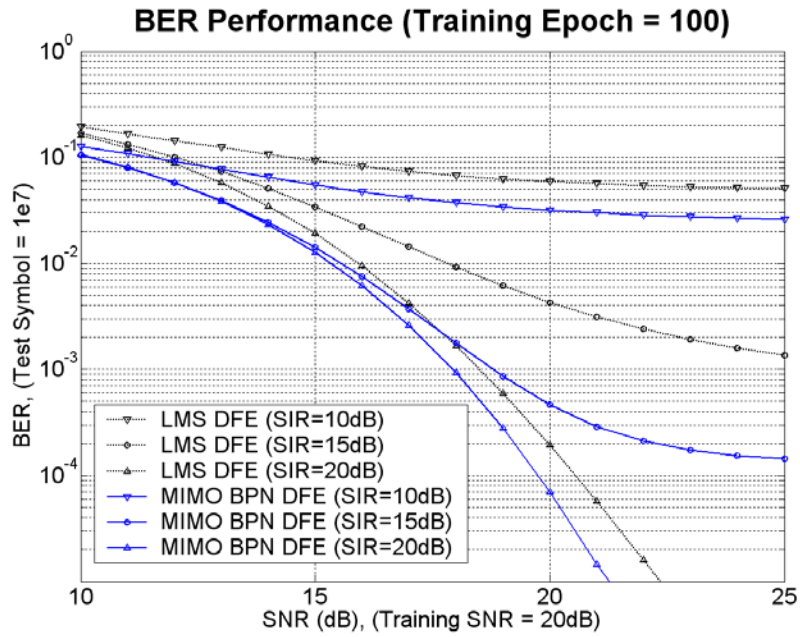


Fig. 4-4: BER vs. SNR for different types of equalizers in the band-limited channels with co-channel interference at SIR=10, 15 and 20dB.

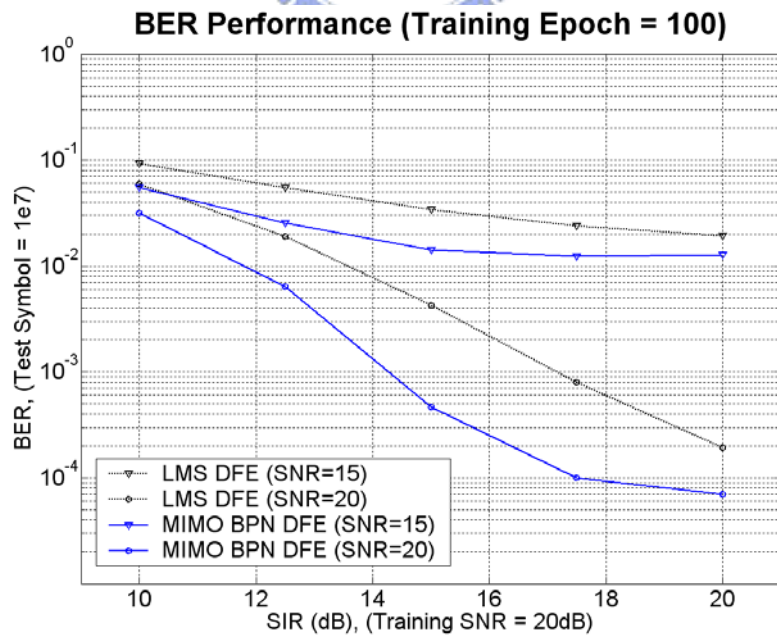


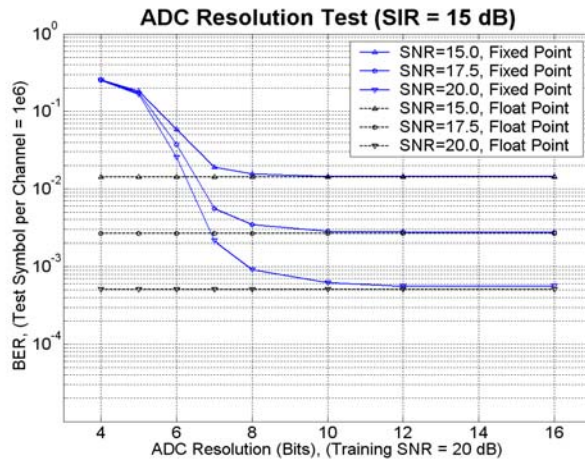
Fig. 4-5: BER vs. SIR for different types of equalizers in the band-limited channels with co-channel interference at SNR= 15 and 20dB.

4-1-3-2 Fixed-Point Simulations

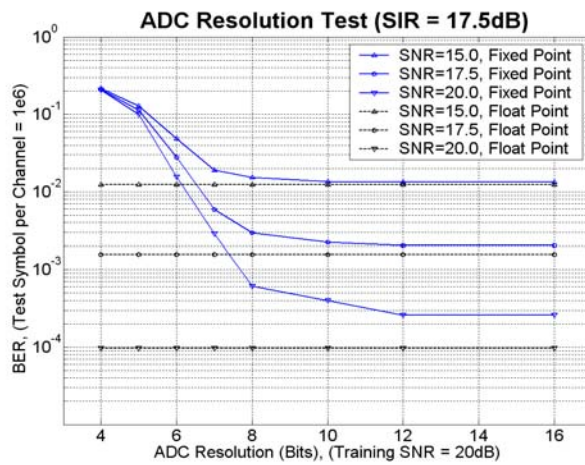
Based on the above floating-point simulation results, the fixed-point simulations of the MIMO MLP/BP-based DFEs are presented. Also, we use a hard limiter to replace the log-sigmoid function for low cost, leading to decreased system performance. The best weighting parameters yielded by the floating-point simulations are applied to the fixed-point simulations. In the fixed-point simulations, the test symbol number per channel is equal to 10^6 .

The BER performance under SIR=15dB, 17.5dB, and 20dB for different ADC resolution at SNR=15dB, 17.5dB, and 20dB are shown in Fig. 4-6. A comparison of BER performance versus SNR for different ADC resolution is shown in Fig. 4-7.

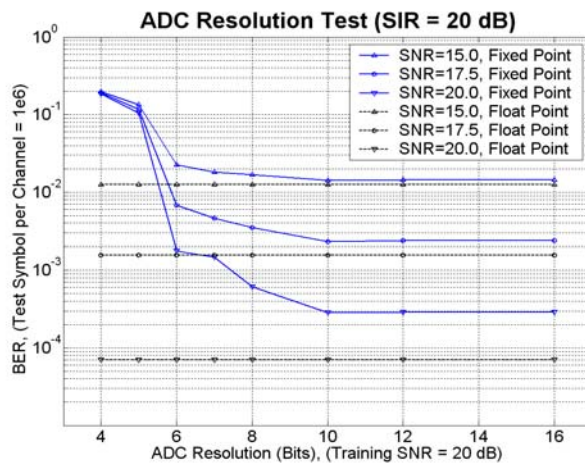
From Fig. 4-6, the acceptable ADC resolution is ten bits. Unfortunately, suitable ten bits ADCs are too expensive for such high-speed applications. Based on the results of chapter 3, we also increase the internal wordlength instead of ADC resolution to achieve acceptable performance with a reasonable cost. The detail of the internal resolution enhancement technique is shown in next subsection.



(a) SIR = 15.0dB

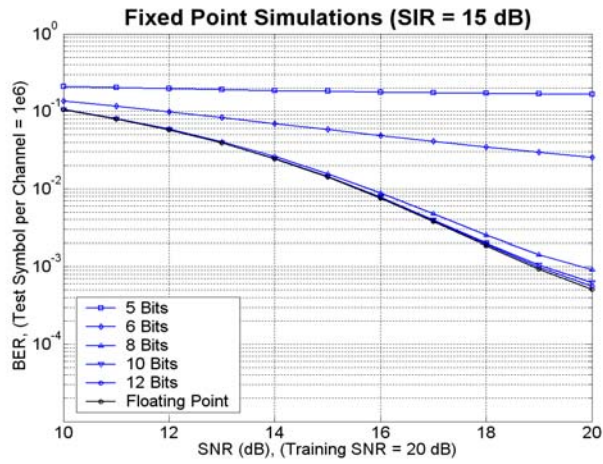


(b) SIR = 17.5dB

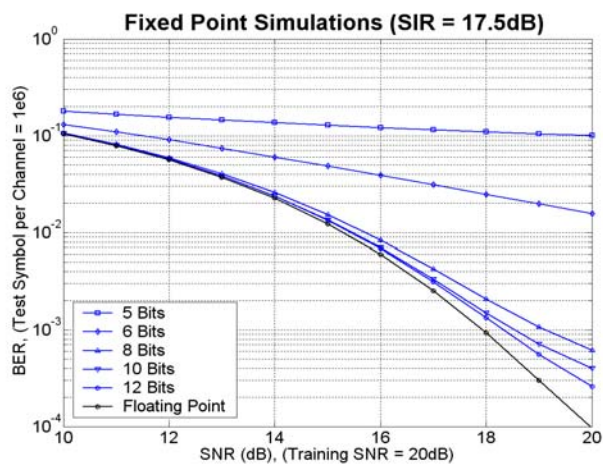


(c) SIR = 20.0dB

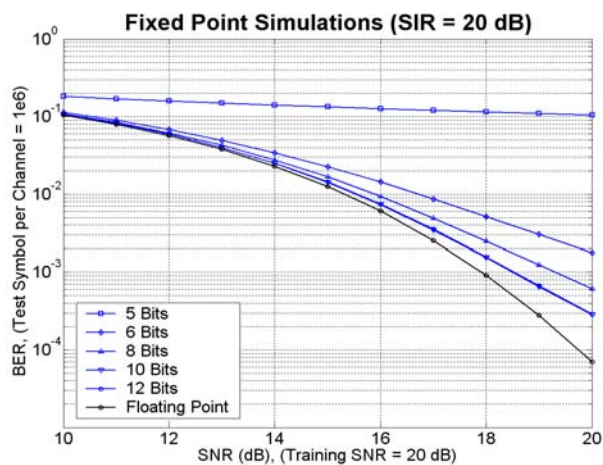
Fig. 4-6: BER performance under SIR=15dB, 17.5dB, and 20dB for different ADC resolution at SNR=15dB, 17.5dB, and 20dB.



(a) SIR = 15.0dB



(b) SIR = 17.5dB



(c) SIR = 20.0dB

Fig. 4-7: BER performance vs. SNR for different ADC resolution at SIR=15dB, 17.5dB, and 20dB.

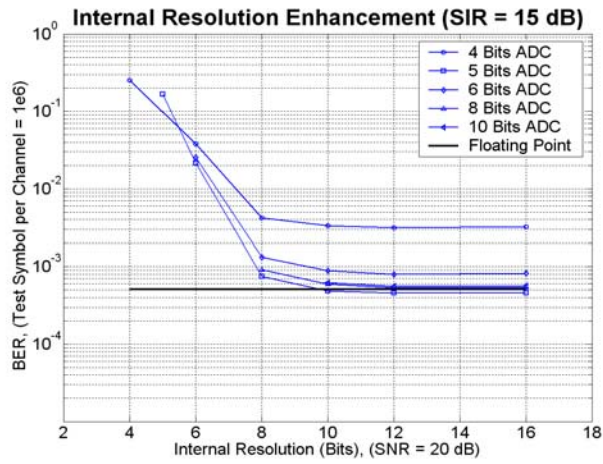
4-1-3-3 Internal Resolution Enhancement

For sensible cost consideration, the internal resolution enhancement technique has been applied to the proposed equalizer. We consider adding internal resolution to increase the performance under low ADC resolution. Thus, we can use lower resolution ADCs to obtain a similar performance.

The BER performance under SIR=15dB, 17.5dB, and 20dB for different ADC resolution with different internal resolution at SNR=20dB is shown in Fig. 4-8. The comparisons of BER performance versus SNR under SIR=15dB, 17.5dB, and 20dB with different ADC resolutions and different internal resolutions are shown in Fig. 4-9.

From Fig. 4-8 and Fig. 4-9, we suggest the most suitable wordlength configuration is five bits ADC with ten bits internal resolution. The internal resolution enhancement technique can significantly improve BER performance and achieves a better compromise between cost and performance.

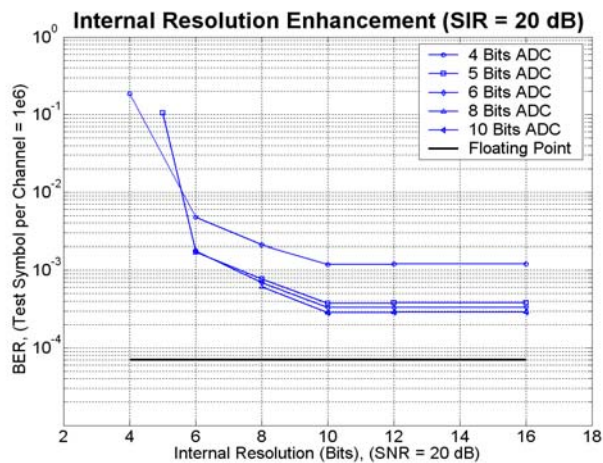
Finally, we summarize the simulation results that apply the suggested wordlength configuration for the LMS DFEs and the MIMO MLP/BP-based DFEs. A comparison of BER performance versus SNR for the referred and the proposed equalizers at SIR=15.0dB, 17.5dB, and 20.0dB is shown in Fig. 4-10. The proposed scheme significantly outperforms the LMS DFE when large CCI presents. By this approach, we can realize the MIMO MLP/BP-based DFEs with reasonable cost.



(a) SIR = 15.0dB

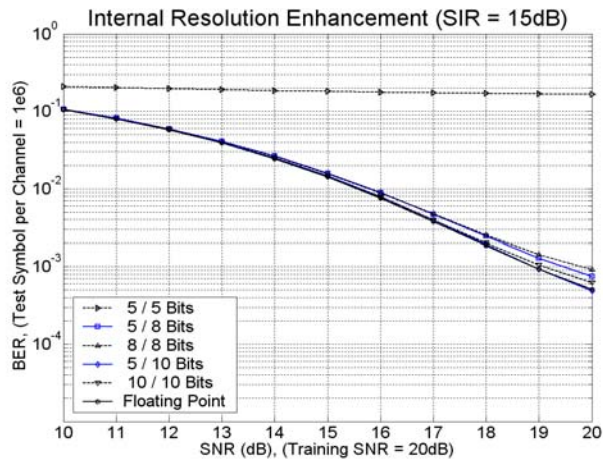


(b) SIR = 17.5dB

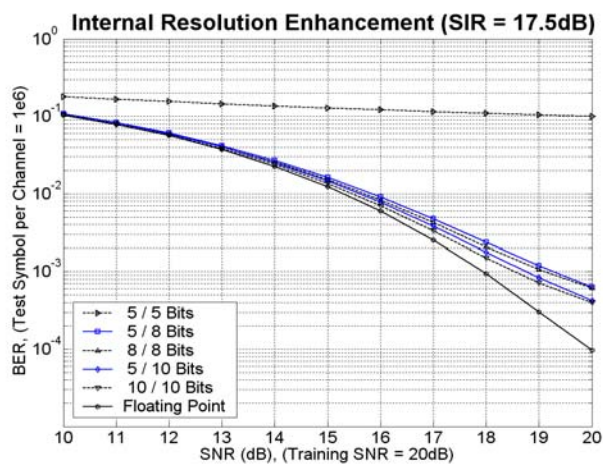


(c) SIR = 20.0dB

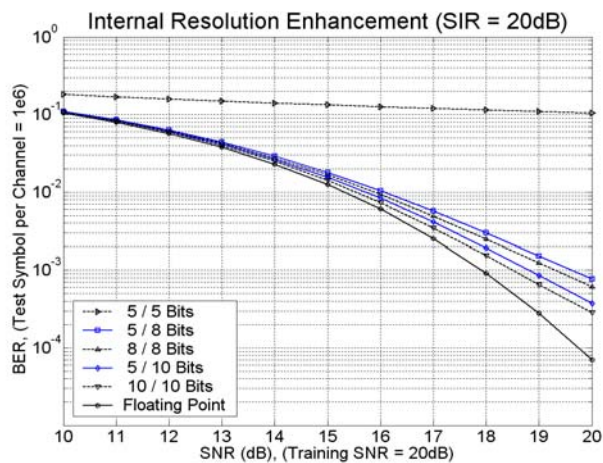
Fig. 4-8: BER performance under SIR=15dB, 17.5dB, and 20dB for different ADC resolution with internal resolution enhancement technique at SNR=20dB.



(a) SIR = 15.0dB



(b) SIR = 17.5dB



(c) SIR = 20.0dB

Fig. 4-9: BER performance vs. SNR with different ADC resolution and different internal resolution at SIR=15dB, 17.5dB, and 20dB.

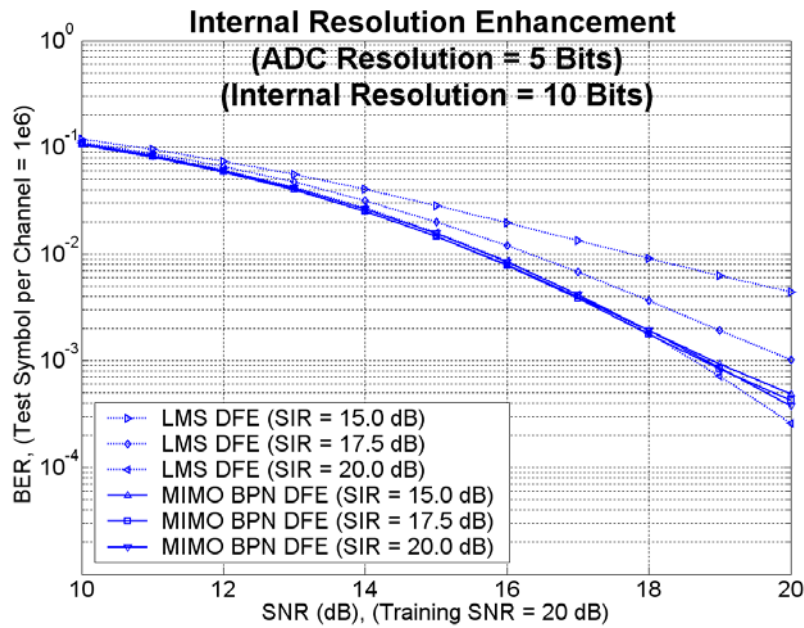


Fig. 4-10: BER performance vs. SNR for the LMS DFEs and MIMO MLP/BP-based DFEs at SIR=15.0dB, 17.5dB, and 20.0dB.



4-1-4 Summary

The proposed scheme can overcome ISI while suppress CCI. According to the simulation results, the MIMO MLP/BP-based DFE can recover severe distorted NRZ signals and suppress CCI to achieve better BER performance than LMS DFEs in the band-limited channels in which the data rate is ten times as much as the channel bandwidth. Because the proposed equalizer is a multi-input multi-output architecture, we can extend the input and output number for more complex system.

In the fixed-point simulations, the proposed equalizer also outperforms the LMS DFE. Since suitable high-speed ADCs are expensive, the internal resolution enhancement technique has been applied to the LMS DFEs and the MIMO MLP/BP-based DFEs to provide acceptable performance with lower resolution ADCs. This method will results in

a better compromise between cost and performance. Moreover, the proposed scheme significantly outperforms the LMS DFE when large CCI presents.

However, the performance of the MIMO MLP/BP-based DFEs is not good enough under small background noise with large co-channel interference conditions. For such situations, the MIMO GMLP/BP-based DFEs can provide better performance. The detail of the GMLP/BP-based DFEs is shown in next section.

4-2 MIMO GMLP/BP-based DFEs for Overcoming ISI and CCI in Wireline Band-limited Parallel Channels

Referring to the MIMO MLP/BP-based DFEs and the GMLP/BP-based DFEs, the MIMO GMLP/BP neural networks are realized as waveform equalizers for distorted nonreturn-to-zero data recovery in band-limited channels with co-channel interference. From the simulation results, we note that the proposed design can recover severe distorted NRZ data as well as suppress ISI, CCI and AWGN. As a result, the better performance as compared to the LMS DFEs and the MIMO MLP/BP-based DFEs is achieved in the wireline band-limited channels with co-channel interference. In this work, we assume that the parallel interconnection paths lay on a plane within a chip or within a printed circuit board (PCB).

This section is organized as follows. The equivalent channel model is presented in subsection 1 while subsection 2 shows the proposed architecture. Afterward, the simulation conditions and results show in subsection 3. Finally, we make a summary in subsection 4.

4-2-1 Multi-channel Environment within a Plane

In this work, the channel characteristics are same as those in the previous section except the weighting of co-channel interference between different channels. We assume that the parallel interconnection paths lay on a plane within a chip or within a PCB. Because the effect of CCI should be proportional to the distance with an inverse ratio, it is a worse case that uses sorted uniform distribution random values between 1 and 0 to simulate the effects between different channels. By this way, we construct an N-by-N symmetric matrix and normalize this matrix to make the sum of squares of all elements be N. The weighting of co-channel interference between different channels is shown in Table 4-3 where N is equal to 8.



Table 4-3: Weighting of co-channel interference between different channels on a plane.

	1	2	3	4	5	6	7	8
1	0	0.7070	0.5984	0.3760	0.3112	0.1641	0.1576	0.1338
2	0.7070	0	0.4131	0.3155	0.2690	0.1800	0.1398	0.0215
3	0.5984	0.4131	0	0.5883	0.4451	0.3705	0.2296	0.0353
4	0.3760	0.3155	0.5883	0	0.6650	0.4303	0.4189	0.0002
5	0.3112	0.2690	0.4451	0.6650	0	0.5375	0.2003	0.1160
6	0.1641	0.1800	0.3705	0.4303	0.5375	0	0.3726	0.1420
7	0.1576	0.1398	0.2296	0.4189	0.2003	0.3726	0	0.6319
8	0.1338	0.0215	0.0353	0.0002	0.1160	0.1420	0.6319	0

4-2-2 MIMO GMLP/BP-based DFE

In this work, the I/O format is same as that in section 4-1. The neural network architecture is similar to that in section 3-2. The block diagram of the MIMO generalized MLP/BP-based DFE is shown in Fig. 4-11. This MIMO generalized MLP/BP-based DFE is the single hidden layer MLP architecture. The inputs of the MIMO generalized MLP/BP-based DFE consist of feed-forward signals, which come from the input symbols by tapped-delay-line registers, and feedback signals, which come from previous decisions by another tapped-delay-line registers. Because the order of the neuron of the generalized MLP/BP neural networks is more than one, it is necessary to generate the power terms for the inputs in each layer. Although the complexity of the MIMO GMLP/BP-based DFE is higher than that of the MIMO MLP/BP-based DFE, the MIMO GMLP/BP-based DFE provide better performance.

Same as the previous configurations, all equalization schemes in this work have 11 symbols per channel in the forward part and 5 symbols per channel in the feedback part. We also assume there are 8 parallel channels in this system. The number of neurons in the input layer is equal to 128 (16-by-8). The MLP/BP-based DFEs uses the single hidden layer MLP architecture. The number of neurons in the hidden layer is 16. Since all the proposed equalization schemes have a single output per channel, the number of neurons in the output layer is equal to 8 (1-by-8). The summation function order of the generalized MLP/BP-based DFEs is restricted to 1, 2, and 3 that is denoted by “Order 1”, “Order 2”, and “Order 3”, respectively.

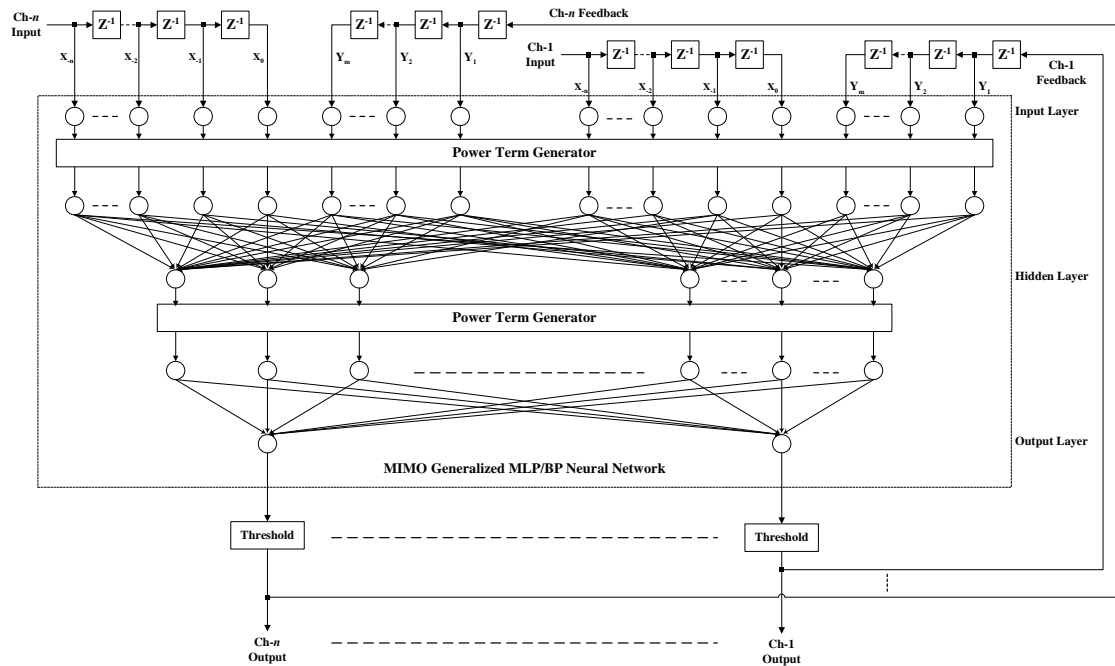


Fig. 4-11: The MIMO generalized MLP/BP-based DFEs.



4-2-3 Simulation Results

The performance of the MIMO generalized MLP/BP-based DFE is evaluated through the simulations for the distorted NRZ signal recovery in the band-limited channels with co-channel interference. The data rate is ten times of the channel bandwidth. It is a wireline application so we can select a longer training set to achieve better performance.

In the training procedure, the length of the training set is equal to 10^4 symbols and the total training epochs are 10^2 . The two-phase learning is used with the learning rate of $0.5 (2^{-1})$ when the mean square error of the training set is larger than 10^{-3} , and the learning rate of $0.125 (2^{-3})$, otherwise. When the training epochs exceed eighty percent of the total epochs, the best parameters will be recorded to achieve the lowest mean square error of the training set in the last twenty percent of the training epochs. Hence the steady-state

training results can be recognized. In fact, the simulations indicate no unstable problems as all training processes are converged.

Because different initial conditions lead to different effects, the non-training evaluation set that has 10^5 symbols is used to examine the training quality of numerous independent simulation outcomes. After numerous independent training and evaluation runs, those yielding better outcomes will be chosen to perform a long trial with the test set, and then the best one will be the final test result. The length of the test set is 10^7 symbols, and the evaluation set is its subset. In this work, we execute fifty independent runs and select the best one as the final result.

Similarly, we compare the performance of our proposed approach with that of a set of LMS DFEs. We use a LMS DFE without cross inputs for a channel among these parallel channels. The simulation conditions are listed in Tab. 4-4.

The band-limited channel described by the transfer function, $H_0(z) = 0.4665 + 0.2489z^{-1} + 0.1328z^{-2} + 0.0708z^{-3} + 0.0378z^{-4}$, with the co-channel interference described by the transfer function, $C_r(z) = 0.408 + 0.816z^{-1} + 0.408z^{-2}$, is used to estimate the system performance of the LMS DFEs, the MIMO MLP/BP-based DFE, and the MIMO generalized MLP/BP-based DFE. This ISI channel response indicates that the data rate is ten times of the channel bandwidth. The training noise and the evaluation noise are assumed to be SNR=20dB, and SNR of the test signal is between 10dB and 25dB. The signal to co-channel interference ratio (SIR) is equal to 10, 12.5, 15, 17.5, and 20, respectively.

Fig. 4-12 shows the comparisons of the BER performance vs. SNR for the LMS DFEs, the MIMO MLP/BP-based DFE, and the MIMO GMLP/BP-based DFE in the band-limited channels with different SIR. In this figure, we find that the MIMO GMLP/BP-based DFE outperform the MIMO MLP/BP-based DFE under small

background noise with large co-channel interference. Considering different SIR in the band-limited channels at SNR=15dB and 20dB, Fig. 4-13 also shows the comparisons of the BER performance vs. SIR for the LMS DFEs, the MIMO MLP/BP-based DFE, and the MIMO GMLP/BP-based DFE. As compared with LMS DFEs and the MIMO MLP/BP-based DFE, the MIMO GMLP/BP-based DFE can improve the SIR performance about 2.5dB and 0.3dB at BER=10⁻³. Moreover, we can find that the suitable summation function order is equal to two when small interference presented, or three when large distortion appeared.

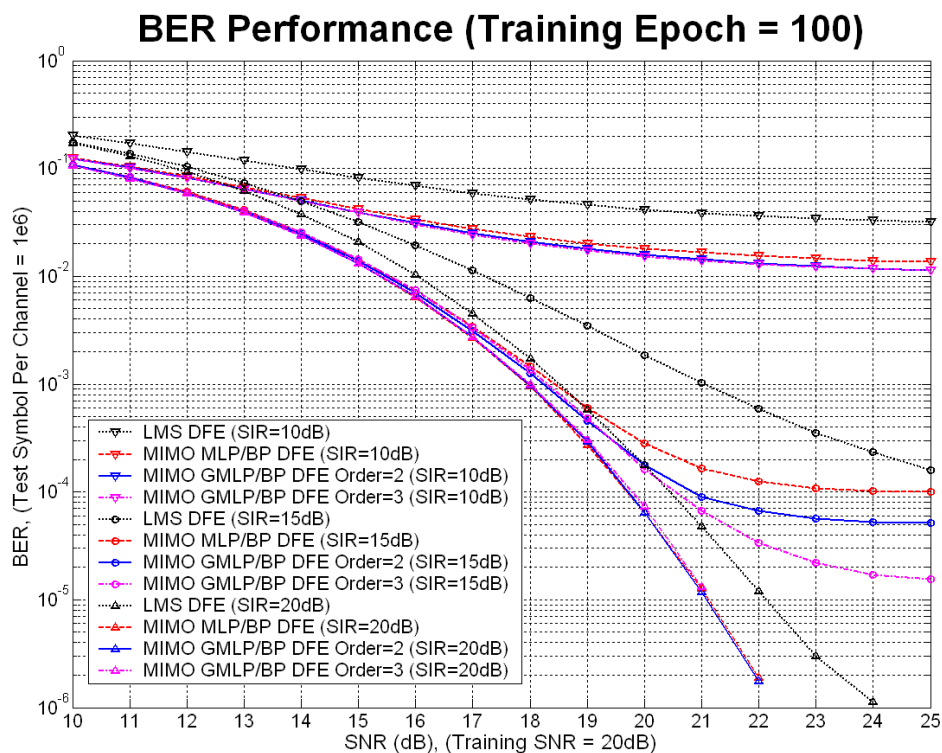


Fig. 4-12: BER vs. SNR for different types of equalizers in the wireline band-limited channels with co-channel interference at SIR=10, 15 and 20dB.

Table 4-4: Simulation conditions for MIMO GMLP/BP-based DFE.

Simulation Conditions	LMS DFEs	MIMO GMLP/BP-based DFE
Input Channel Number	1	8 channels
Forward Length	11 symbols	
Feedback Length	5 symbols	
Input Number per Channel	16 symbols	
Input Numbers	16	128 (16x8)
Hidden Neuron Number	---	16
Output Number	1	8
Summation Function Order	---	1, 2, and 3
Training Set	10 ⁴ symbols	
Evaluation Set	10 ⁵ symbols	
Test Set	10 ⁶ symbols	
Training Epochs	100 cycles	
Re-training Times	1	50
Learning Rate Searching Range	2 ⁰ ~ 2 ⁻¹⁰	2 ⁰ ~ 2 ⁻⁴ / 2 ⁰ ~ 2 ⁻⁴
Most Suitable Learning Rate	2 ⁻⁸	2 ⁻¹ / 2 ⁻³ (Two phase learning, MSE Bound=10 ⁻³)
Training SNR	20 dB	
Test SNR	10 to 25 dB (Step = 1 dB)	
SIR	10, 12.5, 15, 17.5, and 20 dB	
Equalizer Number for 8 channels	8	1

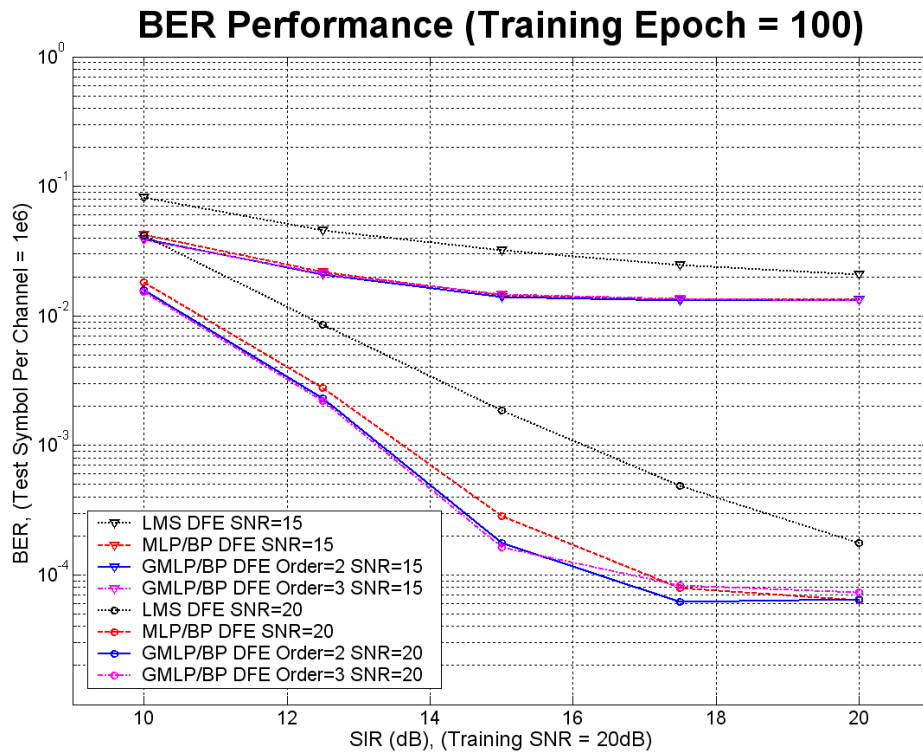
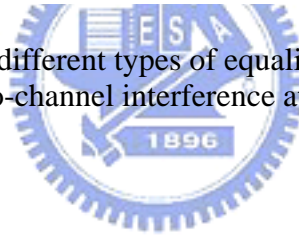


Fig. 4-13: BER vs. SIR for different types of equalizers in the wireline band-limited channels with co-channel interference at SNR= 15 and 20dB.




4-2-4 Summary

According to the simulation results, the MIMO GMLP/BP-based DFE can recover severe distorted NRZ signals and suppress CCI to achieve better BER performance than LMS DFEs and the MIMO MLP/BP-based DFE in wireline band-limited channels in which the data rate is ten times as much as the channel bandwidth. Also the proposed scheme is a multi-input multi-output architecture, we can extend the input and output number for more complex system. Overall, the MIMO GMLP/BP-based DFE can yield a substantial improvement over the MIMO MLP/BP-based DFE that performs better than the LMS DFEs.



CHAPTER 5

MLP/BP-based Soft DFEs with TCM for Wireless Communications



For more efficient data transmissions, a new MLP/BP-based channel equalizer is proposed to compensate for multi-path fading in wireless applications. In this chapter, for better system performance, we apply the soft output and the soft feedback structure as well as the soft decision channel decoding. Moreover, to improve packet error rate (PER) and bit error rate (BER), we search for the optimal scaling factor of the transfer function in the output layer of the MLP/BP neural networks and add small random disturbances to the training data. As compared with the conventional MLP/BP-based DFEs and the soft output MLP/BP-based DFEs, the proposed MLP/BP-based soft DFEs under multi-path fading channels can improve over 3dB ~ 0.6dB at PER=10⁻¹ and over 3.3dB ~ 0.8dB at BER=10⁻³.

The system diagram of wireless digital communication systems is shown in Fig. 5-1. This chapter is organized as follows. The wireless channel environment is presented in section 1. Section 2 makes a discussion for the error control coding while section 3 shows

the architecture of the MLP/BP-based soft DFEs with bit-interleaved TCM. Afterward, the simulation results show in section 4. Finally, we make a summary in section 5.

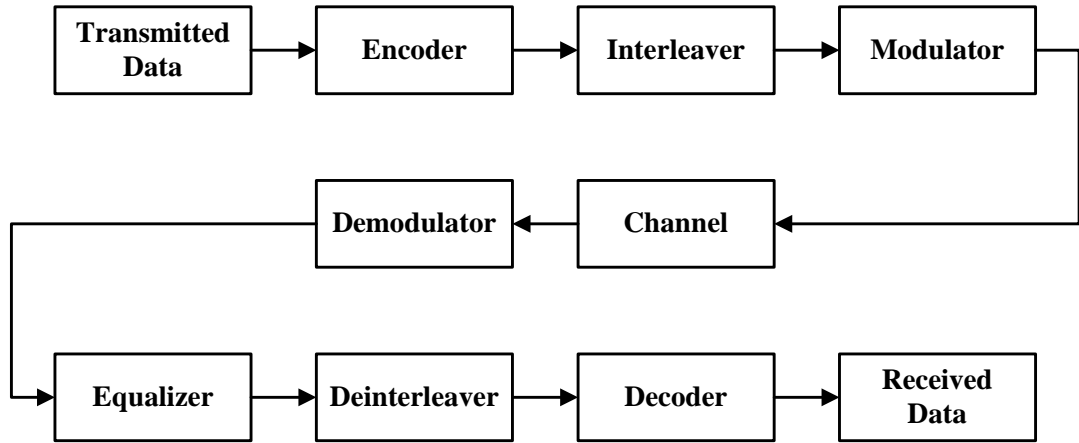


Fig. 5-1: System Diagram.



5-1 Wireless Channel Environment

The description of the equivalent channel model for wireless digital transmission systems is shown in Fig. 5-2. In this model, a finite impulse response (FIR) filter is used to model the ISI channel response and the AWGN is used to model the background noise. The equivalent FIR filters of the multi-path fading channels are time varying. In this work, we assume the FIR filter coefficients constant within a packet interval. Nevertheless, in the fast channel variation, we can select a smaller packet to avoid this problem.

The ISI channel response with AWGN can be written as follows:

$$H(z) = h_0 + h_1 \cdot z^{-1} + h_2 \cdot z^{-2} + \dots + h_L \cdot z^{-L}, \quad (5-1)$$

$$h_m = A_m \cdot e^{j\phi_m}, \quad (5-2)$$

$$y_k = \sum_{i=0}^L h_i \cdot x_{k-i}, \quad (5-3)$$

$$\hat{y}_k = y_k + n_k, \quad (5-4)$$

where $H(z)$ is the transfer function of the ISI channel; h_m is the coefficient of the channel response that is a complex value; L is the length of the channel response; A_m is the magnitude of h_m ; φ_m is the phase of h_m ; x_k is the input sequence; y_k is the channel output which is warped by ISI only; n_k is the AWGN; \hat{y}_k is the received signal which is distorted by both ISI and AWGN.

In this work, we assume that the channel length is six, and the transmission modulation is QPSK. In (5-2), we generate the magnitude by uniform distribution random values between 0 to 1 and the phase by different uniform distribution random values from 0 to 2π . The filter responses are normalized to unity. The channel responses of the multi-path fading channels are shown in Fig. 5-3 and their frequency responses are illustrated in Fig. 5-4.

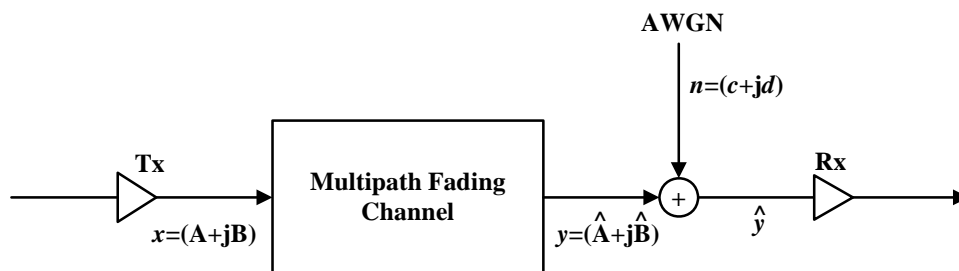


Fig. 5-2: The Equivalent Model for the Multi-path Fading Channels.

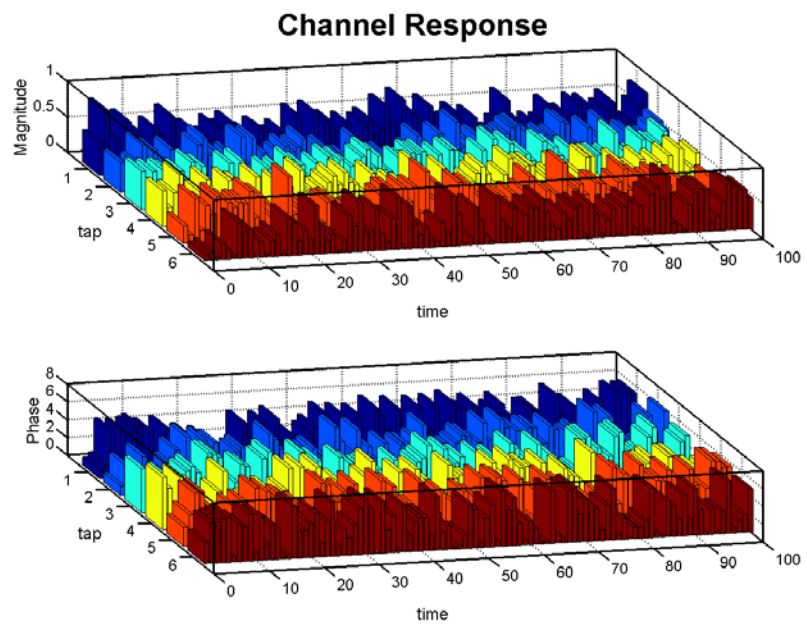


Fig. 5-3: Channel Responses of Multi-path Fading Channels.

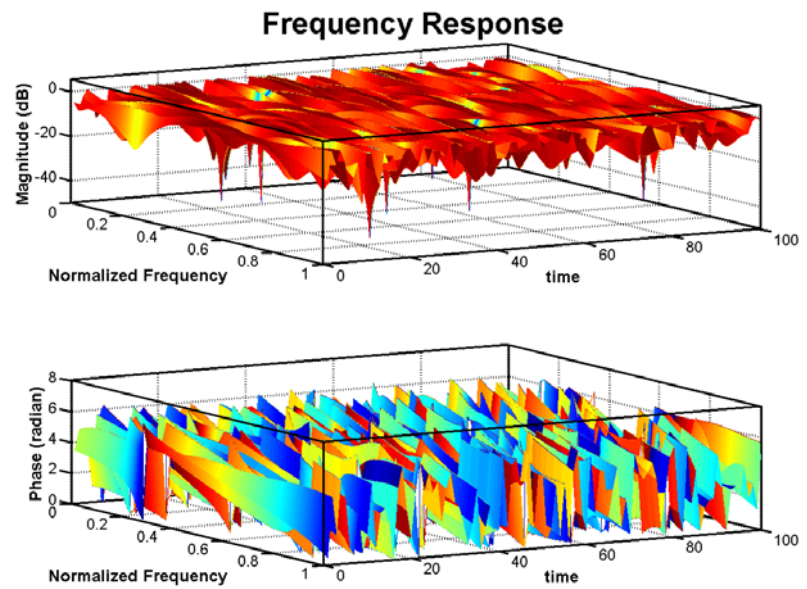
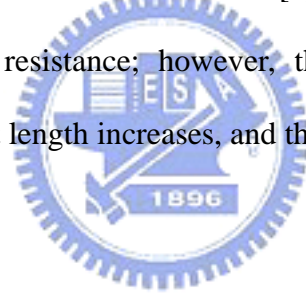


Fig. 5-4: Frequency Responses of Multi-path Fading Channels.

5-2 Error Control Coding

Error control coding is often applied in a communication system to enhance the error performance. Among the well-known coding techniques, the convolutional code would be the most popular one that provides the superior error correction capacity and has reasonable decoding complexity. The Viterbi algorithm [7] is a maximum likelihood decoding for convolutional codes. With the probabilistic soft inputs, the Viterbi decoder can optimally decode the received codeword. In the present wireless system, the bit interleaved 64 states convolutional codes is adopted while considering the system complexity and the error performance.

The bit interleaving is included for the fading channel to achieve a decoding performance close to that in the AWGN channel [8]. A larger convolutional code can further provide better error resistance; however, the decoding complexity increases exponentially as the constraint length increases, and the decoder would be unacceptable in real applications.



5-3 Architecture

In this section, the MLP/BP-based soft DFE with bit-interleaved trellis coded modulation (TCM) is presented for the distorted QPSK signal recovery in multi-path fading channels under different AWGN power. For better performance, we select the unipolar sigmoid function with the scaling adjustment as the transfer function of the MLP/BP neural networks and show as below.

$$f(net_{nj}) = \frac{1}{1 + e^{-K \cdot net_{nj}}}, \quad (5-5)$$

where K is the scaling factor.

As compared with the conventional hard output MLP/BP-based DFE, we apply the soft decision channel decoding to the soft output MLP/BP-based equalization schemes for better performance. The soft output features of the equalizer are quite suitable for the soft decision channel decoding and work much better than the conventional hard output one. Moreover, we apply not only the soft output but also the soft decision to the MLP/BP-based DFE to further advance the decoding performance of the soft decision channel decoder.

In this section, we first report the proposed MLP/BP-based soft DFE architecture. Subsequently, the solution for the soft decision channel decoding and the interleaving is presented – Combine this neural-based soft equalization scheme and bit-interleaved trellis coded modulation to achieve better system performance in wireless applications.

5-3-1 The MLP/BP-based Soft DFEs

We apply the soft output and the soft decision feedback structure to MLP/BP-based channel equalizers for the soft decision channel decoding and improve whole performance on multi-path fading channels. The block diagram of the MLP/BP-based soft DFEs is shown in Fig. 5-5. We use a single-hidden-layer MLP/BP neural network architecture, where the log-sigmoid function is used as the transfer function of the neurons. There are four tapped delay line registers for I-channel input, I-channel feedback, Q-channel input, and Q-channel feedback, respectively. The MLP/BP neural network has two output neurons that correspond to I-channel output and Q-channel output.

In order to increase the performance, we find the optimal scaling factor for the transfer function in the output layer of the MLP/BP neural networks and add extra small random disturbances to the training data. The scaling factor adjustment enlarges the mapping range of the output of the MLP/BP-based soft DFEs and improves the soft

decision channel coding. With the extra small random disturbances in the training data, the training results are able to avoid the local minimum of the cost function, achieving better training quality. The suitable scaling factor and the disturbance magnitudes are selected by experiences and experiments.

In this work, we search the most suitable input configuration by assuming different forward taps and feedback taps of the equalizers. As a result, all neural-based equalization schemes have 17 symbols in the forward part and 8 symbols in the feedback part. Because the signal includes real part and imaginary part, we separate the input symbols to I-channel and Q-channel. Accordingly, the number of neurons in the input layer is equal to 50 (25×2). All of the neural-based equalizers in this work use the single hidden layer MLP architecture. The number of neurons in the hidden layer is equal to 25. Since all of the equalization schemes produce the detection of a QPSK symbol each time, the number of neurons in the output layer is equal to 2 (1×2), corresponding to the outputs of I-channel and Q-channel.

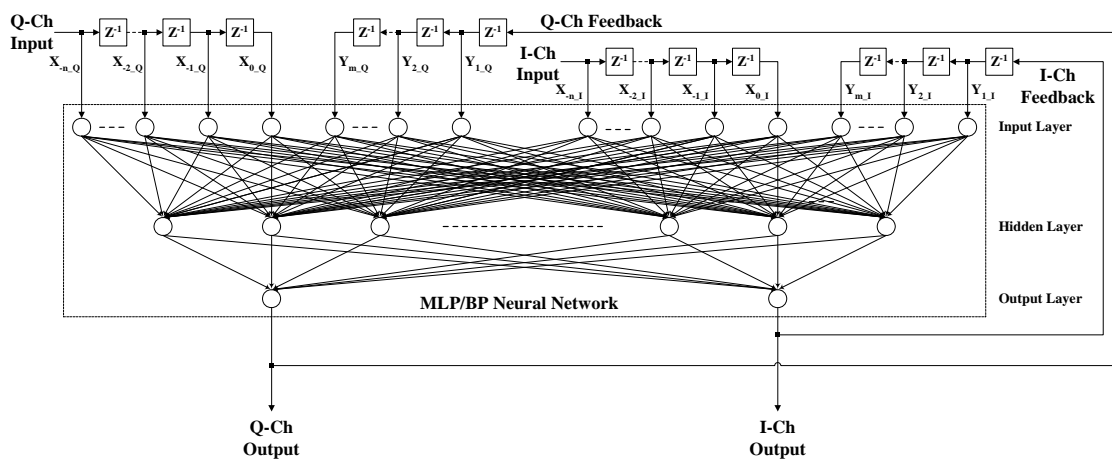


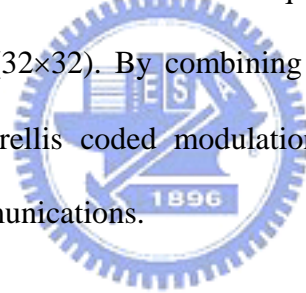
Fig. 5-5: MLP/BP-based Soft DFEs for Wireless Applications.

5-3-2 Soft Decision Channel Coding and Interleaving

Based on the soft outputs from the equalization, we use the soft inputs Viterbi decoder to improve the decoding performance. As compared with the hard-decision decoding algorithm, about 2dB-3dB improvement in SNR can be achieved [10]. The survivor memory is also truncated to be five times the constraint length for negligible truncation error.

Besides, the bit interleaving is integrated to increase the decoding performance. The size of the bit interleaving relates to the channel response length, the frame size of equalizers, and the decoding complexity, a trade-off between the performance and the cost. We decide the bit interleaving size from the channel models as well as the experiments.

In this work, the coding rate of the TCM is equal to $1/3$, and the size of the block interleaver is equal to 1024 (32×32). By combining this neural-based soft equalization scheme and bit-interleaved trellis coded modulation, we can enhance whole system performance in wireless communications.



5-4 Simulation Results

The overall performance of the MLP/BP-based soft DFEs with bit-interleaved TCM is evaluated through the simulations for the distorted QPSK signal recovery in multi-path fading channels under different AWGN power. In these simulations, we apply the proposed architecture to different packet size and prove the proposed scheme with better performance.

The length of the training symbols within a packet is equal to 128 symbols and the total training epochs are 40. When the training epochs exceed fifty percent of total epochs,

the best parameters will be recorded to achieve the lowest mean square error of the training set. The length of transmitted data within a packet is 10^3 , 2×10^3 , 4×10^3 , and 8×10^3 bits, respectively. There are 10^3 packets tested in different configurations.

In this work, different learning rates, equal to 1, 0.5, 0.25, and 0.125, have been evaluated for all of the equalization schemes. For the conventional MLP/BP-based DFE, the soft output MLP/BP-based DFE, the MLP/BP-based soft DFE, and the MLP/BP-based soft DFE with transfer function scaling factor adjustment, the most suitable learning rate is equal to 0.5, 0.25, 0.25, and 0.5, respectively.

For the MLP/BP-based soft DFEs, different scaling factor of the transfer function in the output layer of the MLP/BP neural networks, equal to 1, 0.5, 0.25, and 0.125, have been evaluated. For this application, the most suitable scaling factor is 0.5. Moreover, different magnitudes of extra small random disturbances have been added to the training data to improve the training quality. From experiments, the most suitable magnitude is about 10% of the training signal. Thus, the proposed MLP/BP-based soft DFEs has included the suitable scaling factor to the transfer function of the output neurons and added the suitable magnitude of extra random disturbances to the training data.

In this work, the system configurations and simulation conditions are listed in Tab. 5-1. When the packet data length is equal to 10^3 bits, the PER performance for different types of equalizers is shown in Fig. 5-6. As compared with the conventional MLP/BP-based DFE and the soft output MLP/BP-based DFE, the proposed MLP/BP-based soft DFE under multi-path fading channels with AWGN can improve over 3.0dB and 0.6dB at $\text{PER}=10^{-1}$. When the packet data length is set to 8×10^3 bits, the PER performance for different types of equalizers is shown in Fig. 5-7. The proposed approach improves 0.4dB over the soft output MLP/BP-based DFE and 3.4dB over the conventional MLP/BP-based DFE at $\text{PER}=10^{-1}$. Fig. 5-8 shows the PER performance for

different types of equalizers with different packet data length at $E_b/N_0 = 7.5\text{dB}$ and 10.0dB . We can observe the large packet size results in poor performance. Since the multi-path fading channels are time varying, we select a smaller packet size for faster channel variant rate. Also, a smaller packet size is selected for large background noise.

For data communications, we focus on the PER performance, whereas the BER performance is the major concern for audio or multi-media communications. When the packet data length is equal to 10^3 bits, the BER performance for different types of equalizers is shown in Fig. 5-9. As compared with the conventional MLP/BP-based DFE and the soft output MLP/BP-based DFE, the proposed MLP/BP-based soft DFE under multi-path fading channels with AWGN can improve over 3.6dB and 0.9dB at $\text{BER}=10^{-3}$. When the packet data length is 8×10^3 bits, the BER performance for different equalizer types is shown in Fig. 5-10. As compared with the conventional MLP/BP-based DFE and the soft output MLP/BP-based DFE, the proposed MLP/BP-based soft DFE under multi-path fading channels with AWGN can improve over 3.3dB and 0.8dB at $\text{BER}=10^{-3}$. The BER performance for different types of equalizers with different packet data length at $E_b/N_0 = 7.5\text{dB}$ and 10.0dB is shown in Fig. 5-11. The PER performance improvement at $\text{PER}=10^{-1}$ and the BER performance improvement at $\text{BER}=10^{-3}$ are listed in Tab. 5-2.

Table 5-1: System configurations and simulation conditions.

Type	MLP/BP-based DFE		MLP/BP-based Soft DFE	
	Hard Output	Soft Output	Without Scaling factor adjustment	With Scaling Factor adjustment
Forward Length	17 symbols			
Feedback Length	8 symbols			
Input Tap Number	25 symbols			
Input Neuron Numbers	50 (25×2)			
Hidden Neuron Number	25			
Output Neuron Number	2 (1×2)			
Training Symbol Number	128 symbols			
Training Epochs	40 cycles			
Packet Data Length	1K, 2K, 4K, and 8K			
Test Packet Number	1000 packets			
Learning Rate Searching Range	$2^0 \sim 2^{-3}$			
Most Suitable Learning Rate	2^{-1}	2^{-2}	2^{-2}	2^{-1}
Scaling Factor Searching Range	---	---	---	$2^0 \sim 2^{-3}$
Most Suitable Scaling Factor	---	---	---	2^{-1}
Test Eb/N ₀	5dB – 13 dB (Step=0.5dB)			

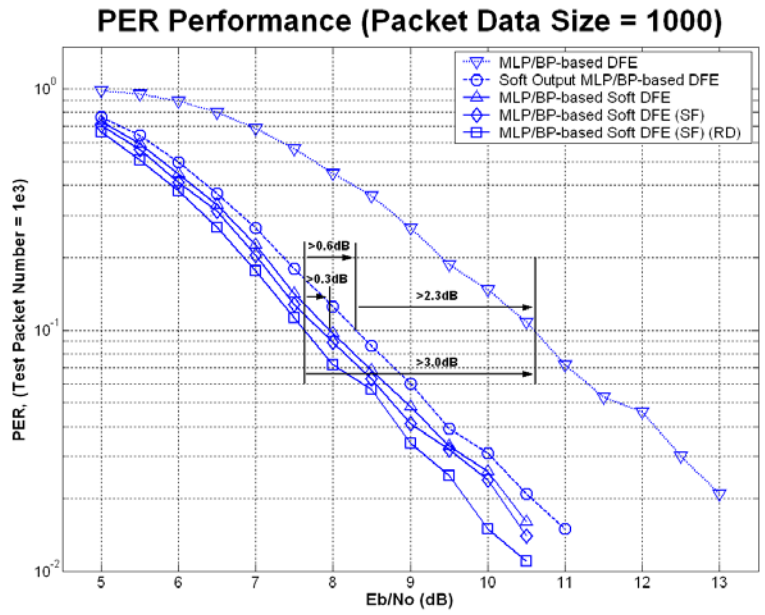


Fig. 5-6: PER Performance for different types of equalizers when packet data length is equal to 10^3 .

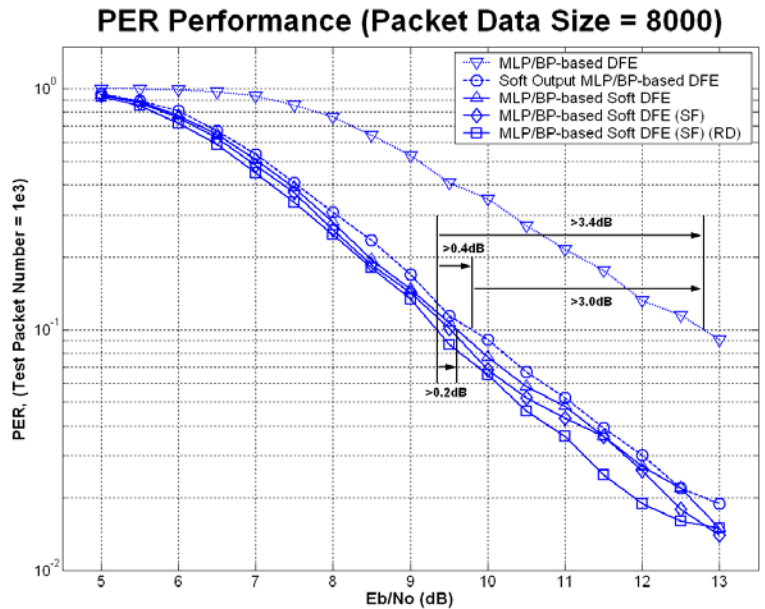


Fig. 5-7: PER Performance for different types of equalizers when packet data length is equal to 8×10^3 .

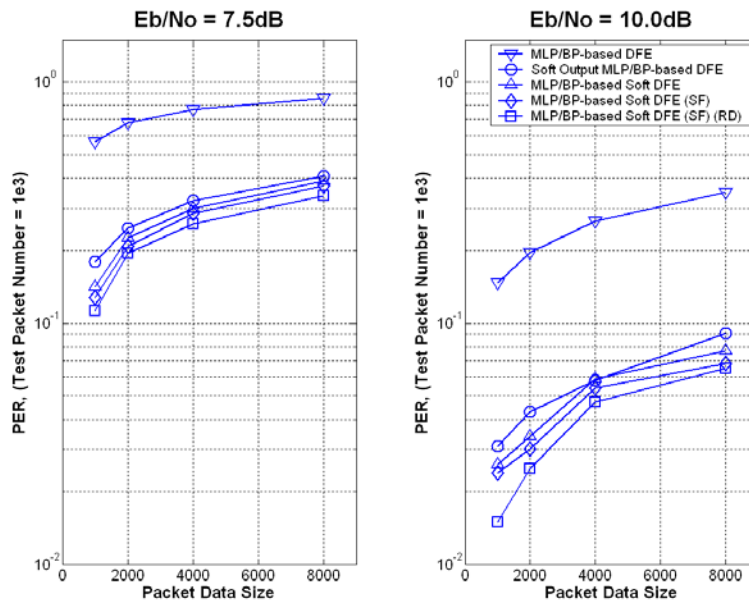


Fig. 5-8: PER Performance for different types of equalizers with different packet data length at $E_b/N_0 = 7.5\text{dB}$ and 10.0dB .

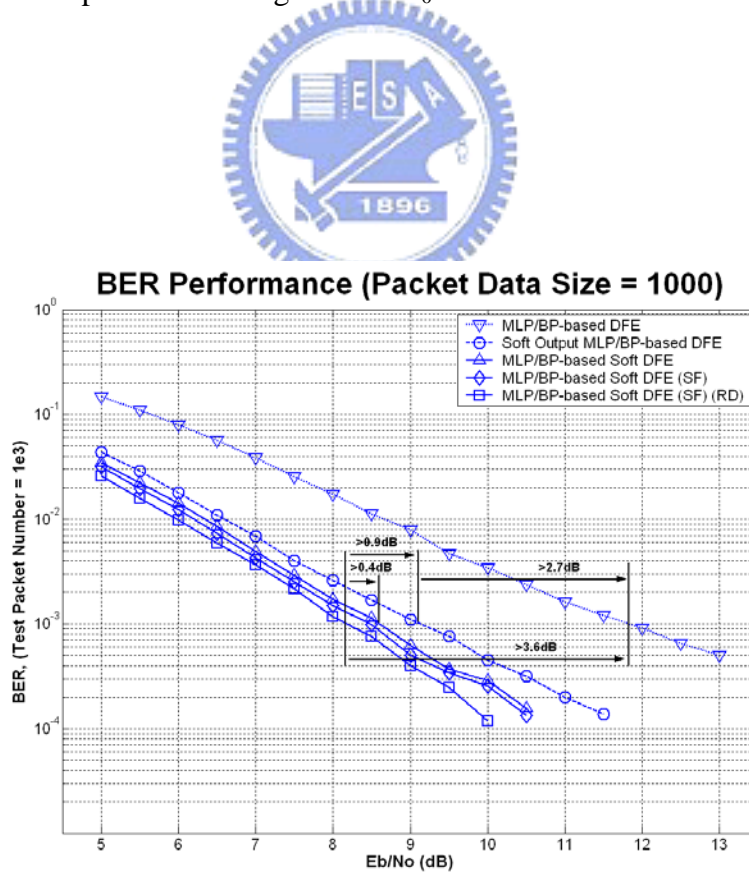


Fig. 5-9: BER Performance for different types of equalizers when packet data length is equal to 10^3 .

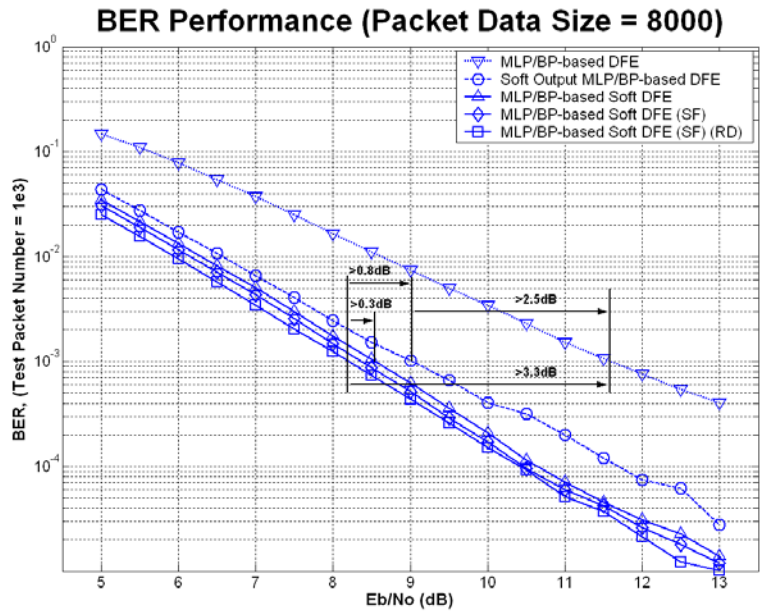


Fig. 5-10: BER Performance for different types of equalizers when packet data length is equal to 8×10^3 .

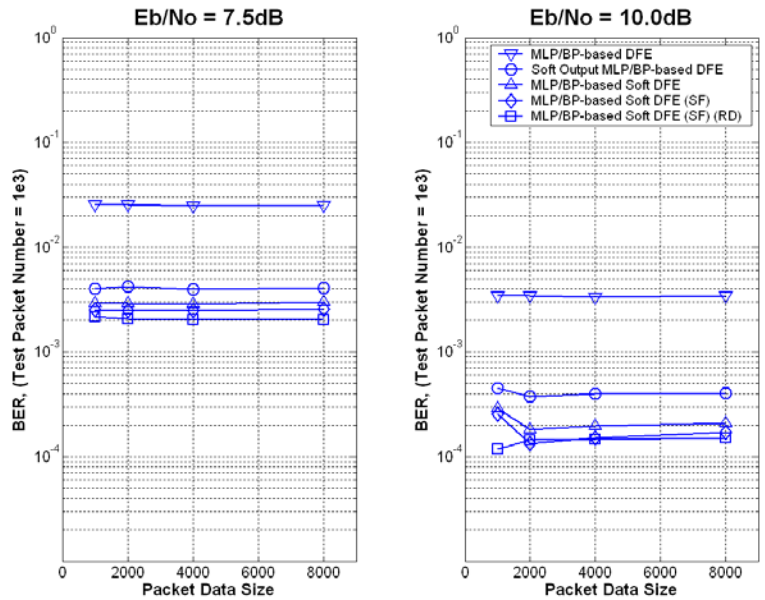


Fig. 5-11: BER Performance for different types of equalizers with different packet data lengths at $E_b/N_0 = 7.5\text{dB}$ and 10dB .

Table 5-2: The PER and BER performance improvement.

Type	MLP/BP-based DFE		MLP/BP-based Soft DFE	
	Hard Output	Soft Output	Original Setting	With Scaling Factor Adjustment and Extra Random Disturbances
Packet Data Length	Eb/N ₀ Improvement at PER=10 ⁻¹			
1K	---	> 2.3 dB	> 2.6 dB	> 3.0 dB
2K	---	> 2.5 dB	> 2.7 dB	> 3.0 dB
4K	---	>2.3 dB	>2.6 dB	> 2.8 dB
8K	---	> 3.0 dB	> 3.2 dB	> 3.4 dB
Packet Data Length	Eb/N ₀ Improvement at BER=10 ⁻³			
1K	---	> 2.7 dB	> 3.2 dB	> 3.6 dB
2K	---	> 2.7 dB	>3.1 dB	> 3.4 dB
4K	---	> 2.6 dB	> 3.1 dB	> 3.4 dB
8K	---	> 2.5 dB	> 3.0 dB	> 3.3 dB

5-5 Summary

With the soft output and the soft decision, the MLP/BP-based channel equalizers can offer more information for the soft decision channel decoding. Moreover, the system performance is further improved by searching the most suitable scaling factor for the transfer function in the output neurons and adding the suitable magnitude of extra small random disturbances to the training data. The proposed approach is applied to compensate

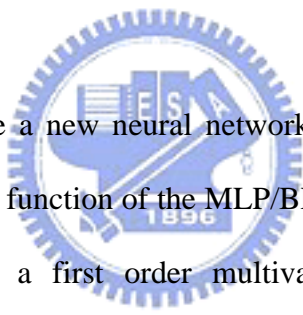
for the distorted QPSK signals in multi-path fading channels with AWGN and results in a significant performance improvement. In conclusion, the proposed MLP/BP-based soft DFE with bit-interleaved TCM provides a potential solution for wireless communications.



CHAPTER 6

Conclusion and Future Works

6-1 Conclusion



In this study, we propose a new neural network model that applies a multivariate power series as the summation function of the MLP/BP neural networks. Compared to the conventional approach using a first order multivariate polynomial, the boundaries separating the pattern space change from piecewise linear into piecewise nonlinear. In addition, when deduced by the gradient steepest descent method, the corresponding training algorithm is a gradient method; consequently, the convergence solutions exist. Therefore, this new model is a generalized MLP/BP neural network (GMLP/BP) that is more flexible than other piecewise linear approaches because of the nonlinear separating pattern space. The traditional MLP/BP neural network is a special case of the proposed generalized MLP/BP neural network.

As the channel equalization schemes can be thought of a mapping from the received waveform to the transmitted data. The pattern recognition techniques have been used to identify the severely distorting data. Having the capability of classifying the sampling

pattern and fault tolerance, artificial neural networks are very suitable for the channel equalizers. As a result, we apply the traditional and the generalized MLP/BP neural networks to channel equalization designs. From the simulation results, the proposed neural-based channel equalization schemes can outperform the conventional LMs and LMS DFEs.

For wireline communications, we apply the MLP/BP-based channel equalization schemes to different applications. In the wireline band-limited channels that the data rate is about ten times as much as the channel bandwidth, the MLP/BP-based DFEs provide better performance, tolerate sampling clock skew, and permit channel response variance. However, the traditional MLP/BP-based DFEs are not good enough for the severe ISI channels with nonlinear distortions. In such channels, the GMLP/BP-based DFEs can outperform the traditional MLP/BP-based DFEs that do better than the LMS DFEs. In wireline band-limited parallel channels, the MIMO MLP/BP-based DFEs and the MIMO GMLP/BP-based DFEs can suppress ISI, CCI and AWGN, simultaneously. By the computer simulations, the MIMO GMLP/BP-based DFEs can yield a substantial improvement over the MIMO MLP/BP-based DFEs that perform better than a set of the LMS DFEs.

For wireless communications, a modified approach, which is also based on the MLP/BP neural network, is presented. We apply the soft output and the soft decision feedback structure to the MLP/BP-based channel equalization scheme that concatenates with the soft decision channel decoder to improve whole performance on multi-path fading channels. Moreover, the performance of the MLP/BP-based soft DFE is also increased with the optimal scaling factor searching of the transfer function in the output layer of the MLP/BP neural networks and extra small random disturbances added to the training data. By the simulations, the MLP/BP-based soft DFEs with bit-interleaved TCM

outperform the MLP/BP-based DFEs with bit-interleaved TCM and the soft output MLP/BP-based DFEs with bit-interleaved TCM in multi-path fading channels.

6-2 Future Works

In this thesis, we have proposed the generalized MLP/BP-based DFEs and applied to wireline communications. Moreover, we also apply the MLP/BP-based soft DFEs with bit-interleaving soft decision channel coding to wireless communications. For further improvements, we are deducing a general form of MLP/BP neural networks in the complex domain. It should be applied to wireless communications.

Now, we are tuning the training parameters of the GMLP/BP-based soft DFEs to solve the overfitting problem for wireless communications. Moreover, the MIMO MLP/BP-based soft DFEs and the MIMO GMLP/BP-based soft DFEs will be developed for wireless communications.

To realize the proposed neural-based equalization schemes for different applications, several hardware designs are currently under investigation. The MLP/BP-based DFEs and the GMLP/BP-based DFEs can be applied to wireline high-speed peripheral interface. The MIMO MLP/BP-based DFEs and the MIMO GMLP/BP-based DFEs should be applied to high-speed system bus. The MLP/BP-based soft DFEs with bit-interleaving TCM are possible solutions in wireless communications. Although the architecture of the proposed equalization schemes is more complex than that of the conventional methods, we think that the rapid progress of VLSI technology will afford more complex approaches for better performance. Also, we can use digital signal processors to realize the proposed neural-based equalization schemes as soft-define radios (SDR). The implementations of the proposed neural-based channel equalization schemes are our research activities in the

future.

Our approaches show very good results for channel equalization applications. Further research activities have been initiated to explore how to improve and implement such techniques for wireline and wireless communications. Still, there are many open problems for further research activities.



References

- [1] S. Haykin, *Communication Systems 3e*, Wiley, 1994.
- [2] B. Sklar, *Digital Communications: Fundamentals and Applications 2e*, Prentice Hall, 2001.
- [3] J. G. Proakis, and M. Salehi, *Contemporary Communication Systems using MATLAB*, Brooks/Cole, 2000.
- [4] K. A. Al-Mashouq, and I. S. Reed, "The Use of Neural Nets to Combine Equalization with Decoding for Severe Intersymbol Interference Channels," *IEEE Trans. Neural Networks*, vol. 5, no. 6, pp. 982-988, Nov. 1994.
- [5] B. S. Song, and D. C. Soo, "NRZ Timing Recovery Technique for Band-Limited Channels," *IEEE J. Solid-State Circuits*, vol. 32, no. 4, pp. 514-520, Apr. 1997.
- [6] W. V. Etten, "An Optimum Linear Receiver for Multiple Channel Digital transmission Systems," *IEEE Tran. Commun.*, vol. 23, no. 8, pp. 828-834, Aug. 1975.
- [7] A. J. Viterbi, "Error bounds for convolutional codes and asymptotically optimum decoding algorithm," *IEEE Trans. Inform. Theory*, vol. IT-13, no. 2, pp. 260-269, Apr. 1967.
- [8] G. Caire, G. Taricco, and E. Biglieri, "Bit-interleaved coded Modulation," *IEEE Trans. Inform. Theory*, vol. 44, no. 3, pp. 927-946, May 1967.
- [9] Y. Chen, K. B. Letaief, and J. C. I. Chuang, "Soft-Output Equalization and TCM for Wireless Personal Communication Systems," *IEEE J. Select Areas Commun.*, vol. 16, no. 9, pp. 1679-1690, Dec. 1998.
- [10] W. H. Gerstaecker, R. R. Müller, and J. B. Huber, "Iterative Equalization with Adaptive Soft Feedback," *IEEE Trans. Commun.*, vol. 48, no. 9, pp. 1462-1466, Sep. 2000.
- [11] S. Haykin, "Adaptive Digital Communication Receivers," *IEEE Commun. Mag.*, vol. 38, no. 12, pp. 106-114, Dec. 2000.
- [12] D. E. Rumelhart, and J. L. McClelland, *Parallel Distributed Processing: Explorations in the Microstructure of Cognition, Vol. 1: Foundations*, PDP Research Group Cambridge, MA: MIT Press, 1986.

- [13] B. Widrow, and M. A. Lehr, "30 Years of Adaptive Neural Networks: Perceptron, Madaline, and Backpropagation," *Proc. IEEE*, vol. 78, no. 9, pp. 1415-1442, Sep. 1990.
- [14] S. Haykin, *Neural Networks: A Comprehensive Foundation 2e*, Prentice Hall, 1998.
- [15] R. L. Kennedy, Y. Lee, B. V. Roy, C. D. Reed, and R. P. Lippmann, *Solving Data Mining Problems Through Pattern Recognition*, pp. 10.23-10.32, Prentice Hall, 1998.
- [16] C. T. Lin, and C. S. G. Lee, *Neural Fuzzy Systems*, Prentice Hall, 1999.
- [17] T. R. Hsu, T. Y. Hsu, H. Y. Liu, S. D. Tzeng, J. N. Yang and C. Y. Lee, "A MLP/BP-based Equalizer for NRZ Signal Recovery in Band-Limited Channels," *Proc. 43rd IEEE Midwest Symp. Circuits and Syst. (MWSCAS)*, vol. 3, pp. 1340-1342, 2000.
- [18] T. R. Hsu, J. N. Yang, T. Y. Hsu, and C. Y. Lee, "MLP/BP-based Decision Feedback Equalizers with High Skew Tolerance in Wireline Band-Limited Channels," *WSEAS Trans. Commun.*, vol. 5, no. 2, pp. 239-245, Feb. 2006.
- [19] T. R. Hsu, T. Y. Hsu, J. T. Yang, and C. Y. Lee, "Multi-Input Multi-Output MLP/BP-based Decision Feedback Equalizers for Overcoming Intersymbol Interference and Co-Channel Interference in Wireline Band-Limited Channels," *WSEAS Trans. Circuits and Syst.*, vol. 5, no. 4, pp. 477-484, Apr. 2006.
- [20] T. R. Hsu, *The Research of Applying the Generalized Perceptron Neural Network Model to Speech Recognition*, Master's thesis, Feng-Chia University, Taichung, Taiwan, 1994.
- [21] T. R. Hsu, T. Y. Hsu, C. Y. Hsiao, and C. C. Lai, "The Research of Applying the Generalized Perceptron Neural Network Model to Speech Recognition," *Proc. National Symp. Telecommun.*, pp. 316-321, 1994.
- [22] T. R. Hsu, C. C. Lin, T. Y. Hsu, and C. Y. Lee, "Generalized MLP/BP-based Decision Feedback Equalizers for Severe Intersymbol Interference Channels in Wireline Applications," Submitted to *IEEE Trans. Neural Networks* at Jan. 2005, Revised at Oct. 2005, Ref.#: TNN05-P410.
- [23] T. R. Hsu, C. C. Lin, T. Y. Hsu, and C. Y. Lee, "MIMO Generalized MLP/BP-based DFEs for Overcoming ISI and CCI in Wireline Band-Limited Channels," Will be submitted to *IEICE Trans. Commun.*.
- [24] T. R. Hsu, C. C. Lin, T. Y. Hsu, and C. Y. Lee, "MLP/BP-based Soft Decision Feedback

Equalization with TCM for Wireless Applications,” Submitted to *IEICE Trans. Commun.*, at Jun. 2006, Conditional Acceptance at Jul. 2006, Ref.#: 2006EAL2066.

- [25] Y. S. Sohn, S. J. Bae, H. J. Park, C. H. Kim, and S. I. Cho, “A 2.2Gbps CMOS Look-Ahead DFE Receiver for Multidrop Channel with Pin-to-Pin Time Skew Compensation”, *Proc. IEEE Custom Integrated Circuits Conf. (CICC)*, pp. 473-476, 2003.
- [26] J. E. Jaussi, G. Balamurugan, D. R. Johnson, B. Casper, A. Martin, J. Kennedy, N. Shanbhag and R. Mooney, “8-Gb/s Source-Synchronous I/O Link with Adaptive Receiver Equalization, Offset Cancellation, and Clock De-Skew”, *IEEE J. Solid-State Circuits*, vol. 40, no. 1, pp. 80-88, Jan. 2005.
- [27] S. J. Bae, H. J. Chi, H. R. Kim, and H. J. Park, “A 3Gb/s 8b Single-Ended Transceiver for 4-Drop DRAM Interface with Digital Calibration of Equalization Skew and Offset Coefficients”, *Proc. IEEE Int. Solid-State Circuits Conf. (ISSCC)*, pp. 520-521, 2005.
- [28] S. Chen, S. Gunn, and C. J. Harris, “Decision Feedback Equaliser Design Using Support Vector Machines,” *IEE Proc. Vision, Image and Signal Processing*, vol. 147, no. 3, pp. 213-219, Jun. 2000.
- [29] S. Chen, and C. J. Harris, “Design of the Optimal Separating Hyperplane for the Decision Feedback Equalizer Using Support Vector Machines,” *Proc. IEEE Int. Conf. Acoust., Speech, and Signal Processing (ICASSP)*, vol. 5, pp. 2701-2704, Jun. 2000.
- [30] S. Chen, A. K. Samingan and L. Hanzo, “Optimal Decision Feedback Equaliser for M-PAM Signals Using Support Vector Machine Solution,” *Electronics Lett.*, vol. 36, no. 20 pp. 1742-1744, Sep. 2000.
- [31] B. Sklar, “How I Learned to Love the Trellis,” *IEEE Signal Processing Mag.*, vol. 20, no. 3, pp. 87-102, May 2003.
- [32] A. Pages, M. A. Lagunas, M. Nájjar, and A. I. Pérez Neira, “The K-Filter: A New Architecture to model and design non-linear system from Kolmogorov’s Theorem”, *Signal Processing*, vol. 44, no. 3, pp. 249-267, Jul. 1995.
- [33] R. Hecht-Nielsen, “Counterpropagation Networks,” *Proc. Int. Conf. Neural Networks*, vol. 2, pp. 19-32, 1987.
- [34] C. Shang, M. J. J. Holt, and C. F. N. Cowan, “Log-Likelihood Adaptive Algorithm in

- Single-Layer Perceptron Based Channel Equalisation,” *Electronics Lett.*, vol. 31, no. 22, pp. 1900-1902, Oct. 1995.
- [35] S. Chen, G. J. Gibson, and C. F. N. Cowan, “Adaptive Channel Equalisation Using a Polynomial-Perceptron Structure,” *IEE Proc. I. Commun., Speech and Vision*, vol. 137, no. 5, pp. 257-264, Oct. 1990.
- [36] Z. J. Xiang, G. G. Bi, and T. Le-Ngoc, “Polynomial Perceptrons and Their Applications to Fading Channel Equalization and Co-Channel Interference Suppression,” *IEEE Trans. Signal Processing*, vol. 42, no. 9, pp. 2470-2480, Sep. 1994.
- [37] Z. J. Xiang, and G. G. Bi, “A New Lattice Polynomial Perceptron and Its Applications to Frequency-Selective Fading Channel Equalization and ACI Suppression,” *IEEE Trans. Commun.*, vol. 44, no. 7, pp. 761-767, Jul. 1996.
- [38] W. S. Gan, J. J. Soraghan, and T. S. Durrani, “New Functional-Link Based Equaliser,” *Electronics Lett.*, vol. 28, no. 17, pp. 1643-1645, Aug. 1992.
- [39] W. S. Gan, J. J. Soraghan, and T. S. Durrani, “Functional-Link Model for Adaptive Channel Equaliser,” *Proc. IEEE Int. Conf. Acoust., Speech, and Signal Processing (ICASSP)*, vol. 3, pp. 309-312, 1994.
- [40] J. C. Patra, R. N. Pal, R. Baliarsingh, and G. Panda, “Nonlinear Channel Equalization for QAM Signal Constellation Using Artificial Neural Networks,” *IEEE Trans. Syst., Man and Cybern. B*, vol. 29, no. 2, pp. 262-271, Apr. 1999.
- [41] A. Hussain, J. J. Soraghan, and T. S. Durrani, “A New Adaptive Functional-Link Neural-Network-Based DFE for Overcoming Co-Channel Interference,” *IEEE Trans. Commun.*, vol. 45, no. 11, pp. 1358-1362, Nov. 1997.
- [42] A. Hussain, J. J. Soraghan, and L. Thornton, “Combatting Co-Channel Interference in Mobile Radio Systems Using a Novel Non-linear DSP Architecture,” *Proc. IEE Colloquium Novel DSP Algorithms and Architectures for Radio Syst.*, pp. 7/1-7/7, 1999.
- [43] G. Paterson, and J. J. Soraghan, “Functional Link Equaliser with Decision Selection for Combatting Cochannel Interference,” *Proc. 13th IEEE Workshop Statistical Signal Processing*, pp. 191-196, 2005.
- [44] H. Lin, and K. Yamashita, “A Fast Clustering Algorithm for Equalization Using RBF Network,” *Proc. 3rd IEEE Int. Conf. Knowledge-Based Intell. Inform. Eng. Syst.*, pp.

349-352, 1999.

- [45] S. Chen, B. Mulgrew, and S. McLaughlin, "Adaptive Bayesian Decision Feedback Equaliser Based on a Radial Basis Function Network," *Proc. IEEE Int. Conf. Commun. (ICC)*, vol. 3, pp. 1267-1271, 1992.
- [46] I. Howitt, J. H. Reed, V. Vemuri, and T.C. Hsia, "RBF Growing Algorithm Applied to the Equalization and Co-Channel Interference Rejection Problem," *Proc. IEEE Int. Conf. Neural Networks*, vol. 6, pp. 3571-3576, 1994.
- [47] B. Mulgrew, "Applying Radial Basis Functions," *IEEE Signal Processing Mag.*, vol. 13, no. 2, pp. 50-65, Mar. 1996.
- [48] S. H. Heo, S. K. Park, and S. W. Nam, "Channel Equalization for Severe Intersymbol Interference and Nonlinearity with a Radial Basis Function Neural Network," *Proc. IEEE Int. Joint Conf. Neural Networks (IJCNN)*, vol. 6, pp. 3992-3995, 1999.
- [49] Q. Gan, P. Saratchandran, N. Sundararajan, and K. R. Subramanian, "A Complex Valued Radial Basis Function Network for Equalization of Fast Time Varying Channels," *IEEE Trans. Neural Networks*, vol. 10, no. 4, pp. 958-960, Jul. 1999.
- [50] J. C. Patra, and R. N. Pal, "Adaptive Channel Equalization Using Counter Propagation Network," *Proc. IEEE ICCS*, vol. 1, pp. 149-153, 1994.
- [51] G. J. Gibson, S. Siu, and C. F. N. Cowen, "Multilayer Perceptron Structures Applied to Adaptive Equalisers for Data Communications," *Proc. IEEE Int. Conf. Acoust., Speech, and Signal Processing (ICASSP)*, vol. 2, pp. 1183-1186, 1989.
- [52] Q. Zhang, "Adaptive Equalization Using the Backpropagation Algorithm," *IEEE Trans. Circuits and Syst.*, vol. 37, no. 6, pp. 848-849, Jun. 1990.
- [53] S. Siu, G. J. Gibson, and C. F. N. Cowen, "Decision Feedback Equalization Using Neural Network Structures," *Proc. 1st IEE Int. Conf. Artificial Neural Networks*, pp. 125-128, 1989.
- [54] S. Siu, G. J. Gibson, and C. F. N. Cowen, "Decision Feedback Equalisation Using Neural Network Structures and Performance Comparison with Standard Architecture," *IEE Proc. I. Commun., Speech and Vision*, vol. 137, no. 4, pp. 221-225, Aug. 1990.
- [55] M. Meyer, and G. Pfeiffer, "Multilayer Perceptron Based Decision Feedback Equalisers

- for Channels with Intersymbol Interference," *IEE Proc. I. Commun., Speech and Vision*, vol. 140, no. 6, pp. 420-424, Dec. 1993.
- [56] A. Zerguine, A. Shafi, and M. Bettayeb, "Multilayer Perceptron-Based DFE with Lattice Structure," *IEEE Trans. Neural Networks*, vol. 12, no. 3, pp. 532-545, May 2001.
- [57] T. L. Clarke, "Generalization of Neural Networks to the Complex Plane," *Proc. IEEE Int. Joint Conf. Neural Networks (IJCNN)*, vol. 2, pp. 435-440, 1990.
- [58] G. M. Georgiou, and C. Koutsougeras, "Complex Domain Backpropagation," *IEEE Trans. Circuits and Syst. II: Analog and Digital Signal Processing*, vol. 39, no. 5, pp. 330-334, May 1992.
- [59] T. Kim, and T. Adali, "Fully Complex Backpropagation for Constant Envelope Signal Processing," *Proc. IEEE Workshop Neural Networks for Signal Processing*, vol. 1, pp. 231-240, 2000.
- [60] H. Leung, and S. Haykin, "The complex backpropagation algorithm," *IEEE Trans. Signal Processing*, vol. 39, no. 9, pp. 2101-2104, Sep. 1991.
- [61] N. Benvenuto, and F. Piazza, "On the complex backpropagation algorithm," *IEEE Trans. Signal Processing*, vol. 40, no. 4, pp. 967-969, Apr. 1992.
- [62] C. H. Chang, S. Siu, and C. H. Wei, "Decision Feedback Equalization Using Complex Backpropagation Algorithm," *Proc. IEEE Int. Symp. Circuits and Syst. (ISCAS)*, vol. 1, pp. 589-592, 1997.
- [63] P. R. Chang, B. F. Yeh, and C. C. Chang, "Adaptive Packet Equalization for Indoor Radio Channel Using Multilayer Neural Networks," *IEEE Trans. Veh. Technol.*, vol. 43, no. 3, pp. 773-780, Aug. 1994.
- [64] P. R. Chang, and B. C. Wang, "Adaptive Decision Feedback Equalization for Digital Satellite Channels Using Multilayer Neural Networks," *IEEE J. Select. Areas Commun.*, vol. 13, no. 2, pp. 316-324, Feb. 1995.
- [65] N. W. K. Lo, and H. M. Hafez, "Neural Network Channel Equalization," *Proc. IEEE Int. Joint Conf. Neural Networks (IJCNN)*, vol. 2, pp. 981-986, 1992.
- [66] P. R. Chang, and B. C. Wang, "Neural-Net-Based Receiver Structures for Single- and Multi-amplitude Bandlimited Signals in CCI and ACI channels," *IEEE Trans. Veh.*

Technol., vol. 46, no. 3, pp. 791-798, Aug. 1997.

- [67] S. S. Yang, C. L. Ho, and C. M. Lee, "HBP: Improvement in BP Algorithm for an Adaptive MLP Decision Feedback Equalizer," *IEEE Trans. Circuits and Syst. II: Express Briefs*, vol. 53, no. 3, pp. 240-244, Mar. 2006.
- [68] T. Adali, and M. K. Sonmez, "Channel Equalization with Perceptrons: an Information-Theoretic Approach," *Proc. IEEE Int. Conf. Acoust., Speech, and Signal Processing (ICASSP)*, vol. 3, pp. 297-300, 1994.
- [69] T. Adali, X. Liu, and M. K. Sonmez, "Conditional Distribution Learning with Neural Networks and Its Application to Channel Equalization," *IEEE Trans. Signal Processing*, vol. 45, no. 4, pp. 1051-1064, Apr. 1997.
- [70] C. T. Lin, and C. F. Juang, "An Adaptive Neural Fuzzy Filter and Its Applications," *IEEE Trans. Syst., Man and Cybern. B*, vol. 27, no. 4, pp. 262-271, Aug. 1997.

